VOLUME 34 AUGUST 1956 NUMBER 8

Canadian Journal of Chemistry

Editor: LÉO MARION

Associate Editors:

HERBERT C. BROWN, *Purdue University*
A. R. GORDON, *University of Toronto*
C. B. PURVES, *McGill University*
Sir ERIC RIDEAL, *Imperial College, University of London*
J. W. T. SPINKS, *University of Saskatchewan*
E. W. R. STEACIE, *National Research Council of Canada*
H. G. THODE, *McMaster University*
A. E. VAN ARKEL, *University of Leiden*

Published by THE NATIONAL RESEARCH COUNCIL

OTTAWA CANADA

CANADIAN JOURNAL OF CHEMISTRY

(*Formerly Section B, Canadian Journal of Research*)

Under the authority of the Chairman of the Committee of the Privy Council on Scientific and Industrial Research, the National Research Council issues THE CANADIAN JOURNAL OF CHEMISTRY and six other journals devoted to the publication, in English or French, of the results of original scientific research. Matters of general policy concerning these journals are the responsibility of a joint Editorial Board consisting of: members representing the National Research Council of Canada; the Editors of the Journals; and members representing the Royal Society of Canada and four other scientific societies.

The Chemical Institute of Canada has chosen the Canadian Journal of Chemistry and the Canadian Journal of Technology as its medium of publication for scientific papers.

EDITORIAL BOARD

Representatives of the National Research Council

A. N. Campbell, *University of Manitoba*
G. E. Hall, *University of Western Ontario*
H. G. Thode, *McMaster University*
D. L. Thomson, *McGill University*
W. H. Watson (Chairman), *University of Toronto*

Editors of the Journals

D. L. Bailey, *University of Toronto*
T. W. M. Cameron, *Macdonald College*
J. B. Collip, *University of Western Ontario*
G. A. Ledingham, *National Research Council*
Léo Marion, *National Research Council*
R. G. E. Murray, *University of Western Ontario*
G. M. Volkoff, *University of British Columbia*

Representatives of Societies

D. L. Bailey, *University of Toronto*
Royal Society of Canada
T. W. M. Cameron, *Macdonald College*
Royal Society of Canada
J. B. Collip, *University of Western Ontario*
Canadian Physiological Society
R. G. E. Murray, *University of Western Ontario*
Canadian Society of Microbiologists
H. G. Thode, *McMaster University*
Chemical Institute of Canada
T. Thorvaldson, *University of Saskatchewan*
Royal Society of Canada
G. M. Volkoff, *University of British Columbia*
Royal Society of Canada; Canadian Association of Physicists

Ex officio

Léo Marion (Editor-in-Chief), *National Research Council*
F. T. Rosser, Director, Division of Administration, *National Research Council*

Manuscripts for publication should be submitted to Dr. Léo Marion, Editor-in-Chief. Canadian Journal of Chemistry, National Research Council, Ottawa 2, Canada.
(For instructions on preparation of copy, see **Notes to Contributors** (inside back cover).)

Proof, correspondence concerning proof, and orders for reprints should be sent to the Manager, Editorial Office (Research Journals), Division of Administration, National Research Council, Ottawa 2, Canada.

Subscriptions, renewals, requests for single or back numbers, and all remittances should be sent to Division of Administration, National Research Council, Ottawa 2, Canada. Remittances should be made payable to the Receiver General of Canada, credit National Research Council.

The journals published, frequency of publication, and prices are:

Canadian Journal of Biochemistry and Physiology	Bimonthly	$3.00 a year
Canadian Journal of Botany	Bimonthly	$4.00 a year
Canadian Journal of Chemistry	Monthly	$5.00 a year
Canadian Journal of Microbiology	Bimonthly	$3.00 a year
Canadian Journal of Physics	Monthly	$4.00 a year
Canadian Journal of Technology	Bimonthly	$3.00 a year
Canadian Journal of Zoology	Bimonthly	$3.00 a year

The price of single numbers of all journals is 75 cents.

Canadian Journal of Chemistry

Issued by THE NATIONAL RESEARCH COUNCIL OF CANADA

VOLUME 34 AUGUST 1956 NUMBER 8

THERMAL NEUTRON CAPTURE CROSS SECTION OF Ce^{142} [1]

BY L. P. ROY[2] AND L. YAFFE

ABSTRACT

The cross section of Ce^{142} has been determined by the activation method and found to be 0.95 ± 0.05 barns relative to a value of $\sigma_{Co^{59}} = 36.3$ barns. Disintegration rates were determined by a 4π counter. The value obtained agrees with that of Katcoff *et al.* (1949) also obtained by the activation method but differs markedly from that of Pomerance (1952).*

INTRODUCTION

In the course of some related work (11) it became necessary to determine the capture cross section of Ce^{142} as accurately as possible. Bothe (1), by the activation method, had obtained a value of 1.1 barns relative to a value of 49 barns for the capture cross section σ of Ho^{165}. Using the most recent value of $\sigma_{Ho^{165}} = 64$ barns (7, 12), then $\sigma_{Ce^{142}} = 1.4$ barns according to Bothe. Katcoff *et al.* (5) obtained a value of 0.95 ± 0.18 barns by the activation method using uranium metal as a flux monitor. Pomerance (8) used the pile oscillator technique to obtain a value of 1.8 ± 0.2 barns for isotopically enriched Ce^{142}. He used $\sigma_{Au^{197}} = 95$ barns as a standard. Using the more recent value of 98.7 barns (2) Pomerance's value becomes 1.9 barns. The spread in these values was too great to be used in our work and large enough to warrant a redetermination of $\sigma_{Ce^{142}}$ by the activation method using improved techniques.

If naturally-occurring cerium were irradiated in a nuclear reactor the following first-order reactions would occur:

(1) $_{58}Ce^{136}$ (0.193% of natural cerium)

(n, γ)

$$_{58}Ce^{137} \xrightarrow[36\text{ hr.}]{\text{E.C.}} {}_{57}La^{137} \xrightarrow[>400\text{ yr.}]{\text{E.C.}} {}_{56}Ba^{137}\ \text{(stable)}$$

[1]*Manuscript received March 23, 1956.*

Contribution from the Radiochemistry Laboratory, Department of Chemistry, McGill University, Montreal, with financial assistance from the National Research Council of Canada and the Atomic Energy Control Board.

[2]*Holder of a Shawinigan Chemical Scholarship (1952–53), a National Research Council Studentship (1953–54), and a Province of Quebec Bursary (1954–55). Present address: Atomic Energy of Canada Limited, Chalk River, Ont.*

*NOTE ADDED IN PROOF.—*Dr. Pomerance has been kind enough to inform us that his sample of enriched Ce^{142} showed a detectable amount (<1500 p.p.m.) of cadmium. His calculations show that, if the sample contained exactly 1500 p.p.m. of cadmium, his value for the cross section of Ce^{142} would be 1.0 ± 0.2 barns.

(2) $_{58}Ce^{138}$ (0.250% of natural cerium)

(n, γ)

$_{58}Ce^{139} \xrightarrow[140\text{ d.}]{\text{E.C.}} {}_{57}La^{139}$ (stable)

(3) $_{58}Ce^{140}$ (88.47% of natural cerium)

(n, γ)

$_{58}Ce^{141} \xrightarrow[32\text{ d.}]{\beta^-} {}_{59}Pr^{141}$ (stable)

(4) $_{58}Ce^{142}$ (11.07% of natural cerium)

(n, γ)

$_{58}Ce^{143} \xrightarrow[33\text{ hr.}]{\beta^-} {}_{59}Pr^{143} \xrightarrow[13.5\text{ d.}]{\beta^-} Nd^{143}$ (stable)

Owing to the multiplicity of radioactive cerium isotopes formed it is obviously very difficult to measure Ce^{143} directly. However it is possible to determine the activity of the Ce^{143} produced by separating and measuring its 13.5 day Pr^{143} daughter.

The differential equations involved are well known and it can be shown that the activity of Pr^{143} at any time t_1 after the irradiation is given by

$$[1] \qquad \lambda_2 C_{t_1} = \frac{\lambda_1\lambda_2}{\lambda_1-\lambda_2} B_T(e^{-\lambda_2 t_1} - e^{-\lambda_1 t_1}) + C_T\lambda_2 e^{-\lambda_2 t_1},$$

where B_T and C_T are the numbers of atoms of Ce^{143} and Pr^{143} respectively formed after a time of irradiation T and

$$[2] \qquad B_T = \frac{nvA\sigma_0}{\lambda_1}(1-e^{-\lambda_1 T})$$

and

$$[3] \qquad C_T = \frac{nvA\sigma_0}{\lambda_2}(1-e^{-\lambda_2 T})\frac{-nvA\sigma_0}{\lambda_1-\lambda_2}(e^{-\lambda_2 T} - e^{-\lambda_1 T}).$$

A is the number of atoms of Ce^{142} present during the irradiation in a neutron flux of nv neutrons/cm.^{2}/sec. and is assumed to be constant. σ_0, σ_1 and λ_1, λ_2 are cross sections and disintegration constants respectively, the subscripts 0, 1, 2 referring to Ce^{142}, Ce^{143}, and Pr^{143} respectively.

EXPERIMENTAL

Samples of spectroscopically pure cerium oxide were sealed into small quartz ampoules and irradiated in a position in the NRX Chalk River heavy water reactor where the neutron spectrum was predominantly thermal. With each sample was enclosed a piece of fine weighed cobalt wire which was used as a flux monitor.

After irradiation the cerium oxide was dissolved in boiling concentrated sulphuric acid to which a few drops of 30% hydrogen peroxide was added. Ten milligrams of praseodymium carrier was added and the rare earths precipitated by the cautious addition of ammonium hydroxide. The precipi-

tate was dissolved in nitric acid and cerium separated by oxidation with solid potassium bromate and precipitation as ceric iodate. The supernatant, containing the praseodymium, was neutralized by cautious addition of concentrated sodium hydroxide which precipitated praseodymium hydroxide. The precipitate was dissolved, cerium carrier was added, and the entire cycle of cerium removal and praseodymium precipitation was repeated six or seven times. The final precipitate of praseodymium hydroxide was dissolved in 1 ml. of 6 *N* hydrochloric acid and made up to standard volume. The absolute disintegration rate was determined by the use of a 4π counter as described by Pate and Yaffe (6).

The cobalt wire monitor was dissolved in 1 ml. aqua regia, the solution made to standard volume, and its activity determined in a similar manner.

The chemical yield of the praseodymium was determined by precipitating it from the master solution as praseodymium oxalate and drying it to $Pr_2(C_2O_4)_3 \cdot 9H_2O$.

RESULTS AND DISCUSSION

The Pr^{143} was identified by its half-life. A typical decay curve is shown in Fig. 1. Values obtained from this and other samples which were followed

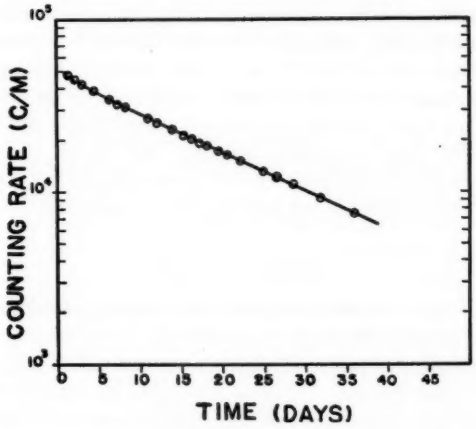

FIG. 1. Decay curve of Pr^{143}.

for about three half-lives ranged between 13.5 and 13.7 days. As can be seen from the previous discussion the only activity which could interfere from the cerium irradiation would be La^{137} which would not be separated from the praseodymium by the chemical procedures employed. A simple calculation shows that, owing to its long half-life, the La^{137} contribution to the activity will be negligible. Freedom from other rare earth radioactive impurities is attested to by the fact that the half-life obtained is very close to the currently accepted value (3, 4, 9, 10).

Table I shows the flux values obtained from the cobalt monitor. $\sigma_{Co^{59}}$ was taken as 36.3 (13) after correction for the more recent value of $\sigma_{Au^{197}} = 98.7$ barns (2).

TABLE I

NEUTRON FLUX VALUES OBTAINED FROM COBALT MONITOR

Sample No.	Co^{59} atoms, $\times 10^{-19}$	Time, sec. $\times 10^{-4}$	Co^{60}, dis./sec. $\times 10^{-5}$	Calc. flux, n./cm.^{2}/sec. $\times 10^{-12}$
1	1.17	3.70	6.1	9.24
2	1.17	7.19	3.6	2.80

In Table II are shown the values of the cross section of Ce^{142} as calculated by means of equation [1].

TABLE II

VALUES OF CROSS SECTION OF Ce^{142} OBTAINED

Sample No.	A, Ce^{143} atoms $\times 10^{-18}$	t_1, sec. $\times 10^{-5}$	$\lambda_3 C_{t_1}$, dis./sec. $\times 10^{-5}$	σ_0, barns
1*a*	8.24	1.214	8.44	0.945
1*b*	8.24	1.214	8.46	0.948
1*c*	8.24	1.214	8.44	0.945
2*a*	9.31	2.760	7.98	0.965
2*b*	9.31	2.760	7.94	0.961
2*c*	9.31	2.760	7.98	0.965

An average value of 0.95 ± 0.05 barns was obtained, in excellent agreement with the value of Katcoff *et al.* (5). The error quoted is five times the standard deviation obtained and certainly takes into account systematic errors. It is difficult to understand the higher value obtained by Pomerance.* Two possibilities occur to us. First, the cerium sample used by him might have contained small amounts of high neutron-absorbing rare earth impurities. Secondly Ce^{143} may form a short-lived isomer. The cross section for its formation would not be detected by our technique but would be measured by the pile oscillator method.

ACKNOWLEDGMENTS

One of us (L. P. R.) wishes to express his gratitude to Shawinigan Chemicals Limited, the National Research Council of Canada, and the Province of Quebec for financial assistance during the course of this and allied researches.

REFERENCES

1. BOTHE, W. Z. Naturforsch. 1: 179. 1946.
2. CARTER, R. S., PALEVSKY, H., MYERS, V. W., and HUGHES, D. J. Phys. Rev. 92: 716. 1953.
3. FELDMAN, L., LIDOFSKY, L., MACKLIN, P., and WU, C. S. Phys. Rev. 76: 1888. 1949.
4. INGHRAM, M. G. and HESS, D. C., JR. Phys. Rev. 74: 627. 1948.
5. KATCOFF, S., LEARY, J. A., WALSH, K. A., ELMER, R. A., GOLDSMITH, S. S., HALL, L. D., NEWBURY, E. G., POVELITES, J. J., and WADDELL, J. S. J. Chem. Phys. 17: 421. 1949.
6. PATE, B. D. and YAFFE, L. Can. J. Chem. 33: 15, 610. 1955.
7. POMERANCE, H. Phys. Rev. 83: 641. 1951.
8. POMERANCE, H. Phys. Rev. 88: 412. 1952.
9. POOL, M. L. and KRISBERG, N. L. Phys. Rev. 73: 1035. 1948.
10. POOL, M. L. and KURBATOV, J. D. Phys. Rev. 63: 463. 1943.
11. ROY, L. P. and YAFFE, L. Can. J. Chem. 34: 238. 1956.
12. SEREN, L., FRIEDLANDER, H. N., and TURKEL, S. H. Phys. Rev. 72: 888. 1947.
13. YAFFE, L., HAWKINGS, R. C., MERRITT, W. F., and CRAVEN, J. H. Phys. Rev. 82: 553. 1951.

*See footnote to Abstract.

GRAFT COPOLYMERS OF STYRENE AND METHYL METHACRYLATE

PART II: VISCOSITY BEHAVIOR[1,2]

By M. H. Jones

ABSTRACT

A study of the viscosity behavior of the graft copolymers described in Part I has been made with dilute solutions in benzene at 25°C. Although the slope constants of the Huggins equation increase with the frequency of branching when measurements are made in a capillary viscometer under 'free fall' conditions, this is shown to be attributable to the dependence of viscosity on shear gradient. At a constant shear rate, the Huggins k' values approximate to those of linear polymers. It is suggested that the marked increase in viscosity observed with decreasing shear rate for the graft copolymers is due to molecular entanglement.

INTRODUCTION

Although the viscosity behavior of dilute polymer solutions has been studied actively for a number of years, most of the experimental evidence is concerned with polymers which are essentially linear in structure and little is known of the influence of branching.

Through a modification of the Stokes equation to take into consideration interactions between solvent and polymer molecules, Huggins (7) has derived the expression

$$\eta_{sp}/C = [\eta]+k'[\eta]^2C+k''[\eta]^3C^2+ \ldots$$

relating the reduced viscosity to the concentration of the solution. For sufficiently dilute solutions, only the first two terms of the series are significant. The interaction coefficient, k', is considered to be a constant for a given solvent–polymer system and, in general, is independent of molecular weight. This is similar to the empirical equation of Schulz and Blaschke (12). Increases in the slope constant for high molecular weight fractions from polymerization carried to high conversions, where the rate of transfer to polymer resulting in the formation of branched molecules is more significant, have been attributed to branching (4, 5, 11). A similar explanation has been given to observed increases in k' for soluble fractions of styrene – divinyl benzene copolymers (10, 17) where branching occurs through the unreacted double bonds of the diolefinic units in the polymer chain. Theoretical calculations (14) have supported this contention. However, the results of Thurmond and Zimm (16) show no detectable difference in the slope constant of the Huggins equation between fractions of a styrene – divinyl benzene copolymer and a polystyrene prepared under identical conditions. Decreases in the exponent of the Houwink viscosity – molecular weight relationship for high conversion polybutadienes (8) and soluble crosslinked polystyrenes (8, 16) have also been attributed to branching.

[1]*Manuscript received March 21, 1956.*
Contribution from the Department of Chemistry, Ontario Research Foundation, Toronto 5, Ontario.
[2]*Presented in part at the 6th Canadian High Polymer Forum held at St. Catharines, Ontario, April 14–15, 1956.*

The series of well-characterized branched molecules described in Part I provide a means of studying some of these effects and observing their change with progressive increments of branching.

EXPERIMENTAL

Materials

Samples of homopolymers and random copolymers of styrene and methyl methacrylate were prepared by bulk polymerization using α,α'-azo-bis-isobutyronitrile as initiator. The preparative conditions are recorded in Table I. Polymerizations were limited to small conversions at comparatively

TABLE I

LINEAR POLYMERS AND COPOLYMERS OF STYRENE AND METHYL METHACRYLATE

Polymer	Poly^n Temp. (°C.)	[Initiator] (gm. l.$^{-1}$)	Mole fraction MMA	% Poly^n	% PMMA in copolymer
PS 1	70			12.5	
PS 2	45	0.98		4.8	
PMMA 1	60	1.87		9.3	
PMMA 2	60	0.28		7.4	
Cop 1	60	0.30	0.811	7.1	71
Cop 2	60	0.30	0.682	6.0	60
Cop 3	60	0.30	0.508	5.2	50
Cop 4	60	0.093	0.682	5.2	58

low temperatures; these conditions are such that branching may be considered negligible. The compositions of the copolymers were determined by infrared analysis. The method of synthesis of the graft copolymers has been described in detail in Part I.

Viscosity Measurements

Viscosity measurements were made in benzene solution at 25.0°C. ±0.005°C. using Ubbelohde and Ostwald type viscometers. A large bulb was incorporated in the Ubbelohde viscometer to permit dilution of the solution *in situ*. The Ostwald viscometer was similar to that used by Flory and his co-workers (6) and was designed to study the influence of shear rate on viscosity in the range encountered with the Ubbelohde viscometer. Kinetic energy corrections were calculated from the dimensions of the viscometers using the Wilberforce modification of the Poiseuille equation (1), i.e.

$$\eta = \frac{\pi r^4 hg\rho t}{8lv} - \frac{m\rho v}{8\pi lt}$$

or

$$\eta = A\rho t - \frac{B\rho}{t}.$$

A value of 1.1 (1) was chosen for the constant m and the corrections were applied to the flow times. Hence the corrected flow time

$$t^* = t - \frac{B}{At}.$$

For the Ubbelohde and Ostwald instruments, the maximum kinetic energy corrections for the solvent were 0.9% and 0.5% respectively. As these are small, the arbitrary choice of a value for the empirical constant, m, was considered justifiable. Flow times were determined with a stop watch graduated in 1/10 sec. intervals and the reproducibility of successive readings was better than ±0.1%. The dimensions of the two viscometers are given in Table II together with the corrected flow times for the solvent.

TABLE II

VISCOMETER CONSTANTS

Viscometer	v (cc.)	r (cm.)	l (cm.)	t^* (sec.)
Ubbelohde	2.20	0.0230	13.3	115.1
Ostwald: Upper bulb	2.37	0.0217	19.6	145.9†
Lower bulb	2.74	0.0217	19.6	222.3†

†*For solvent volume of 10.01 cc.*

Solution viscosities at different shear rates for a given polymer concentration were obtained by adding known volumes of the solution to the Ostwald viscometer. The maximum rates of shear, G, were derived from the expression

$$G = rhg\rho/2l\eta\eta_r$$

where η is the viscosity of the solvent and η_r the relative viscosity of the solution. The hydrostatic head, h, of the liquid column in the viscometer was taken as the arithmetic mean of the maximum and minimum heights. Although this differs from the true mean as calculated by a formula of the Meissner type (1), the maximum difference for the present viscometer was less than 1.5%.

Polymer solutions were prepared by shaking known weights of polymer with the solvent for 18 hr. to ensure complete solution. The solutions were filtered through sintered glass disks of medium porosity before transference to the viscometer. The usual precautions were taken to avoid contamination of the viscometers and solutions with dust particles. In general, reduced viscosities were determined at four or more concentrations in the range 0.05–0.40 gm./100 cc. and the parameters of the Huggins equation obtained by the least squares method of calculation.

RESULTS AND DISCUSSION

The parameters of the Huggins equation for the series of graft copolymers determined with the Ubbelohde viscometer under 'free fall' conditions are given in Table III. Similar data on the linear polystyrenes, polymethyl methacrylates, and random copolymers are included for comparison. Usually duplicate determinations were made and the slope constants agreed within 0.02 unit and the intrinsic viscosities within 1%.

The k' values for the linear polymers are constant at approximately 0.35. Even with small amounts of branching, i.e. one to two branches per molecule

TABLE III

HUGGINS PARAMETERS FOR LINEAR AND GRAFT COPOLYMERS—VARIABLE SHEAR GRADIENT

Polymer	$\bar{P}_n$ (backbone)	$\bar{P}_n$ (branches)	Average no. branches per molecule	$[\eta]_{25°C.}$ (dl. gm.$^{-1}$)	k'
A1	2500	4500	1.2	3.26	0.40_5
A2	2500	1500	1.5	1.85	0.38_5
D1	3100	2300	2.6	3.10	0.54_9
D2	3100	1700	3.4	3.10	0.58_7
D3	3100	1600	3.0	3.17	0.61_3
D4	3100	1300	3.3	2.62	0.56_8
E1	3800	1500	1.8	2.99	0.43_1
E2	3800	1500	3.2	3.43	0.54_2
E3	3800	1800	3.9	3.66	0.63_4
E4	3800	1900	5.9	3.99	0.78_0
PS 1				3.16	0.33_5
PS 2				1.73	0.35_8
PMMA 1				1.84	0.35_5
PMMA 2				2.66	0.32_4
Cop 1				1.84	0.35_3
Cop 2				1.66	0.36_6
Cop 3				1.57	0.34_9
Cop 4				2.53	0.34_2

(Polymers A1, A2, and E1) there appears to be a significant increase in k' and, with more highly branched structures, the effect is pronounced. The progressive increase in slope constant with frequency of branching is most clearly demonstrated in the series E1–E4 where the variation in chain length is small compared to the increase in the number of branches. The reduced viscosity – concentration curves for these polymers are illustrated in Fig. 1. The broken lines indicate the slopes that would be obtained at the pertinent intrinsic viscosities for a k' value of 0.35. Although these results were obtained with the same viscometer and consequently at a constant shear stress, the reduced viscosities at each concentration during dilution are measured at progressively increasing shear gradients since these are an inverse function of the solution viscosity. In general, the shear gradients for a viscosity plot varied in the range 500–1500 sec.$^{-1}$.

Studies of the influence of molecular weight and solvent on the shear dependence of viscosity for neutral polymers have been reported by several authors (3, 6, 9, 13). Their results indicate that shear effects may just become significant at molecular weights of the same order as those of the present series of polymers and an investigation of the influence of shear rate was made to determine the magnitude of the effect. Although the range of shear gradients covered was small, a considerable difference in behavior was observed between the linear and branched molecules. Solutions of the polystyrene, polymethyl methacrylate, and the random copolymers, which were believed to have essentially no branching, behaved as Newtonian liquids (Figs. 2 and 3). The graft copolymers showed a marked dependence of viscosity

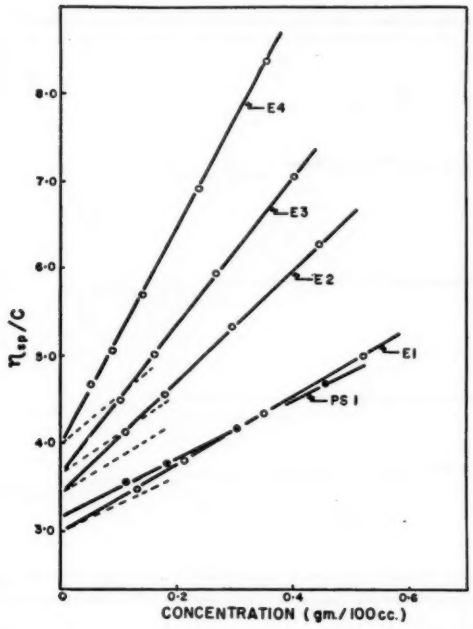

FIG. 1. Reduced viscosity versus concentration plots for graft copolymers E1–E4 with Ubbelohde viscometer.

on shear rate and this was clearly evident for samples having viscosities, and presumably molecular weights, similar to the linear polymers. Reduced viscosity – shear plots for the graft copolymers with the greatest difference in intrinsic viscosity are shown in Figs. 4 and 5. The curvature of the plots precludes the usual practice of extrapolating to zero shear gradient to obtain reduced viscosities that are independent of shear effects, and values for each concentration were taken from the curves at an arbitrary shear rate of 500 sec.$^{-1}$. Huggins plots of these values for two of the graft copolymers (E3 and E4) are illustrated in Fig. 6 together with the curves obtained under 'free fall' conditions with the same viscometer. For the polymer E3 the curves have been displaced downwards 0.5 unit in the ordinate scale for clarity. The values of the Huggins parameters for these two polymers and for a linear polystyrene and polymethyl methacrylate are recorded in Table IV. The significant result is that the slope constants for the graft copolymers, when measured at a constant shear rate, decrease to approximately the value obtained for polymers having a linear structure. This, again, emphasizes the necessity of determining shear dependence in capillary viscometry of high polymer solutions and demonstrates the fact that non-Newtonian behavior may appear as a unique viscosity–concentration effect in a relationship of the Huggins type when results are obtained under 'free fall' conditions. It is obvious that the increases in slope constant for the graft copolymers obtained with the

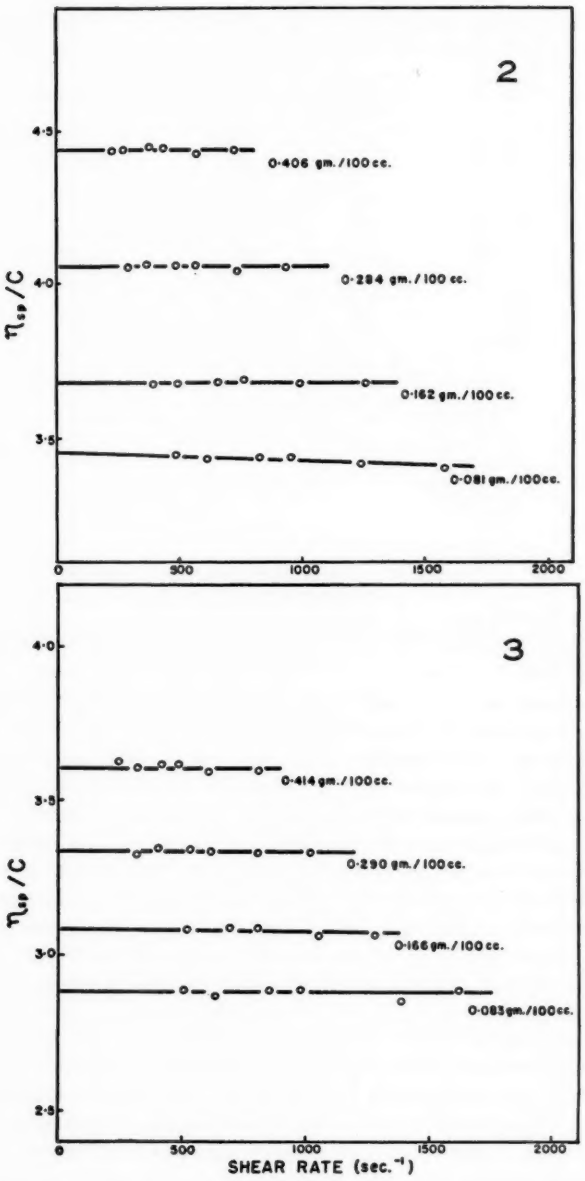

FIG. 2. Reduced viscosity versus shear rate plots for various concentrations of polymer PS 1.

FIG. 3. Reduced viscosity versus shear rate plots for various concentrations of polymer PMMA 2.

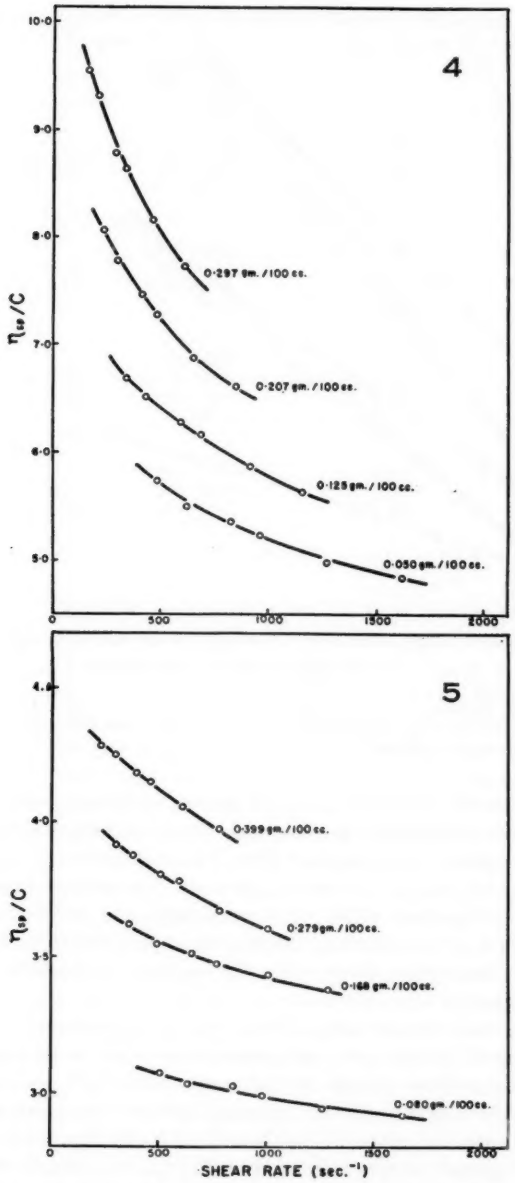

FIG. 4. Reduced viscosity versus shear rate plots for various concentrations of polymer E4.
FIG. 5. Reduced viscosity versus shear rate plots for various concentrations of polymer D4.

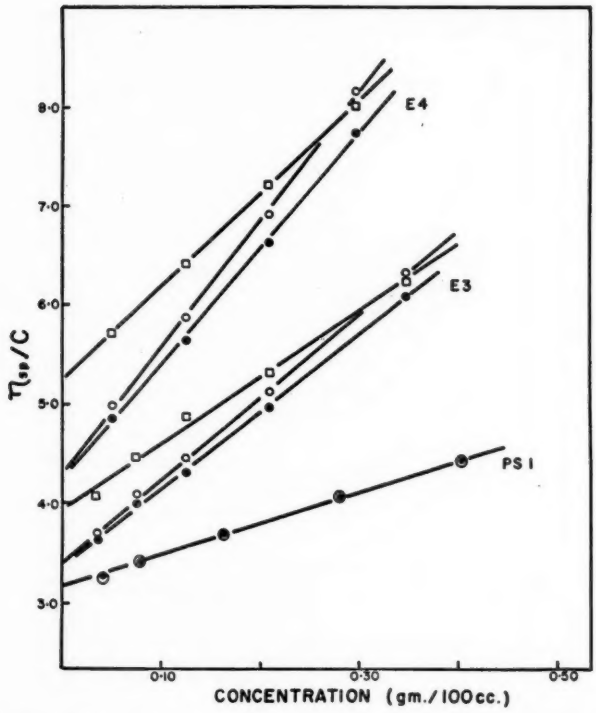

FIG. 6. Reduced viscosity versus concentration plots for graft copolymers E3 and E4 with Ostwald viscometer. Ostwald upper bulb—'free fall', -●-; Ostwald lower bulb—'free fall', -○-; Ostwald, constant $G = 500$ sec.$^{-1}$, -□-.

Ubbelohde viscometer (Table II) are fortuitous. Although the data on the shear dependence of viscosity are limited, slope constants have also been determined at constant shear rates of 250, 750, and 1000 sec.$^{-1}$ where errors due to extrapolation should not be too serious. The values obtained for the polymer E3 are, respectively 0.37, 0.34, and 0.34, and for the polymer E4, 0.39, 0.33, and 0.32. Although there appears to be a slight trend to increasing values of k' with decrease in shear rate, the variation is probably within the experimental accuracy.

It is to be expected that deviations from Newtonian behavior will be determined by the ease of deformation and orientation of the molecules in solution and, consequently, will be related to the molecular weight and 'goodness' of the solvent since these factors govern the extension and softness of the expanded coil. However, it must be assumed that branched molecules, with their greater density of packing, will be less subject to deformation under flow than linear molecules but the observations show that the latter are independent of shear rate. Probably the explanation lies in the greater probability of molecular entanglement with the branched polymers because of the increased number of

TABLE IV

INFLUENCE OF SHEAR RATE ON HUGGINS PARAMETERS FOR LINEAR AND GRAFT COPOLYMERS

Viscometer	Shear rate (sec.$^{-1}$)	$[\eta]_{25°C.}$	k'
Polymer E3			
Ubbelohde	520–1380	3.66	0.63_4
Ostwald: Upper bulb	610–1750	3.84	0.53_2
Lower bulb	470–1380	3.89	0.55_5
	500	4.42	0.35_0
Polymer E4			
Ubbelohde	510–1630	3.99	0.78_0
Ostwald: Upper bulb	610–1620	4.21	0.66_0
Lower bulb	460–1270	4.28	0.70_3
	500	5.25	0.34_0
Polymer PS 1			
Ubbelohde	760–1440	3.16	0.33_5
Ostwald: Upper bulb	720–1780	3.13	0.33_2
Lower bulb	570–1390	3.16	0.31_2
	500	3.20	0.29_3
Polymer PMMA 2			
Ubbelohde	810–1550	2.66	0.32_4
Ostwald: Upper bulb	810–1620	2.71	0.28_8
Lower bulb	640–1280	2.68	0.31_2
	500	2.71	0.29_2

free chain ends. It must be remembered that for polymers in the present molecular weight range, the volume occupied by a single molecule is such that the concentrations employed for viscosity measurements are similar to the requirement for a system of close-packed spheres. From light scattering data (2), it has been estimated that the diameter of the sphere occupied by a polystyrene molecule of molecular weight 10^6 in benzene is approximately 1000 Å and this condition would be equivalent to a concentration of 0.24 gm./100 cc. Thus, for most of the solutions used, the molecules are in close proximity providing a greater concentration of aggregates (15). A combination of factors, such as orientation and deformation of loosely connected coils, may then contribute to the shear dependence.

For the Ubbelohde viscometer and the upper bulb of the Ostwald viscometer, with a solution volume of 10.01 cc., the constant factor in the shear rate expression, i.e. $rhg\rho/2l\eta$, differs by only 0.5%. Thus, the slope constants determined at 'free fall' with these two systems should be practically identical. The fact that the values obtained for the graft copolymers with the Ostwald instrument are lower may be attributable to a greater degree of molecular disentanglement. The differences for the linear polymers are within the experimental accuracy. For the Ubbelohde determinations, dilutions were made in the viscometer and the solutions agitated intermittently for short periods (10–15 min.), whereas for the Ostwald measurements all solutions were shaken for 18 hr. before use. Prolonged agitation may be necessary to establish the aggregation equilibrium between single and double molecules for a given concentration. It was noted that the differences between reduced viscosities

for the two viscometers at similar concentrations and shear rates increased with decreasing concentration.

In conclusion, it may be said that no detectable increase in the slope constant of the Huggins equation was found for a series of polymers with known amounts of branching when measurements were made at a constant shear rate. Although this observation is contrary to theoretical predictions (14), it is recognized that the concentrations employed are such that polymer–polymer interactions will be of importance. Statistical treatments of the hydrodynamic behavior of long chain molecules are usually applied to the idealized condition that the particles are well separated in the solvent. The important difference in behavior between branched and linear molecules appears to be their relative dependence of viscosity on the shear gradient.

ACKNOWLEDGMENTS

The author is indebted to Mr. S. Wasniewski and Mr. K. Parker for technical assistance.

REFERENCES

1. BARR, G. A monograph of viscometry. Oxford University Press, London. 1931.
2. BOUNDY, R. H. and BOYER, R. F. Styrene. A.C.S. Monograph No. 115. 1952. p. 419.
3. CONRAD, C. M., TRIPP, V. W., and MARES, T. J. Phys. & Colloid Chem. 55: 1474. 1951.
4. CRAGG, L. H. and BROWN, A. T. Can. J. Chem. 30: 1033. 1952.
5. CRAGG, L. H. and FERN, G. R. H. J. Polymer Sci. 10: 185. 1953.
6. FOX, T. G., FOX, J. C., and FLORY, P. J. J. Am. Chem. Soc. 73: 1901. 1951.
7. HUGGINS, M. L. J. Am. Chem. Soc. 64: 2716. 1942.
8. JOHNSON, B. L. and WOLFANGEL, R. D. Ind. Eng. Chem. 44: 752. 1952.
9. KRIGBAUM, W. R. and FLORY, P. J. J. Polymer Sci. 11: 37. 1953.
10. MANSON, J. A. and CRAGG, L. H. Can. J. Chem. 30: 482. 1952.
11. MENCIK, Z. and LANIKOVA, J. Makromol. Chem. 14: 118. 1954.
12. SCHULZ, G. V. and BLASCHKE, F. J. prakt. Chem. 158: 130. 1940.
13. SHARMAN, L. J., SONES, R. H., and CRAGG, L. H. J. Appl. Phys. 24: 703. 1953.
14. SIMHA, R. J. Natl. Bur. Standards, 42: 409. 1949.
15. SIMHA, R. J. Colloid Sci. 5: 386. 1950.
16. THURMOND, C. D. and ZIMM, B. H. J. Polymer Sci. 8: 477. 1952.
17. WALKER, O. J. and WINKLER, C. A. Can. J. Research, B, 28: 298. 1950.

THE VIBRATIONAL SPECTRA OF ISOBUTANE AND ISOBUTANE-d_1[1]

By J. C. Evans[2] and H. J. Bernstein

ABSTRACT

The Raman spectra of liquid $(CH_3)_3CH$ and $(CH_3)_3CD$ were obtained photoelectrically and intensities and depolarization ratios measured. The infrared spectra of the corresponding gases were obtained from 3 to 35 μ. A vibrational assignment consistent with depolarization ratios and band contours has been made for the molecules on the basis of C_{3v} symmetry and their spectra correlated.

INTRODUCTION

The vibrational spectrum of isobutane has been the subject of many investigations (7) and several ambiguities remain with regard to vibrational assignments (7). Sheppard and Simpson (7) suggest that further experimental work is required to decide upon the frequency assignment of the deformation modes and the asymmetrical skeletal stretching mode. In order to clarify the situation with regard to this molecule the Raman spectra of liquid $HC(CH_3)_3$ and $DC(CH_3)_3$ have been obtained with depolarization ratios, and the infrared spectra of the vapors have also been examined. The infrared spectrum of the heavy isobutane has been reported previously (2) but no attempt at assignment was made.

EXPERIMENTAL

Isobutane was obtained from a commercial cylinder and the deuterium-substituted compound prepared by Dr. L. C. Leitch.

The Raman spectra of the liquids were obtained at -70°C. in a tube previously described (3) and depolarization ratios measured by comparing spectra obtained first with polaroid film wrapped with its axis parallel to the sample tube and then perpendicular to it. These ratios were corrected for the non-rectilinear irradiation set-up by the method of Rank and Kagarise (6). The mercury 4358 line was used to excite the Raman spectra, the Stokes lines of which are shown in Fig. 1. The photoelectric Raman spectrometer used (8) was operated under the following conditions: slits $\sim$10 cm.$^{-1}$, dynode voltage $=500$ v., with intermediate values of gain and response time. The current in the water-cooled mercury arcs was 17 amp.

The infrared spectra were obtained with a Perkin Elmer Model 112 double pass infrared spectrometer with LiF, NaCl, and CsBr optics. The spectra shown in Figs. 2 and 3 were obtained in a 10 cm. cell at the various pressures and slit widths indicated.

DISCUSSION

Before attempting an assignment for this molecule it is worth while mustering all the information provided by theory. Symmetry considerations limit the discussion of the point group symmetry to either C_3 or C_{3v}. Since steric hind-

[1]*Manuscript received April 9, 1956.*
Contribution from the Division of Pure Chemistry, National Research Council, Ottawa, Canada. Issued as N.R.C. No. 3994.
[2]*Postdoctorate Research Fellow 1953-55.*

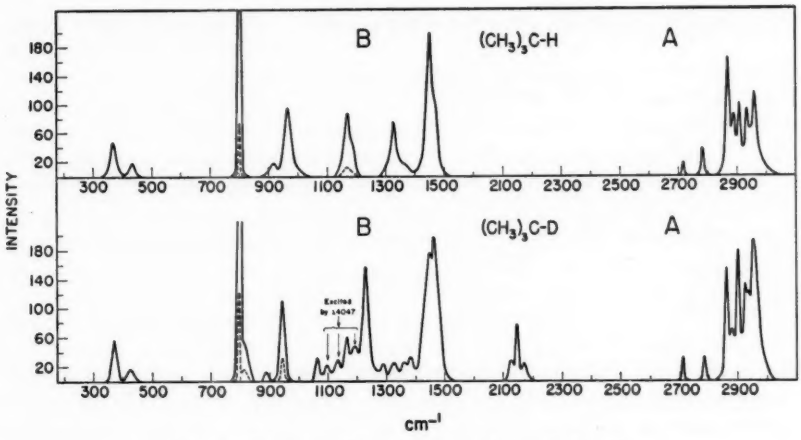

FIG. 1. Raman spectra of light and heavy isobutane.
A: slits 5 cm.$^{-1}$;
B: slits 6 cm.$^{-1}$,
—intensity scale 6× that for field A,
----intensity scale the same as for field A.

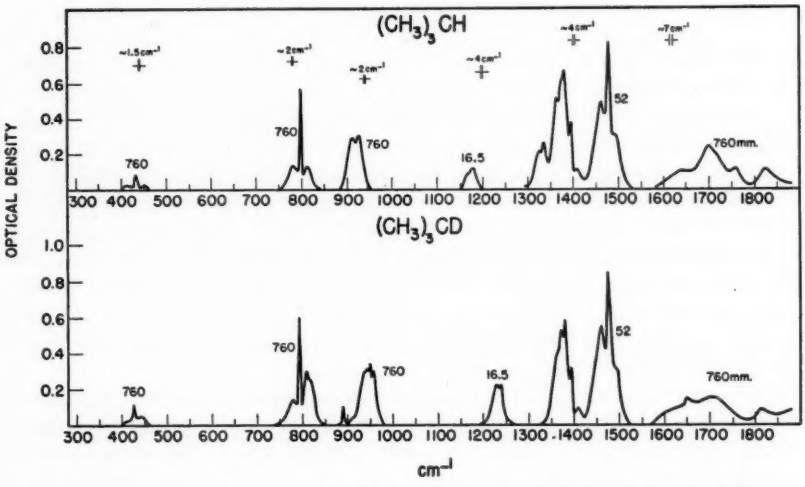

FIG. 2. Infrared spectra of gaseous light and heavy isobutane in the region 300–1800 cm.$^{-1}$.

rance probably rotates the CH_3 groups so that the planes of symmetry of the C_{3v} group are no longer present, one should actually consider isobutane to have the point group symmetry C_3 with the division of fundamentals into $12A+12E$ with all modes active in both Raman effect and infrared absorption. For all practical purposes however we shall consider the molecule to have the higher symmetry of C_{3v} to describe its vibrational spectrum, in accord with

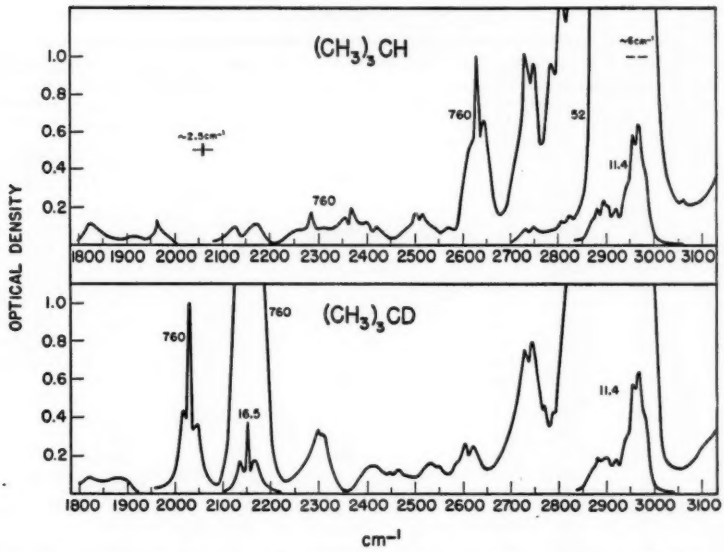

FIG. 3. Infrared spectra of gaseous light and heavy isobutane in the region 1800–3100 cm.$^{-1}$.

previous investigators (7), for which the fundamentals fall into the grouping $8A_1+4A_2+12E$. In this case the $4A_2$ type fundamentals are forbidden in both Raman effect and infrared absorption.

In order to understand the nature of the vibrational spectrum a little more clearly it simplifies matters to consider first the molecule in which the three H atoms of each CH_3 group are replaced by a single particle X. For this molecule then all bending vibrations involving X are external bending modes of the CH_3 group; the only internal mode for the CH_3 group in this molecule corresponds to the stretching vibration ν_{CX}. For the molecule $HC(CX)_3$ of point group C_{3v} there are $5A_1+1A_2+6E$ modes. It is readily seen that the distribution of the bending modes of the X group and, correspondingly, the CH_3 group is $1A_1+1A_2+2E$. In Table I the modes of vibration of isobutane have been classified according to the approximate description of internal and external modes of the CH_3 group and also in terms of other groups in the molecules. Since the internal modes of the CH_3 group are well known (7) and give rise to bands at ~3000 cm.$^{-1}$, 1450 cm.$^{-1}$, and 1350 cm.$^{-1}$, the observed spectrum will be simplified to the extent that the 10 active internal modes of the CH_3 group will appear in the spectrum at the three regions indicated. The remaining bands of the spectrum should belong to the three external bending modes of the CH_3 group and the six modes of the H—C(—C)(—C) group; the E type torsional mode being rarely observed and the A_2 type not allowed. From considerations of this kind we readily see that the isobutane molecule

TABLE I

Species	No.		CH_2 external	CH_3 internal
A_1	ν_1			ν_{CH} unsym.
	ν_2			ν_{CH} sym.
	ν_3	ν_{CH}		
	ν_4			δ_{CH_3} unsym.
	ν_5			δ_{CH_3} sym.
	ν_6		δ_{CCH_2}	
	ν_7	ν_{CC}		
	ν_8	δ_{CCC}		
E	ν_9			ν_{CH} unsym.
	ν_{10}			ν_{CH} unsym.
	ν_{11}			ν_{CH} sym.
	ν_{12}			δ_{CH_3} unsym.
	ν_{13}			δ_{CH_3} unsym.
	ν_{14}			δ_{CH_3} sym.
	ν_{15}	δ_{CH}		
	ν_{16}		δ_{CCH_2}	
	ν_{17}		δ_{CCH_2}	
	ν_{18}	ν_{CC}		
	ν_{19}	δ_{CCC}		
	ν_{20}		Torsion	
A_2	ν_{21}			ν_{CH} unsym.
	ν_{22}		δ_{CCH_2}	
	ν_{23}			δ_{CH_3} unsym.
	ν_{24}		Torsion	

which has 36 degrees of vibrational freedom would be expected to give an observed spectrum of only 12 bands. Further in the Raman spectrum the A_1 type will be polarized and the E type depolarized and in the infrared spectrum of the gas the A_1 type will be parallel with a PR separation* of about 32 cm.$^{-1}$ and a pronounced Q branch (1), whereas the E type bands are perpendicular with less pronounced Q branch (1) and varying spacing due to Coriolis interaction (4).

Finally the Teller–Redlich product rule for isotopic substitution (4) may be used as a final check on the assignment since the theoretical product rule ratios† for the A_1 species is 1.403 and for the E type, 1.382.

The observed Raman spectra and infrared spectra are tabulated and the bands assigned for isobutane and heavy isobutane in Tables II and III respectively, and in Table IV the spectra have been correlated.

It is apparent that the depolarization ratios and infrared band contours unambiguously determine the species of the skeletal deformation modes. The question as to which frequency is to be associated with the degenerate skeletal stretching mode cannot be answered unambiguously since strong coupling in the deuterated molecule makes it impossible to use the isotopic shift as criterion.

**The PR doublet separation was calculated from the formula of Gerhard and Dennison, Phys. Rev. 43: 197. 1933. The moments of inertia of isobutane were calculated assuming $\nu_{CH} = 1.09$, $\nu_{CC} = 1.54$, with all angles tetrahedral and gave*

$$I_A = I_B = 107 \times 10^{-40} \text{ c.g.s. units},$$
$$I_C = 183 \times 10^{-40} \text{ c.g.s. units}.$$

For deuterium-substituted isobutane

$$I_A = I_B \doteqdot 110 \times 10^{-40} \text{ c.g.s. units}.$$

†The moments of inertia required here were those given in footnote (*).

TABLE II

RAMAN SPECTRA OF LIQUID $HC(CH_3)_3$ AND $DC(CH_3)_3$

$\Delta\nu_a$	Isobutane			Assignment	Heavy isobutane		
	$\Delta\nu$	Int.[b]	ρ[c]		$\Delta\nu$	Int.[b]	ρ[c]
2960 (12D)	2958	116	D	ν_9, ν_{10}, ν_{11} (e)	2956	116	D
2936 (5p)	2933	94	0.27	ν_1, (a_1)	*2938	74	0.57
					2927	80	0.43
2908 (6p)	2907	103	0.18	ν_2 (a_1)	2903	108	0.25
2891 (2)	2889	87	0.38	$2\nu_{12}$ or $2\nu_{13}$ (A_1)	2882	42	0.25
2869 (12p)	2869	167	0.13	ν_3 (a_1)	2146	50	0.41
				$(\nu_4+\nu_5\ A_1)$	2864†	87	0.23
2778 (2p)	2783	38	0.58	$2\nu_{12}$ or $\nu_{12}+\nu_{13}$ (A_1)	2782	20	0.57
2714 (5p)	2716	19	0.10	$2\nu_{14}$ (A_1)	2712	19	0.13
	~1468	16	?	ν_4 (a_1)	1463	30	0.8
1452 (7b)D	1450	35	D	ν_{12}, ν_{13} (e)	1450	28	D
				ν_5 (a_1)	1380	6	D
1322 to (3b)D	~1373	3	?	ν_{14} (e)	1358	2	?
1355	1327	13	D	ν_{15} (e)	944	18	D
	1184	8	?	ν_6 (a_1)	1166	10	P
1172 (4b)D	1169	15	D	ν_{16} (e)	1229	25	D
965 (4b)D	966	16	D	ν_{17} (e)	1065	6	D
	917	3	D	ν_{18} (e)	813	~5	D?
795 (10)P	799	76	0.24	ν_7 (a_1)	796	70	0.17
437 (2)P	433	3	0.35	ν_8 (a_1)	426	3	0.23
371 (4b)D	367	8	D	ν_{19} (e)	370	9	D
1098 (½b?)	Not observed			ν_3 excited by λ4047			
					1326‡	4	
				?	1289	4	
				?	891	2	
				ν_1 excited by λ4047	1196	1	
				ν_2 excited by λ4047	1137	1	
				ν_3 excited by λ4047	1096	1	
				?	2168	~10	0.53
				?	2127	~12	0.49

[a] *Raman spectrum given in Kohlrausch, "Ramanspektren", Edwards Bros., Ann Arbor, Mich., 1945, p. 209.*

[b] *Peak heights are given on the same scale for both molecules.*

[c] *These depolarization ratios have been corrected for convergence error. P = polarized, D = depolarized = 0.87.*

* *Fermi resonance with $2\nu_4$ (A_1).*

† *$\nu_4+\nu_5$ (A_1) is a possible explanation for the intensity of 87 at 2864 cm.$^{-1}$ in the spectrum of $DC(CH_3)_3$: also incomplete deuteration. However since the largest change in intensity on deuterium substitution occurs here, i.e. from 167 in the light compound to 87 in the heavy, this band must be identified with the CH stretching mode where deuterium substitution is involved.*

‡ *Due to incomplete deuteration, i.e. $CH(CH_3)_3$ impurity.*

3000–1500 cm.$^{-1}$ Region

From the intensities in Table II it is readily seen that the band at 2869 cm.$^{-1}$ in the light compound has become very much weaker in the deuterated compound compared to the intensities of the other bands in this region. This enables one to identify this frequency with the stretching of the tertiary CH bond. In the infrared spectra the situation is not so simple and indeed it would be very difficult to make this assignment on the basis of infrared data alone. The assignments of the gas frequencies in the infrared are complicated by the extensive overlapping and therefore cannot be considered final. In Table III however this attempt has been made in accordance with expected contours. All observed bands in this region have been assigned except the very

TABLE III

INFRARED SPECTRA OF GASEOUS ISOBUTANE AND ISOBUTANE-d_1

$HC(CH_3)_3$				Assignment	$DC(CH_3)_3$			
ν, cm.$^{-1}$	Int.	Type	*PR* separation		ν, cm.$^{-1}$	Int.	Type	*PR* separation
2980					2980			
—	w.	(∥)	∼40	$2\nu_4$ (A_1)	—	w.	(∥)	∼40
∼2940 sh					∼2940			
2968					2968			
2956	s.	(⊥)		ν_9, ν_{10}, ν_{11} (e)	2956	s.	(⊥)	
—					—			
2920	s.	(∥)		ν_1 (a_1)	2920	s.	(∥)	
2904					2904			
∼2920					∼2920			
2904	s.	(∥)	∼26	ν_2 (a_1)	2904	s.	(∥)	∼26
2894					2894			
—					2166			
2880	m.	(∥)		ν_3 (a_1)	2152	s.	(∥)	32
2872 sh					2134			
∼2824 sh					—			
2806	w.	(∥)		$2\nu_{12}$ or $\nu_{12}+\nu_{13}$ (A_1)	2788	w.	(∥)	
2785					2768			
2748					2744			
2730	w.	(⊥)		$\nu_5+\nu_{13}$ (E)	2730	w.	(⊥)	
2645					—			
2629	w.	(∥)		$\nu_4+\nu_8$ (A_1)	2620	w.	(∥)	
∼2616					2604			
2570	v.w.			?	2584	v.w.		
				?	2550	v.w.		
				?	2535	v.w.		
2516	w.			$\nu_6+\nu_{14}$ (E)				
2502								
2480 sh	w.			?	2464	v.w.		
				?	2446	v.w.		
2422								
2402	v.w.	(⊥)		ν_5+unperturbed ν_{17} (E)?	2410	v.w.		
2371								
2357	w.	(∥)		$2\nu_8$ (A_1)				
—								
∼2310					∼2310			
2286	v.w.	(∥)		$\nu_6+\nu_7$ (A_1)	∼2298	v.w.	(∥)	
∼2265								
2170	v.w.			$\nu_5+\nu_7$ (A_1)				
2125				$\nu_7+\nu_{14}$ (E)				
					2046			
				2×unperturbed ν_{17} (A_1)?	2030	m.	(∥)	28
					2018			
1967	v.w.			$\nu_6+\nu_7$ (A_1)				
				$\nu_5+\nu_{12}$, $\nu_8+\nu_{12}$ (E)	1885	v.w.		
1910	v.w.			$\nu_4+\nu_8$ (A_1)				
1821	v.w.			$\nu_5+\nu_9$ (E)	∼1814	v.w.		
1760	v.w.			$\nu_5+\nu_{10}$ (E)				
1720	v.w.			$\nu_{14}+\nu_{19}$ (A_1)	1710	v.w.		
1698	v.w.			ν_8+unperturbed ν_{15} (E)				
1644	v.w.			ν_{19}+unperturbed ν_{15} (A_1)?	1650	v.w.		
				?	1620			
1493					∼1492			
1477	s.	(∥)	32	ν_4 (a_1)	1477	s.	(∥)	31
1461					1461			
1406					1410			
1394	m.	(∥)	∼35	ν_3 (a_1)	1394	s.	(∥)	∼37
∼1371					∼1373			
1379					1379			
1362	s.	(⊥)		ν_{14} (e)	1362	m.	(⊥)	
1334					956			
1325	m.	(⊥)		ν_{15} (e)	947	s.	(⊥)	

TABLE III (*concluded*)

INFRARED SPECTRA OF GASEOUS ISOBUTANE AND ISOBUTANE-d_1

$HC(CH_3)_3$				Assignment	$DC(CH_3)_3$			
ν, cm.$^{-1}$	Int.	Type	*PR* separation		ν, cm.$^{-1}$	Int.	Type	*PR* separation
1177	m.			ν_8 (a_1)				
~1166	m.			ν_{18} (e)	1238 1228	s.	(⊥)	
				$\nu_{14}-\nu_8$ (E)	942 935 sh	m.	(⊥)	
925 912	s.	(⊥)		ν_{13} (e)	817 808	m.	(⊥)	
				?	~ 907 890	w.	?	
					—			
811 797 781	s.	(∥)	30	ν_7 (a_1)	~ 810 793 779	s.	(∥)	31
~ 445 426 ~ 412	m.	(∥)	~33	ν_6 (a_1)	448 432 ~ 413	m.	(∥)	~35

TABLE IV

VIBRATIONAL ASSIGNMENTS

		$HC(CH_3)_3$		$DC(CH_3)_3$		Product rule ratios	
		Raman liquid	Infrared gas	Raman liquid	Infrared gas	Theor.	Obs. (Raman)
A_1	ν_1	2933	2920	2927	2920	1.40	1.39
	ν_2	2907	2904	2903	2904		
	ν_3	2869	2880	2146	2152		
	ν_4	1468	1477	1463	1477		
	ν_5	1373	1394	1380	1390		
	ν_6	1184	1177	1166			
	ν_7	799	797	796	793		
	ν_8	433	426	426	432		
E	ν_9	2958	2962	2956	2962	1.38	1.37$_5$
	ν_{10}	2958	2962	2956	2962		
	ν_{11}	2958	2962	2956	2962		
	ν_{12}	1450	~1475	1450	~1475		
	ν_{13}	1450	~1475	1450	~1475		
	ν_{14}	~1373	1371	1350	1367		
	ν_{15}	1327	1330	944	952		
	ν_{16}	1169[a]	1166	1229	1233		
	ν_{17}	966[a]		1065	—		
	ν_{18}	917[a]	918	813	812		
	ν_{19}	367	—	370	—		

[a] *Assignment of K. S. Pitzer and J. E. Kilpatrick, Chem. Revs. 39: 435. 1946.*

weak features at 1620, 2446, 2464, 2535, 2550, and 2584 cm.$^{-1}$ in the infrared spectrum of $DC(CH_3)_3$, and the very weak band at 2570 in the infrared spectrum of $HC(CH_3)_3$. In the Raman spectrum of $DC(CH_3)_3$ the bands at 2127 and 2168 cm.$^{-1}$ are difficult to assign on the basis of the observed fundamentals.

Region Below 1500 cm.$^{-1}$

In this region there is little difficulty in assigning the bands between 1480 and 1300 cm.$^{-1}$ but comparison of the spectra of the light and heavy molecules between 1300 and 800 cm.$^{-1}$ shows very little resemblance to what one would expect for this particular deuterium substitution. In Fig. 1 for example the strong band at 1169 in the light compound seems to have been shifted to higher wave number on deuterium substitution whereas the band at 966 cm.$^{-1}$ although shifted in the expected direction to lower wave number has moved too much if the shift in ν_7 is a criterion. In Fig. 2 the anomalous isotopic shifts are even more pronounced in the bands at ~1180 cm.$^{-1}$ and 918 cm.$^{-1}$. There can be no question that there is strong interaction or coupling between these vibrational modes.

One possible set of interactions to account for the observed spectrum is the following. If the bands at 1169 and 1320 cm.$^{-1}$ in the light compound are coupled, the unperturbed position of 1169 may be in the region to give the band at 1229 cm.$^{-1}$ in the deuterated compound. The unperturbed position of the CH deformation mode at 1327 cm.$^{-1}$ would fall perhaps to ~900 cm.$^{-1}$ upon deuterium substitution. This band would be strongly coupled with the unperturbed band at 917 cm.$^{-1}$ (which should be relatively undisplaced in the deuterium compound), to give rise to the bands at 813 and 944 cm.$^{-1}$. Since all bands are strongly coupled in the light compound the unperturbed position of 966 cm.$^{-1}$ may give rise to the band observed at 1065 cm.$^{-1}$ in the heavy compound. The band observed at 1166 cm.$^{-1}$ in the heavy compound is the polarized band arising from the polarized band at 1184 cm.$^{-1}$ in the light compound; this band does not participate in the coupling because it is of different symmetry species from the others. If this coupling system is sensible the ratios to be taken in calculating the product rule are

$$\frac{917}{813} \times \frac{966}{1065} \times \frac{1169}{1229} \times \frac{1327}{944}.$$

Rigorously the product of the ratios of the frequencies of the unperturbed band should be taken but since the interaction displaces bands in pairs by equal amounts in opposite directions and since these displacements are small compared to the band positions the ratios of the observed frequencies might be expected to be very nearly the same as those for the unperturbed values.

Since the change in frequency of all modes other than ν_{15} is expected to be negligible on deuterium substitution the observed product rule ratio will be given by the product of the ratios of the frequencies of the coupled bands. This ratio is calculated to be 1.37_0 which is consistent with the theoretical value of 1.38 given above for the E type modes. It is apparent that assignment of one of 917, 966, and 1169 cm.$^{-1}$ to the degenerate skeletal mode is not forthcoming from the present data; however if the suggested coupling scheme is indicative of the true state of affairs the mode at 1169 cm.$^{-1}$ which has an unperturbed frequency in the twelve hundreds is not a likely candidate for this assignment.

The observed infrared spectrum in the region below 1500 cm.$^{-1}$ has been assigned except for the weak band at 890 cm.$^{-1}$ in $CD(CH_3)_3$ whereas in the Raman spectrum of $DC(CH_3)_3$ the corresponding band at 891 cm.$^{-1}$ and the bands at 1289 cm.$^{-1}$ remain unexplained. The assignment is essentially the same as that of Pitzer and Kilpatrick (5) differing in the following respects:

(i) The A_1 wag of the CH_3 group ν_6 is given here as the Raman band at 1184 cm.$^{-1}$ in preference to the band at 1098 cm.$^{-1}$ which we did not observe in the Raman spectrum. The latter band is probably ν_3 excited by λ4047.

(ii) We have assigned the CH stretching mode frequencies which were all taken as 2950 cm.$^{-1}$ by Pitzer and Kilpatrick for the purpose of thermodynamic calculations.

The present assignment will not alter materially the results of the thermodynamic calculations (5) since the uncertainty introduced in assigning the A_2 wag (ν_{22}) is certainly as large as the present change in vibrational frequencies.

REFERENCES

1. Badger, R. M. and Zumwalt, L. R. J. Chem. Phys. 6: 711. 1938.
2. Condon, F. E., McMurray, H. L., and Thornton, V. J. Chem. Phys. 19: 1010. 1951.
3. Evans, J. C. and Bernstein, H. J. Can. J. Chem. 33: 1792. 1955.
4. Herzberg, G. Infrared and Raman spectra. D. Van Nostrand Company, Inc., New York. 1945.
5. Pitzer, K. and Kilpatrick, J. Chem. Revs. 39: 439. 1946.
6. Rank, D. H. and Kagarise, R. J. Opt. Soc. Amer. 40: 89. 1950.
7. Sheppard, N. and Simpson, D. M. Quart. Revs. (London), 7: 19. 1953.
8. White, J. U., Alpert, N. L., and De Bell, A. G. J. Opt. Soc. Amer. 45: 154. 1955.

ADSORPTION OF OXYGEN BY A SILVER CATALYST[1]

By W. W. Smeltzer,[2] E. L. Tollefson,[3] and A. Cambron[4]

ABSTRACT

An apparatus is described to measure volumetrically the amount of gas adsorbed by a catalyst at constant pressure and at exposure times as short as 0.1 min. The volumes of oxygen adsorbed by a technical silver catalyst at pressures of 200, 400, and 700 mm. and in the temperature range of 180° to 300° C. have been measured. Surface area determinations of 0.33 to 0.38 sq. meter per gm. of catalyst by physical adsorption and chemisorption methods show that each silver atom of the surface is associated with approximately one oxygen adatom at a monolayer coverage. The initial rate of adsorption of oxygen is directly proportional to its pressure. Observed transitions in the oxygen adsorption rates indicate that more than one type of oxygen complex occurs on the catalyst surface. The Elovich equation provides the best approximation of the adsorption rate data but is of limited applicability in interpretation of the mechanism of adsorption. Values of 22–29 kcal./mole and 17–25 kcal./mole have been calculated for the apparent activation energy and isosteric heat of adsorption respectively.

INTRODUCTION

Investigations by Twigg (13, 14) and Orzechowski and MacCormack (8) on the oxidation of ethylene to ethylene oxide and carbon dioxide over a silver catalyst have emphasized the role played by the chemisorption of oxygen in the reaction kinetics. There is, however, meager information about the oxygen adsorption characteristics of silver at elevated temperatures. As part of a program designed to elucidate some of the properties of a technical silver catalyst used in the oxidation of ethylene, the rates of adsorption and volumes of chemisorbed oxygen have been determined as a function of pressure and temperature in this investigation. The results reported are for the operating temperatures and oxygen partial pressures used in reaction studies with a silver catalyst prepared by the method of Cambron and McKim (5).

Thus far, probably the most extensive investigation has been made by Benton and Drake (2) who examined the adsorption of oxygen in the temperature range of −183° C. to 200° C. by a silver catalyst prepared from precipitated silver oxide. Two types of adsorption were found, namely, a practically instantaneous physical adsorption at −183° C. which decreased rapidly with increasing temperature and an activated adsorption which proceeded slowly at 0° C. and increased rapidly at higher temperatures to give a saturation volume nearly independent of temperature over the range of 150° to 200° C. For this latter type of adsorption, the values of the isosteric heat of adsorption and energy of activation were 23–15 kcal./mole and 12.7 kcal./mole respectively.

[1]*Manuscript received April 4, 1956.*
Contribution from the Division of Applied Chemistry, National Research Council, Ottawa, Canada. Issued as N.R.C. No. 3995.
[2]*Present address: Metals Research Laboratory, Carnegie Institute of Technology, Pittsburgh, Pa., U.S.A.*
[3]*Present address: Research Center, Stanolind Oil and Gas Co., Tulsa, Oklahoma, U.S.A.*
[4]*Deceased. Former Director, Division of Applied Chemistry, National Research Council, Ottawa, Canada.*

With the exception of this investigation, little appears in the literature on the adsorption of oxygen by silver at elevated temperatures. Taylor (11) measured the rate of oxygen uptake by silver in the temperature range of 0° to 184° C. and found that the energy of activation decreased with increasing adsorption from 17 to 13 kcal./mole. Twigg (13) found that the change in the electrical resistance ΔR of a silver plated glass wool catalyst increased in the presence of oxygen at a pressure p according to the relationship

$$\Delta R = a\sqrt{p}/(1+b\sqrt{p}), \quad [1]$$

where a and b are constants. Applying values for the solubility of oxygen in silver reported by Steacie and Johnson (10), Twigg was led to the conclusion that the resistance effect was caused primarily by oxygen adsorption. Attempts have been made to determine the number of oxygen atoms complexed with each surface silver atom. Buttner, Funk, and Udin (4) measured the surface tension of solid silver in helium–oxygen mixtures between 870° and 945° C. Using the data with the Gibbs adsorption isotherm, these authors concluded that 1.4 atoms of oxygen were associated with each silver atom at 932° C. Armbruster (1) measured the adsorption of oxygen by silver foil of preferred crystalline orientation in the temperature range of −195° to 20° C. The data were satisfactorily represented by the Langmuir isotherm. Using the calculated monolayer volume, this author concluded that one oxygen molecule was associated with four silver atoms. Since few data are available on the kinetics of oxygen chemisorption on silver above 150° C. and because the oxygen–silver atom ratio shows apparent variations with temperature, the adsorption of oxygen at exposure times as low as 0.1 min. has been measured in the temperature range of 180° to 300° C. in this investigation.

EXPERIMENTAL

Catalyst Preparation

Catalyst I was prepared from an alloy of silver containing 11.3% calcium and 0.11% nickel. A powdered sample in the mesh size range −35 +65 was activated by a steam exposure at 305° C. for seven hours to oxidize the calcium, a leach in boiling 20% acetic acid for four hours, and finally a thorough washing in distilled water. This activation procedure was repeated. Chemical analysis showed that the catalyst contained less than 0.05% calcium and 0.001% nickel. A charge of 49.0 gm. of this catalyst was placed in the adsorption cell.

Catalyst II was prepared from an alloy of silver containing 10.0% calcium, 0.14% nickel, and 0.14% copper. A powdered sample in the mesh range −20 +35 was activated by the above procedure. Chemical analysis showed that the catalyst contained 0.08% nickel, 0.13% copper, and 0.08% calcium. A charge of 50.0 gm. of this catalyst was placed in the adsorption cell.

Catalyst Reference State

In order that the catalyst surface would be in the same reference state before each adsorption run, a standard evacuation temperature of 300° C. was chosen since a reasonable rate of desorption occurred without injury to

the catalyst by sintering. A standard pumping time of 20 hr. was adopted after it was established that the volume of oxygen adsorbed after 40 hr. pumping was the same, within experimental error, as that after 20 hr. for the same experimental conditions.

Apparatus and Procedure

The apparatus for the determination of the gas volumes adsorbed by the silver catalyst at various temperatures and oxygen pressures consisted essentially of an adsorption cell connected to a gas burette and a mercury manometer. With the exception of the pressure control device, the vacuum system was of conventional design and consisted of pressure gauges, an oxygen and argon purification train and storage, a mercury diffusion pump, and other standard accessories.

The furnace, which was positioned around the adsorption cell by a slide, consisted of a 12 in. × 4 in. diameter aluminum cylinder of 1 in. wall thickness wound with a monel heating element and insulated with magnesia. The electrical current through the heater was regulated by a Bristol temperature controller which maintained the catalyst temperature within ±1° C. The temperature of the adsorption cell was measured by two standardized chromel–alumel thermocouples fixed inside the furnace.

Fig. 1 illustrates the adsorption section of the apparatus. The adsorption cell was connected to the gas burette by a short tube and a standard 3 mm. stopcock. To allow for end effects of the furnace on the apparent volume of the adsorption cell, the dead space calibrations were made at the experimental

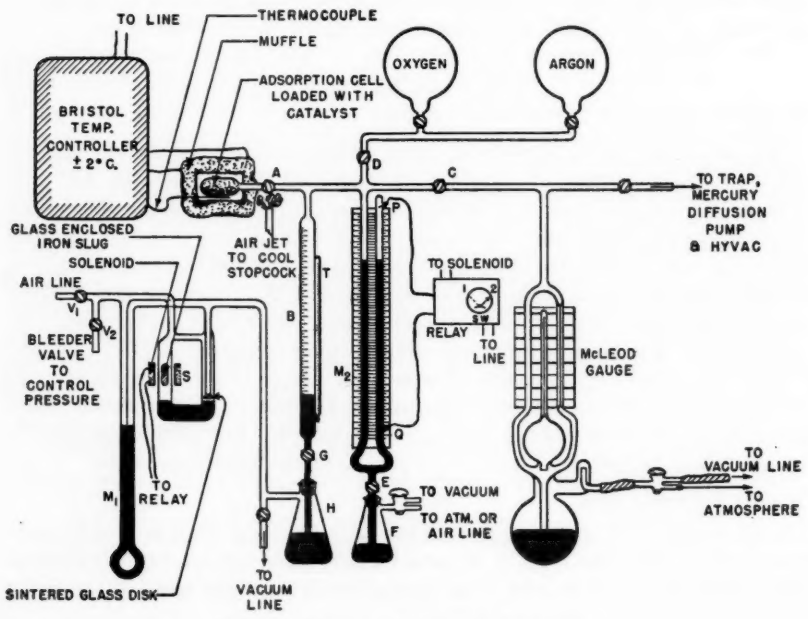

FIG. 1. Diagram of adsorption apparatus.

temperatures with argon. The automatic pressure control device was included in this section of the apparatus to permit burette readings in rapid succession at constant pressure. For this purpose, manometer M_2 was equipped with electrical contacts P and Q and these were connected to the grid circuit of a tube driving a relay. The output of this single pole double throw relay was such that the action of the grid circuit could be reversed. If the output circuit was closed, the solenoid S was energized and raised the glass-enclosed iron slug; simultaneously the mercury level was lowered away from the sintered glass disk in the pressure control device. Thus, air flowed through the disk and raised the mercury in the gas burette when a pressure existed below the control pressure.

Prior to the performance of an adsorption experiment, the standard desorption procedure was performed. The furnace temperature was then set to the desired value and stopcocks A, C, and D were closed. The mercury in burette B was lowered and the manometer M_2 was adjusted so that the column of mercury would contact point P when the system was brought to the run pressure. Stopcock E was then closed and oxygen was admitted through stopcock D from the storage bulb until the mercury in manometer M_2 registered slightly less than the desired run pressure. At this stage, pressure was applied to the mercury surface in flask H by using the relay arrangement. When the stopcock G was opened, the mercury in the gas burette rose until it was automatically stopped when electrical contact was made between the lead P and the mercury column in manometer M_2. After values of the temperature, pressure, and volume had been recorded, the mercury in the burette was raised by a volume equal to that of the dead space of the adsorption cell. An appropriate air pressure differential was then established across manometer M_1 and stopcock A was opened. The volumes of adsorbed oxygen at constant pressure were recorded by burette readings at 0.1 min. intervals or longer.

Materials

The silver–calcium alloys were prepared from high purity Royal Mint silver and high purity calcium supplied by Dominion Magnesium Limited. The minor alloying constituents were prepared from high purity electrolytic copper and Merck nickel shot of 98–99% purity.

The argon and oxygen gases were obtained from commercial cylinders of the Dominion Oxygen Company with a specified purity of at least 99.7%. Prior to storage in the adsorption apparatus these gases were passed through a purification train consisting of ascarite to remove carbon dioxide, heated platinized asbestos in the case of oxygen to remove hydrogen, heated copper in the case of argon to remove oxygen, phosphorus pentoxide to remove water vapor, and a trap at liquid air temperature to remove residual condensible vapors.

RESULTS

The catalyst surface should maintain the same area and properties during the course of experimentation in order that an analysis can be made of the oxygen adsorption results at different temperatures and pressures. Fig. 2 shows the volumes of oxygen adsorbed by Catalyst I with a given set of experimental

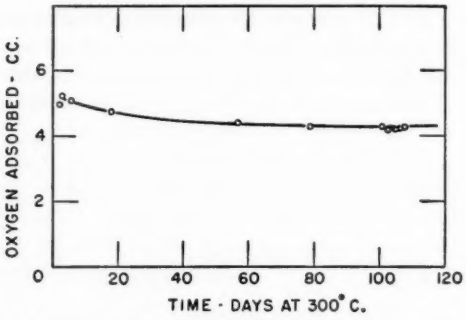

FIG. 2. Adsorption of oxygen by Catalyst I at 260° C. and 400 mm. pressure after evacuation of the catalyst at 300° C. for different time periods.

conditions after the standard evacuation. The volume adsorbed at 400 mm. pressure and 260° C. after the catalyst was maintained at 300° C. for 100 days is approximately 81% of the initially adsorbed volume. Furthermore, the decrease in the adsorption capacity of the catalyst during the last 55 days is less than 5% of the volume adsorbed. The extensive results presented herein for Catalyst I were taken during this period.

Illustrative plots of the volumes of oxygen adsorbed by Catalyst I versus time for each set of adsorption conditions studied in the temperature range of 180° to 300° C. are given in Figs. 3 and 4. There is an initial rapid rate of

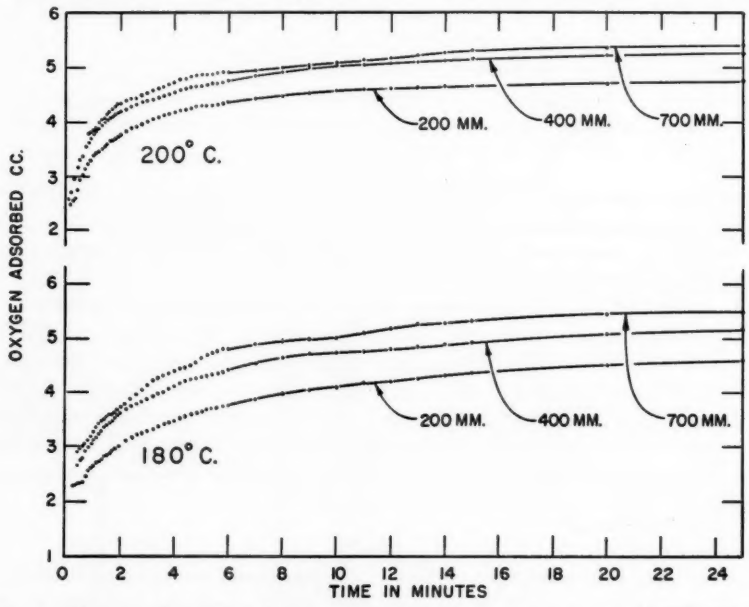

FIG. 3. Oxygen adsorption – time curves for Catalyst I at pressures of 200, 400, and 700 mm. and temperatures of 180° and 200° C.

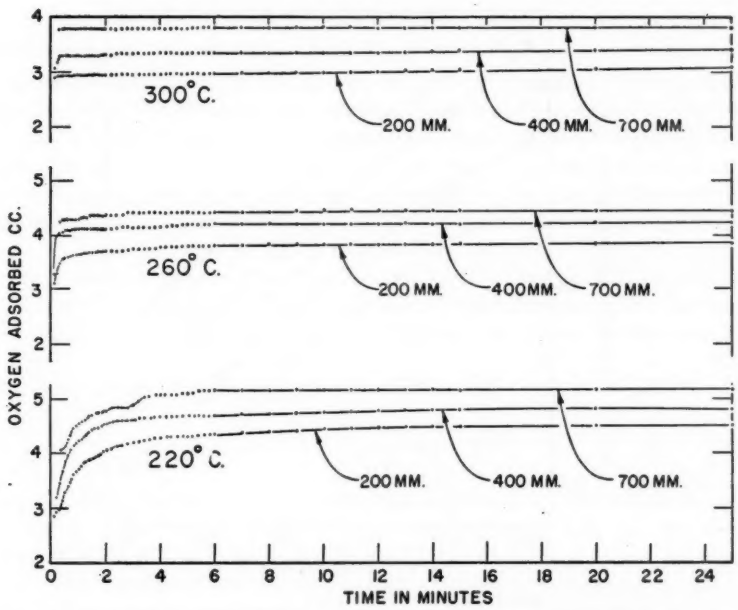

FIG. 4. Oxygen adsorption – time curves for Catalyst I at pressures of 200, 400, and 700 mm. and temperatures of 220°, 260°, and 300° C.

adsorption which increases with increasing temperature. This rate then decreases to a low value and in the temperature range of 200° to 300° C. the volumes of adsorbed oxygen approach their equilibrium values after exposures of 25 min. For example, the adsorption in this temperature range after 15 min. was at least 98% of the total volume adsorbed after 25 min. The small increase in oxygen uptake during the last 10 min. may be due partially to the solubility of oxygen in silver. Isobars of the volumes adsorbed by the catalyst after 25 min. exposure in oxygen and, also, these volumes corrected for the equilibrium solubility of oxygen in silver according to the values given by Steacie and Johnson (10) are illustrated in Fig. 5. Values are not given for 180° C. because adsorption was not complete in the experimental time.

Results for the initial rapid adsorption of oxygen by Catalyst II after exposures of 0.1 min. are illustrated in Fig. 6. Although the rate of adsorption at temperatures above 220° C. was too fast to be measured accurately because of the initial pressure drop in the system, the curves indicate that this initial rate is proportional to the oxygen pressure. Reliance cannot be placed on a comparison of the slopes of the curves at different temperatures, as the adsorption experiments were completed after the catalyst had been evacuated for only one week at 300° C. In a similar manner, the volumes of oxygen adsorbed by Catalyst I after 0.3 min. of exposure are, within the experimental precision, proportional to the oxygen pressure.

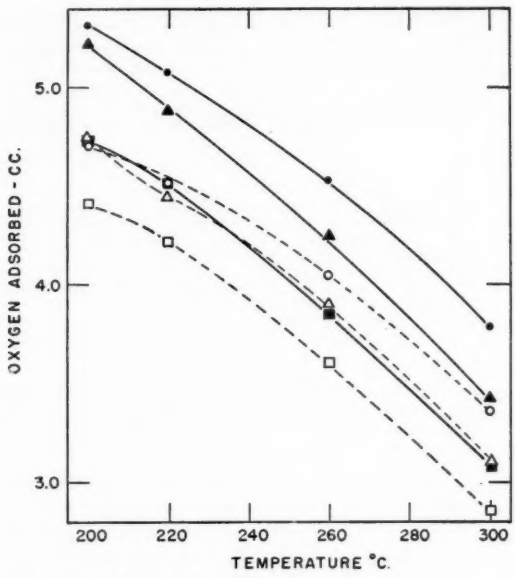

FIG. 5. Isobars of oxygen adsorption by Catalyst I.
■ ▲ ● volumes adsorbed after 25 min. at 200, 400, and 700 mm. pressure respectively with no solubility correction.
□ △ ○ volumes adsorbed after 25 min. at 200, 400, and 700 mm. pressure respectively with solubility correction.

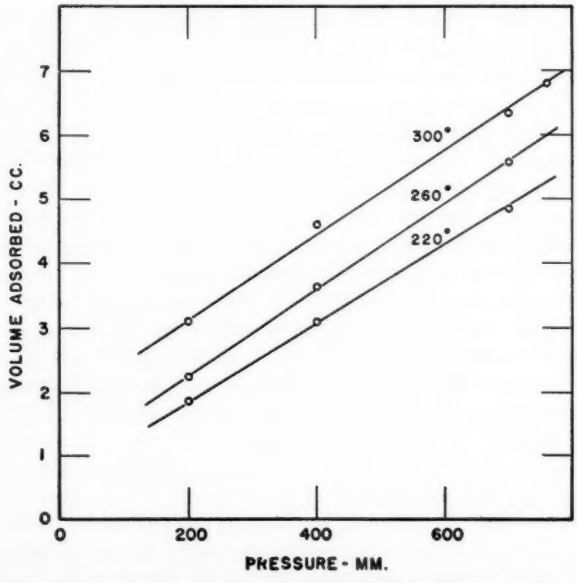

FIG. 6. Volumes of oxygen adsorbed by Catalyst II after 0.1 min. and temperatures of 220°, 260°, and 300° C.

DISCUSSION

Surface Area and Silver-Oxygen Atom Ratio

The isobars of Fig. 5 show that the volume of oxygen finally adsorbed is larger at lower temperatures at constant pressure. This indicates a process involving a state of equilibrium between the adsorbate and the gas phase. In an attempt to determine the catalyst surface area and some properties of the adsorbate, these results are analyzed according to the Langmuir adsorption isotherm. To substantiate this approach, results privately communicated by Drs. A. Orzechowski and K. E. MacCormack on oxygen and krypton adsorption by a catalyst prepared in the same manner as used in this investigation are analyzed according to the Langmuir (7) and Brunauer, Emmett, and Teller (B.E.T.) (3) gas adsorption methods of obtaining surface areas respectively.

One form of the Langmuir isotherm equation is

$$\frac{1}{V} = \frac{1}{V_m bp} + \frac{1}{V_m}, \qquad [2]$$

where p is the pressure, V the volume of gas adsorbed, V_m the volume required to complete a monolayer, and b is a constant. Plots of $1/V$ vs. $1/p$ for the values recorded in Fig. 5 are given in Fig. 7. Linear curves satisfy the results for the temperatures of 200°, 220°, and 260° C. and the pressure range studied. This is valid for both the total uptakes of oxygen and these volumes corrected for solubility of oxygen in the catalyst. The monolayer volume calculated from the intercepts in the temperature range 200°–260° C. varies from 4.8 to

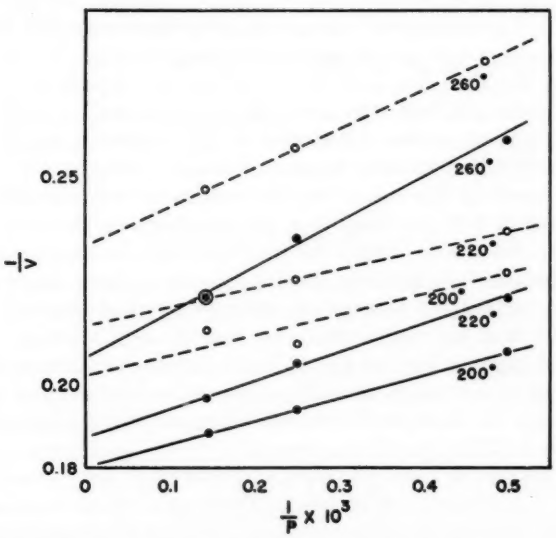

FIG. 7. Langmuir isotherm plots of adsorption data for Catalyst I.
● volumes of oxygen adsorbed after 25 min. with no solubility corrections.
○ volumes of oxygen adsorbed after 25 min. with solubility corrections.

5.6 cc. and, if oxygen solubility is taken into account, from 4.3 to 4.9 cc. Thus, V_m values deviate approximately 15% over the temperature range investigated. If the determination at 220° C. is taken as a mean value, V_m is 5.3 cc. or 4.7 cc. depending upon whether an oxygen solubility correction is made. These values (0.11 or 0.10 cc. per gm. of catalyst) correspond to areas of 0.41 or 0.37 sq. meter per gm. if it is assumed that the cross-sectional area of an oxygen molecule is 14.1 sq. Å.

Orzechowski and MacCormack determined the adsorption isotherm with krypton as the adsorbate at 77.5° K. and, also, the volume of oxygen adsorbed at 220° C. by a 40 gm. sample of catalyst under the experimental conditions employed in this investigation. A surface area of 0.36 sq. meter per gm. of catalyst was obtained from these results when they were analyzed according to the B.E.T. method with the assumption that the cross-sectional area of the krypton molecule was 21.8 sq. Å (9). A Langmuir plot of these results gave a monolayer volume of 4.0 or 3.5 cc. (0.10 and 0.09 cc. per gm. of catalyst) depending upon whether or not oxygen solubility was considered. These latter values, which correspond to surface areas of 0.38 and 0.33 sq. meter per gm., are in agreement with the values determined by the B.E.T. method and, also, with the values of 0.41 and 0.37 sq. meter per gm. determined in this investigation.

This permits a simple approximation to be made as to the number of oxygen atoms complexed with each surface silver atom. If the catalyst surface consists of cubic face-centered crystal faces, the effective area of a silver atom is 8.32 sq. Å. The B.E.T. determination of 0.36 sq. meter corresponds to 4.3×10^{18} atoms of silver. This number is equivalent to either 0.04 or 0.08 cc. of oxygen depending upon whether one or two atoms of oxygen are adsorbed by two silver atoms. The monolayer volumes ranging from 0.09 to 0.10 and 0.10 to 0.11 cc. of oxygen per gm. of catalyst determined from the results of Orzechowski and MacCormack and this investigation, respectively, indicate that one oxygen atom is adsorbed by each silver atom under saturation conditions. Despite this agreement, the calculation is only a first approximation as only one type of crystalline face has been considered.

The agreement of the values for the monolayer volume determined by a Langmuir and B.E.T. analysis does not substantiate the view that simple Langmuir considerations satisfy the characteristics of oxygen chemisorption on silver. This is so because, first, the calculated monolayer volume varies with temperature, second, the energy of adsorption is not constant, and, third, another analytical expression may be used to represent the experimental results. The Langmuir plots of Fig. 7, which do not yield a common intercept, illustrate the first limitation. An examination of the isosteric heat of adsorption, Q, may be used to illustrate the second limitation. Q may be evaluated from the equation

$$[3] \qquad Q = \frac{1}{R}\left(\frac{d \ln p}{d(1/T)}\right)_{V, A},$$

where R is the gas constant and p is the equilibrium pressure of a specified volume V of adsorbate at a temperature T on a surface of constant area A.

Although the accuracy is poor, the values calculated for the isosteric heat of adsorption (using the volumes of oxygen adsorbed shown in Fig. 5 without corrections for oxygen solubilities) vary from 25 to 17 kcal./mole for surface coverages of 68 to 82%. These values, which are in agreement with those reported by Benton and Drake (2), illustrate that the isosteric heat of adsorption is not constant even at large surface coverages.

The agreement of the experimental results, which may be fitted to the Langmuir isotherm equation, with the expression

$$V = a\sqrt{p}/(1+b\sqrt{p}), \quad [4]$$

where V is the volume of adsorbed gas, p is the equilibrium pressure, and a and b are constants, illustrates the third limitation. This expression is similar to equation (1) found by Twigg (13) to satisfy the variation of the electrical resistance of silver in the presence of oxygen. To distinguish the applicability of these isotherm equations, measurements must be extended over a larger pressure range. We stress that the Langmuir isotherm equation has been applied arbitrarily over a limited pressure and temperature range to calculate the monolayer volume.

Adsorption Kinetics

In recent papers, Taylor and Thon (12) and Landsberg (6) have shown that the rates of chemisorption of several gases on solid surfaces may be represented by the Elovich equation,

$$dq/dt = ae^{-\alpha q}, \quad [5]$$

where q is the amount of gas adsorbed, t is the time, and a and α are constants. The integrated form of this equation is

$$q = (2.3/\alpha)\log(t+t_0) - (2.3/\alpha)\log t_0 \quad [6]$$

if $t_0 = 1/\alpha a$. Thus, with a correctly chosen t_0, the plot of q as a function of $\log(t+t_0)$ should give a linear curve with slope $2.3/\alpha$. Also, a, which represents the initial rate of adsorption for $q = 0$, may be evaluated. If t_0 is too small to be assigned a value, a may be evaluated from

$$q_t = (1/\alpha)\ln(1+\alpha a t) \quad [7]$$

if q_t represents the amount of gas adsorbed after time t. Orzechowski and MacCormack (8) have fitted the data of Benton and Drake (2) for the chemisorption of oxygen by silver to an equation of this type, one valid for the approximate range $0.3 < \theta < 0.5$ and another for the range $0.5 < \theta < 0.7$ where θ is the fraction of the monolayer. In each range, a was directly proportional to the oxygen pressure.

Although the adsorption versus time curves of Figs. 3 and 4 show that the Elovich logarithmic rate equation may not be expected to completely fit the adsorption results, it is advantageous to apply this equation in a discussion of the adsorption kinetics. Plots of the adsorbed volumes on Catalyst I versus the logarithm of time for the temperature range of 180° to 260° C. and an oxygen pressure of 200 mm. are shown in Fig. 8. There are, at the temperatures

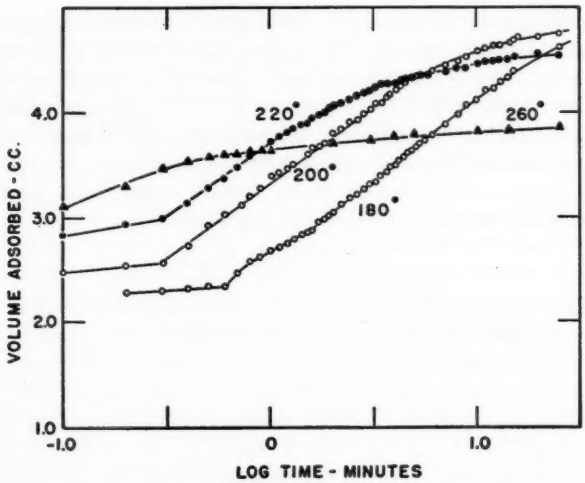

FIG. 8. Adsorption data at 200 mm. pressure for Catalyst I plotted according to the Elovich equation.

of 180°, 200°, and 220° C., abrupt changes in the slopes of the curves within the range of 2.2 to 3.0 cc. of adsorbed gas to regions of practically constant slopes. These latter slopes decrease at higher surface coverages in a manner which is more pronounced at higher temperatures. For the experimental conditions studied, the initial abrupt changes occur only at coverages corresponding to less than 3 cc. of adsorbed gas. It is assumed that α and a may be evaluated from the constant slopes and the volumes of gas adsorbed in these regions (equation [7]). These values and the surface coverages for which the curves are of approximately constant slope are recorded in Table I. Values are recorded only for the temperature range of 180° to 220° C. as the adsorption rate is too rapid at higher temperatures to determine the functional relationship with time.

The calculated values for an initial rate of adsorption, a, increase with pressure and temperature. The dependence of the rate on pressure cannot be determined because the evaluations are not sufficiently accurate. However, the results presented in Fig. 6 indicate that this rate is directly proportional to the pressure. Moreover, it is to be noted that the calculated values for this initial rate are much larger than the experimentally determined values. In Fig. 9 plots are shown of the logarithms of the calculated and experimentally determined values for the initial rate of adsorption versus the reciprocal of the absolute temperature. As a measure of the experimentally determined rate, the reciprocals of the times required to adsorb 3 cc. of oxygen on Catalyst I at 200 mm. pressure of oxygen were used. The apparent energies of activation calculated from the slopes of the least squares lines are 27–29 kcal./mole and 22 kcal./mole for the calculated and experimentally determined initial rates of adsorption respectively. This latter value of 22 kcal./mole is larger than the

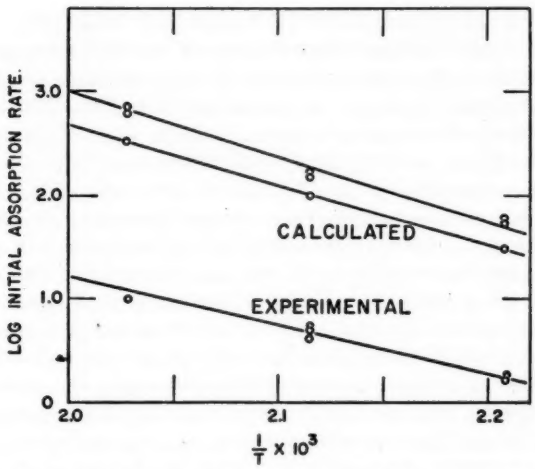

FIG. 9. Arrhenius plots of initial rates of oxygen adsorption on Catalyst I.

values of 17 to 13 kcal./mole reported by Taylor (11) and Benton and Drake (2).

The surface coverages recorded in Table I illustrate that the curves of constant slopes are confined to the approximate range $0.5 < \theta < 0.9$ if the experimental results are plotted according to the Elovich equation. In this analysis, t_0 was assumed to be equal to zero as positive values of this constant gave no better fit of the data to the equation. The above range corresponds to

TABLE I

VALUES OF CONSTANTS α AND a OF ELOVICH EQUATION AND SURFACE COVERAGE θ FOR WHICH EQUATION IS APPLICABLE

Temperature, °C.	Pressure, mm.	α, 1/cc.	a, cc./min.	θ, fraction of monolayer
180	200	1.5	30	0.5–0.8
	400	1.4	60	0.5–0.9
	700	1.3	55	0.6–0.9
200	200	1.5	100	0.5–0.8
	400	1.4	150	0.5–0.8
	700	1.4	160	* –0.9
220	200	1.7	320	0.6–0.7
	400	1.6	630	* –0.8
	700	1.5	670	* –0.9

*Not observed.

that of $0.5 < \theta < 0.7$ found by Orzechowski and MacCormack (8) from an analysis of the data on oxygen adsorption on silver at lower temperatures. Also, the abrupt changes in the slopes of the Elovich curves at a surface coverage of approximately 0.5 are similar to a break in the curve for the adsorption

of hydrogen on zinc oxide found by Taylor and Thon (12). These authors suggest that abrupt changes in the slopes of the Elovich curves indicate a change from one kind of site to another at a certain stage of adsorption.

This investigation supports the view that more than one kind of site is involved in the chemisorption of oxygen on silver. Figs. 3 and 4 show that the curves for adsorption at 180°, 200°, and 220° C. have transitions due to differences in the adsorption rates at 0.6, 0.2, and 0.2 min. respectively after the beginning of the adsorption runs. These abrupt changes in the adsorption–time curves and the curves for data plotted according to the Elovich equation occur at approximately half coverage of the catalyst surface. This suggests that initially the surface is rapidly covered by oxygen so that each oxygen atom is associated with two silver atoms. A relatively slow rearrangement of adatoms may then occur which permits further adsorption until one oxygen atom is associated with each silver atom. If this is correct, the different kinds of adsorption sites may be associated with differences in the bonding of oxygen with silver. For example, on the basis of surface geometry and bond angles,

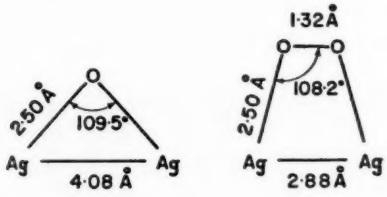

two species could exist on a catalyst surface at the interatomic cubic lattice spacings of 4.08 Å and at the spacings for closest approach of silver atoms of 2.88 Å. Consequently, equilibria between the silver surface atoms and oxygen gas may be represented by the equations

[8] $$4Ag_{(surface)} + O_{2(g)} = 2Ag_2O_{(complex)},$$

[9] $$2Ag_2O_{(complex)} + O_{2(g)} = 2Ag_2O_{2(complex)}.$$

The observed transitions in the adsorption rates then indicate approximately the termination of process [8] and the commencement of process [9]. In the temperature range of 180° to 220° C. process [8] is rapid whereas process [9] is relatively slow. Both of these processes are rapid at 260° and 300° C. as the transitions were not observed. This postulate of two surface oxygen complexes is only a crude approximation as no significance is given to the influence of variations in the energy properties of different crystalline faces on the kinetics of adsorption, and cognizance is given to only the abrupt changes in the slopes of the Elovich curves. Although these latter abrupt changes occur at surface coverages of approximately 0.5, this does not disprove the proposal by Orzechowski and MacCormack (8) that different kinds of adsorption sites may be associated with different crystalline faces.

GENERAL DISCUSSION

In an attempt to account for the observed phenomena, it has been postulated that the catalyst surface area may be determined by the Langmuir and B.E.T. gas adsorption methods and that at least two oxygen complexes are formed on the catalyst surface. These postulates lead to a qualitative interpretation of the adsorption kinetics and emphasize opposing views on the chemisorption of oxygen on a silver catalyst. Twigg (13, 14) and Orzechowski and MacCormack (8), in their investigations on the oxidation of ethylene with a silver catalyst, have proposed that only single oxygen adatoms are involved in the adsorption and reaction kinetics and that proposed mechanisms are applicable to homogeneous and heterogeneous surfaces. Twigg assumes that the formation of ethylene oxide and carbon dioxide requires one and two favorably situated oxygen adatoms respectively. Selective poisoning is attributed to an alteration in the configuration of these adatoms. Orzechowski and MacCormack propose that both reactions involve single oxygen adatoms and that different energetic considerations account for the formation of ethylene oxide and carbon dioxide. According to their postulated reaction mechanism, selective poisoning is attributed to preferential poisoning of different crystalline planes or to the formation of impurity centers which influence the activation energies of the several reaction paths. On the other hand, transitions in the adsorption–time curves of this investigation at surface coverages of approximately 0.5 indicate that at least two oxygen complexes occur with one and two oxygen atoms equivalent to two silver atoms. If significance may be attached to the calculated initial rate of adsorption (Table I) for the formation of the latter complex, this rate is of a sufficient magnitude to influence the reaction kinetics of ethylene oxidation. Selective poisoning may then be attributed to the preferential alteration in concentration of these different complexes. This concept of paired oxygen adatoms is different from that proposed by Twigg in that specific account is taken of the surface geometry and complete dissociation of adsorbed molecular oxygen need not occur. This study emphasizes that further experimental data are required for an understanding of the oxygen chemisorption phenomena on silver and that extreme caution must be used in representing the adsorption of oxygen by an analytical rate equation in reaction studies involving a silver catalyst.

ACKNOWLEDGMENTS

The authors wish to express their thanks to Mrs. Mary Marks Raal, Mrs. Barbara McPhee Burford, and Mr. D. Harwood who assisted in obtaining the presented data.

REFERENCES

1. ARMBRUSTER, M. H. J. Am. Chem. Soc. 64: 2545. 1942.
2. BENTON, A. F. and DRAKE, L. C. J. Am. Chem. Soc. 56: 255. 1934.
3. BRUNAUER, S., EMMETT, P. H., and TELLER, E. J. Am. Chem. Soc. 60: 309. 1938.
4. BUTTNER, F. H., FUNK, E. R., and UDIN, H. J. Phys. & Colloid Chem. 56: 657. 1952.

5. CAMBRON, A. and MCKIM, F. L. W. U.S. Patent No. 2,562,857. 1951; Can. Patent No. 475,366. 1951.
6. LANDSBERG, P. T. J. Chem. Phys. 23: 1079. 1955.
7. LANGMUIR, I. J. Am. Chem. Soc. 40: 1361. 1918.
8. ORZECHOWSKI, A. and MACCORMACK, K. E. Can. J. Chem. 32: 388, 415, 443. 1954.
9. PICKERING, H. L. and ECKSTROM, H. C. J. Am. Chem. Soc. 74: 4775. 1952.
10. STEACIE, E. W. R. and JOHNSON, F. M. G. Proc. Roy. Soc. (London), A, 112: 542. 1926.
11. TAYLOR, H. Z. physik. Chem. Bodenstein Festband, 475. 1931.
12. TAYLOR, H. A. and THON, N. J. Am. Chem. Soc. 74: 4169. 1952.
13. TWIGG, G. H. Proc. Roy. Soc. (London), A. 188: 92, 105, 123. 1946.
14. TWIGG, G. H. Trans. Faraday Soc. 42: 284. 1946.

THE REACTION OF DEUTERIUM ATOMS WITH ETHYLENE[1]

By S. Toby[2] and H. I. Schiff

ABSTRACT

Deuterium was dissociated on a hot tungsten filament and the atom concentration measured by isothermal calorimetry. The recombination coefficient of deuterium atoms on a glass surface, coated with metaphosphoric acid, was found to be 3.8×10^{-5}, and similar to that found for hydrogen atoms. The reactions of H-atoms and D-atoms with ethylene were found to be very rapid. The effects on the yields of the products and on their isotopic composition of variations of reactant flow rate, atom concentration, pressure, and atom-detector position were studied. The major products were methanes, ethanes, and ethylenes, with minor amounts of propanes and butanes. The methanes were always highly deuterated while the ethanes were slightly deuterated. A mechanism is proposed to explain the observations based on a flow pattern in the reaction zone. The possibility of differences in the reaction rates of variously deuterated intermediates is also discussed.

INTRODUCTION

The homogeneous reaction between atomic hydrogen and ethylene occurs so rapidly that little is known of the detailed mechanism. Investigations using isotopic hydrogen have been largely qualitative (19, 11). This paper reports an attempt to obtain quantitative data on the products of the reaction between deuterium atoms and ethylene.

EXPERIMENTAL

The method used to produce and detect the deuterium atoms was similar to that used by LeRoy for hydrogen (2, 3, 7). About 2% of the hydrogen or deuterium in a fast flowing gas stream was dissociated into atoms on an electrically heated tungsten filament. The detector was a tightly wound platinum spiral, mounted on a rack which could be moved by a pinion attached to a standard tapered joint. Two teflon gaskets placed on the inner joint prevented the "Apiezon" grease from being squeezed out during rotation and kept the system vacuum-tight. This arrangement had the advantage of eliminating sliding contacts and permitted a constant lead resistance regardless of detector position. The wattage dissipated by the detector was determined from its resistance and the voltage drop across it.

To conserve deuterium, the gas was circulated during an experiment by connecting the vent of the rotary pump through a refrigerated trap to a return line. Blank experiments showed that the exchange between the deuterium and the pump oil was less than 0.5% for six hours' circulation.

The reaction vessel was 22.5 cm. long and 25 mm. in diameter and was coated with metaphosphoric acid. The speed of gas circulation was 1400 $cm.^3$/sec., corresponding to a linear flow rate of 280 cm./sec. through the reaction chamber and a maximum reaction time of 0.08 sec.

[1]*Manuscript received April 3, 1956.*
Contribution from the Department of Chemistry, McGill University, Montreal, Quebec.
[2]*Holder of a National Research Council Studentship, 1953–54, and of a Province of Quebec Scholarship, 1954–55. Present address: Division of Pure Chemistry, National Research Council, Ottawa.*

Deuterium was prepared from 99.7% deuterium oxide obtained from Atomic Energy of Canada Limited. The deuterium oxide was allowed to react with a carefully degassed mixture of zinc and freshly dehydrated calcium oxide. Deuterium was then evolved at 500°C. (9, 12) by the reaction:

$$Ca(OD)_2 + Zn \rightarrow D_2 + CaZnO_2.$$

The yield of deuterium depended on the rate of heating of the furnace due to the competing reaction:

$$Ca(OD)_2 \rightarrow CaO + D_2O$$

which occurs at temperatures above 350°C. Yields as high as 90% of the theoretical value were obtained with rapid furnace heating. Mass spectral analysis showed the product to be 96% D_2, the remainder being almost entirely HD. Since the reaction under investigation also produced HD as one of the products, additional quantities of D_2 were periodically added to the system to prevent the deuterium content of the circulating gas from dropping below 96%.

The ethylene, obtained from the Ohio Chemical Company, was "trap-to-trap" distilled several times. The center fraction was 99.9% pure, with ethane as the only detectable impurity. About four millimoles of ethylene-d_4 was kindly supplied by Dr. L. C. Leitch of the National Research Council, Ottawa.

Deuterium atoms were allowed to react at room temperature with the ethylene in a conventional fast flow system. The effects of variation of reactant flow rate, atom concentration, deuterium pressure, and atom-detector position were investigated.

The products were condensed in two large, liquid-nitrogen cooled traps, the second of which contained silica gel to retain the methanes. The total "condensible" fraction was first measured volumetrically. The sample was then divided in two and the mass spectrum of one portion determined. Unsaturates were removed from the other portion with acid mercuric sulphate solution (8) and the remaining saturated hydrocarbons analyzed mass spectrometrically. The analysis of the unsaturates was then obtained from the difference between the spectra of the treated and the untreated portions.

Since standard samples of all the deuterated products were not available, approximate procedures were required to interpret the mass spectra. From a mixture known to contain only methane-d_3 and methane-d_4, the probability factors a and b for the ease of removal of H- and D-atoms respectively from the parent molecule were measured for the mass spectrometer used. The values of these parameters for the other methanes were then estimated by linear extrapolation (20), and the mass spectra for all four deuteromethanes were calculated.

The deuteroethanes were analyzed at reduced electron energies (25) using data kindly supplied by Dr. D. P. Stevenson of the Shell Development Company. Analyses were also performed at 70 volts electron energy, using published data (20) for ethane-d_1, -d_2, -d_3, and -d_6, and calculated spectra (24) for ethane-d_4 and -d_5. Since highly deuterated ethanes were present in relatively small amounts, the errors involved in using the calculated spectra were not serious. The agreement between analyses at normal and reduced electron energies was satisfactory.

The deuteroethylenes were analyzed with the aid of published spectra (6). Small quantities of deuteropropanes and deuterobutanes were also found. Their total quantity was estimated from the sum of the ion currents in the "C_2" and "C_4" mass number region.

RESULTS

The Recombination of Hydrogen and Deuterium Atoms

Dingle and LeRoy found (7) that straight lines could be drawn through both first and second order plots for H-atom recombination, and so were unable to assess the relative importance of heterogeneous and homogeneous recombination reactions. We obtained similar results for both H- and D-atoms. Average values for the "pseudo" first order rate constant k', and the "pseudo" second order rate constant k'', for H- and D-atoms are given in Table I. The value for

TABLE I

PSEUDO RATE CONSTANTS FOR H-ATOM AND D-ATOM RECOMBINATION

$k_H' = 3.82 \pm 0.12$ sec.$^{-1}$ $k_D' = 2.77 \pm 0.08$ sec.$^{-1}$	$\frac{k_H'}{k_D'} = 1.38$
$k_H'' = (2.52 \pm 0.06) \times 10^9$ cm.^{3} sec.$^{-1}$ mole^{-1} $k_D'' = (1.66 \pm 0.04) \times 10^9$ cm.^{3} sec.$^{-1}$ mole^{-1}	$\frac{k_H''}{k_D''} = 1.52$

k_H' can be compared with Dingle and LeRoy's value (7) of 4.80 sec.$^{-1}$. The ratio of either the first or the second order rate constants for hydrogen and deuterium should be less sensitive to wall conditions than the individual values, and clearly indicates that H-atoms recombine faster than D-atoms. There are no data with which these ratios can be compared, but Amdur (1) gives a value of 1.36 for k_D'''/k_H''', the ratio of the third order rate constants at 30°C.

The heterogeneous recombination of atoms can also be expressed in terms of a recombination coefficient γ, which may be defined as the ratio of the number of atoms recombining on a surface to the total number striking that surface (21), and is, therefore, independent of the geometry of the apparatus. It can be calculated from the relation

$$\gamma = 2k'r/V$$

where V is the mean atomic velocity and r the radius of the tube. Table II shows the values obtained in this and in other investigations. It will be seen that the values of γ for H- and D-atoms are equal within experimental error. This suggests that any difference between the first order recombination rates is due only to the differences in atomic velocities.

The Reaction of H- and D-Atoms with Ethylene

Preliminary experiments with H-atoms showed that ethane and methane were the main products of the reaction, along with small amounts of propane and butane. The amounts of various products formed in the reaction with D-atoms are given in Table III. Fig. 1 shows the percentage of each product

TABLE II

RECOMBINATION COEFFICIENT FOR GLASS SURFACE COATED WITH METAPHOSPHORIC ACID

Author	Atoms	$\gamma \times 10^5$	Temp., °C.
Poole (17)	H	3.9	Room temp.
Smith (22)	H	2	15
Dingle and LeRoy (7)	H	4.5	5
This work	H	3.8	25
This work	D	3.9	25

TABLE III

VARIATION WITH REACTANT FLOW

Run	Temp., °C.	Total press., mm. Hg	Partial press. atoms, mm. Hg	Partial press. ethylene, mm. Hg	Percentage products			
					Methanes	Ethanes	*d*-Ethylenes	C_3, C_4
D-21	24.0	1.36	0.0246	0.0182	97.9	2.1	0	0
D-20	23.5	1.37	0.0191	0.025	98.7	1.3	0	0
D-17	23.0	1.34	0.0222	0.0510	84.2	12.6	2.9	0.3
D-27	25.8	1.36	0.0222	0.0599	73.0	—	—	—
D-14	22.0	1.36	0.0199	0.132	70.5	18.5	8.7	2.2
D-12	25.5	1.38	0.0211	0.235	59.2	22.5	14.1	4.2
D-11	25.5	1.41	0.0186	0.239	59.4	23.3	12.7	4.6
D-24	25.0	1.37	0.0216	0.312	53.9	25.0	16.3	4.9
D-18	23.5	1.36	0.0217	0.414	52.4	25.9	19.1	2.6
D-26	25.5	1.36	0.0199	0.491	52.0	26.6	17.9	3.6
D-25	26.5	1.36	0.0241	0.525	51.2	26.7	15.7	6.4
D-15	24.0	1.34	0.0210	0.559	49.4	24.6	20.4	5.6
D-16	23.5	1.35	0.0221	0.625	51.6	24.3	19.6	4.4

as a function of ethylene flow rate normalized for a D-atom flow rate of 1.0 micromoles per second; the amount of each of the deuterated methanes, ethanes, and ethylenes is plotted against reactant flow rate in Figs. 2, 3, and 4 respectively.

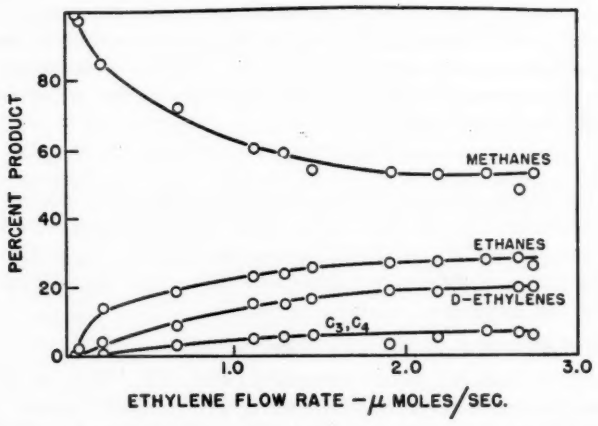

FIG. 1. Variation of total products with ethylene flow rate.

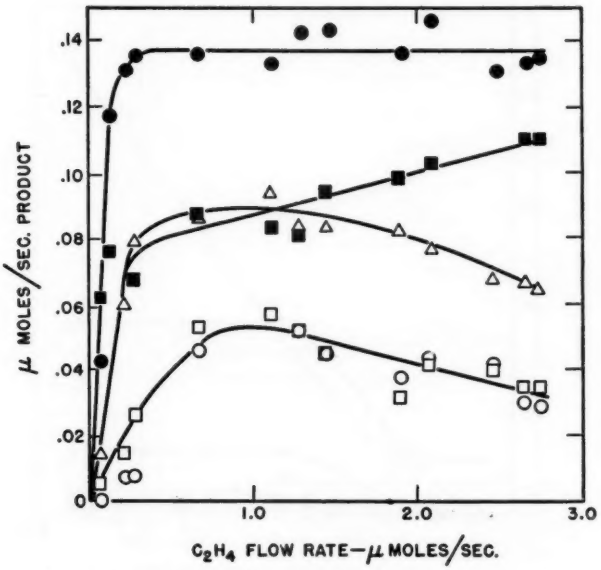

FIG. 2. Variation of methanes with ethylene flow rate.
○, CH_4; □, CH_3D; △, CH_2D_2; ●, CHD_3; ■, CD_4.

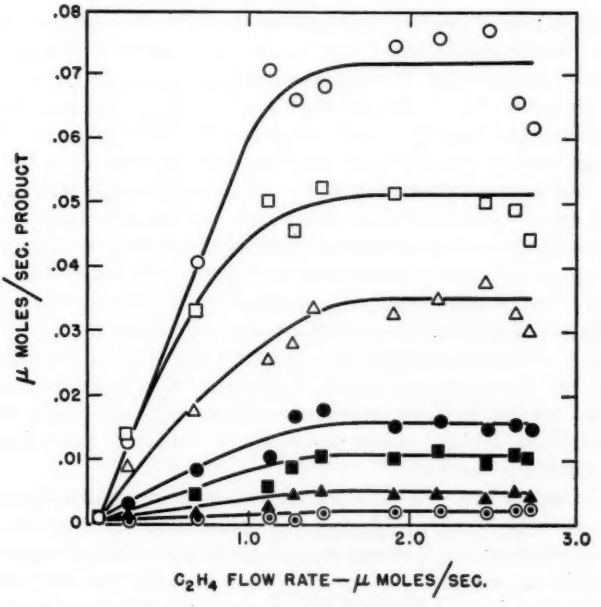

FIG. 3. Variation of ethanes with ethylene flow rate.
○, C_2H_6; □, C_2H_5D; △, $C_2H_4D_2$; ●, $C_2H_3D_3$; ■, $C_2H_2D_4$; ▲, C_2HD_5; ⊙, C_2D_6.

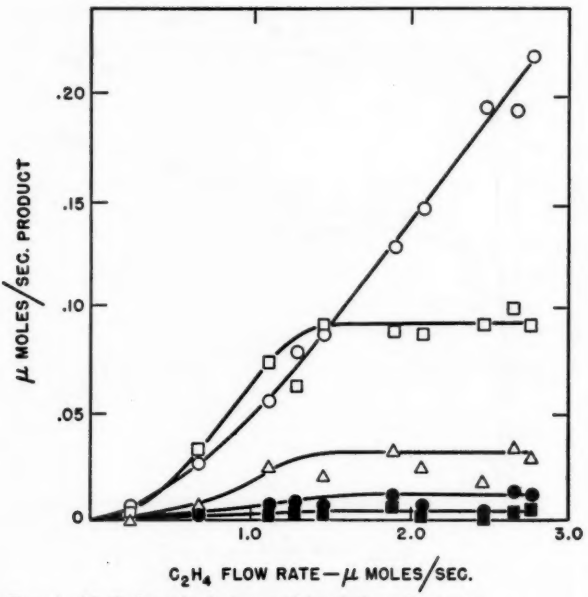

FIG. 4. Variation of ethylenes with ethylene flow rate.
○, $C_2H_4/10$; □, C_2H_3D; △, $C_2H_2D_2$; ●, C_2HD_3; ■, C_2D_4.

The extent of deuteration of any product can be conveniently expressed in terms of the "deuterium number", i.e. the average number of deuterium atoms per molecule of that product. The variation of deuterium number with ethylene flow rate is shown in Fig. 5. The deuterium numbers for the ethylenes do not include unexchanged reactant, and no values are shown at low flow rates, where the amount of unexchanged ethylene was too small for quantitative analysis. In one series of experiments the deuterium pressure was varied while the partial pressure of D-atoms was maintained at 0.028 mm. Hg by controlling the dissociator temperature; the partial pressure of ethylene was 0.017 mm. Hg. The results are plotted along with deuterium numbers in Fig. 6. The deuterium number was pressure dependent only in the case of ethane—with increasing pressure ethane-d_1 became more abundant than ethane-d_0.

Three experiments were performed in which the atom concentration was varied while the deuterium and ethylene pressures were kept constant. Table IV shows the results, and, for comparison, some published data for the reaction of ethylene with H-atoms produced by mercury photosensitization and by the discharge method.

Since all atoms striking the detector are recombined, an attempt was made to alter the reaction time by placing the detector in the reaction chamber during an experiment. Fig. 7 shows the results of a number of experiments in which the detector position was varied from just below the exit tube of the reaction vessel (its normal position during other experiments) to just below the ethylene inlet jet.

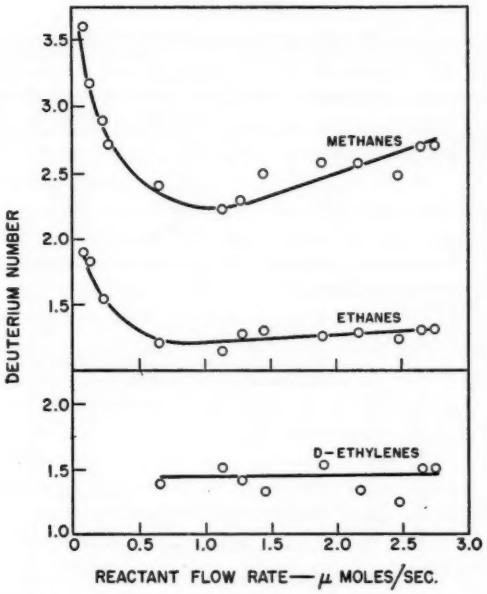

FIG. 5. Variation of deuterium number with ethylene flow rate.

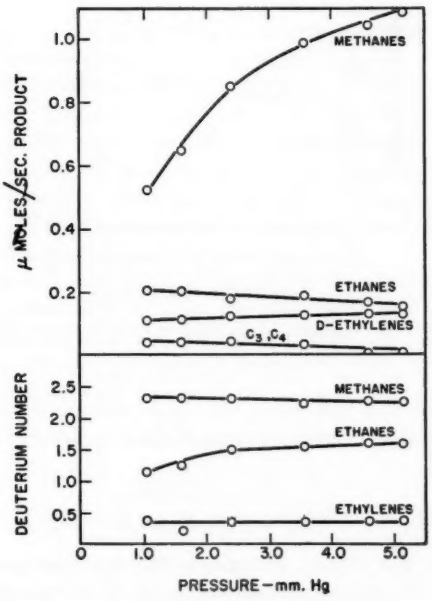

FIG. 6. Variation of products with total pressure.

TABLE IV

VARIATION WITH ATOM CONCENTRATION

Reference	Atoms	Ratio $\frac{\text{atoms}}{\text{reactant}}$	Percentage		
			Methane	Ethane	Butane
Moore and Taylor (16)	H	*ca.* 10^{-3}	2	14	84
This work	D	0.58	57.6	36.8	5.5[b]
This work	D	1.32	72.2	24.4	3.3[b]
This work	D	2.28	76.0	22.5	1.5[b]
H. I. Schiff (unpublished work)[a]	H	*ca.* 20	92.7	7.3	0

[a] *Traces of acetylene were also found.*
[b] *Includes some propane.*

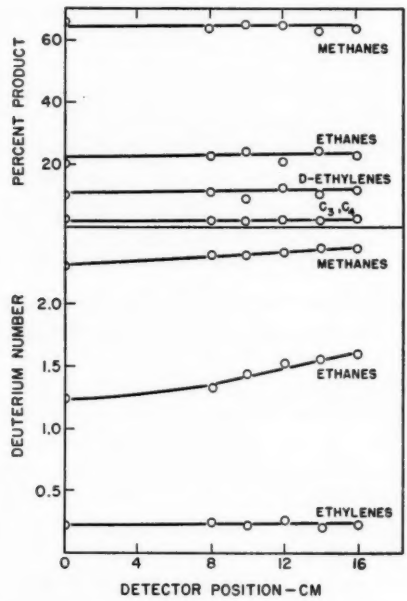

FIG. 7. Variation of products with detector position.

These results indicate that the reaction zone did not extend more than 2 cm. from the inlet jet which corresponds to a reaction time of less than 0.007 sec. The reactions:

$$H + C_2H_4 \rightarrow C_2H_5, \qquad [1]$$

$$D + C_2H_4 \rightarrow C_2H_4D \qquad [1a]$$

must therefore be very fast and have collision yields greater than 10^{-4}, in agreement with previously reported values (4, 5, 15) for reaction [1].

DISCUSSION

Perhaps the most unexpected result of this investigation was the production of C_2H_6 and C_2H_5D as the most abundant ethanes in the reaction between D-atoms and ethylene. The amounts of these products were much too large to be accounted for by the hydrogen impurity in the deuterium. Other possible explanations for their occurrence were therefore analyzed. The following possibilities were considered:

(1) *The preferential dissociation of H_2 on the dissociator filament due to its higher dissociation equilibrium constant relative to D_2.* However, calculation showed that this would increase the H-atom concentration by at most 0.1% of the total atom concentration. HD, the largest impurity in the deuterium, dissociates less readily at 2000°A. than does D_2.

(2) *The exchange of D-atoms with the phosphoric acid wall poison.* If the entire increase in HD content observed when the deuterium was circulated for several hours in the absence of ethylene is attributed to this exchange, the maximum production of H-atoms would correspond to less than 1% of the total atom concentration.

(3) *Back diffusion of ethylene to the dissociator.* When helium was substituted for the deuterium 100% recovery of the ethylene was obtained.

(4) *Loss of methane from the silica gel trap and its subsequent dissociation on the tungsten filament.* In view of the excellent mass balances obtained this could not have occurred to any appreciable extent. Moreover, the dissociation of the methanes would not be a good source of H-atoms since they were found to be highly deuterated.

(5) *Heterogeneous reactions occurring on the atom detector.* Experiments with the detector completely removed gave identical results.

(6) *Exchange of the ethanes with the mercuric sulphate solution during the removal of the olefins.* The unsaturates were removed from several samples by reaction with purified bromine; no differences were found.

(7) *Errors in mass spectral analyses due to the lack of standard gases.* Although these errors are difficult to assess quantitatively, comparison of analyses performed both at high and at low electron energies showed that the order of abundance of the deuteroethanes was correct.

Since none of these possibilities is capable of explaining the production of light ethanes, it is reasonable to conclude that these were indeed products of the reaction between D-atoms and ethylene. This can be shown to be stoichiometrically possible. The reactions forming the major products can be formally represented by the equations:

$$\tfrac{1}{2}C_2H_4 + \alpha D \rightarrow C_2D_\alpha H_{4-\alpha} + (\alpha-2)\ H \text{ for methanes,}$$

$$C_2H_4 + \beta D \rightarrow C_2D_\beta H_{4-\beta} + \beta H \text{ for ethylenes, and}$$

$$C_2H_4 + \gamma D \rightarrow C_2D\gamma H_{6-\gamma} + (\gamma-2)H \text{ for ethanes,}$$

where α, β, and γ represent the deuterium numbers of the products. In a typical experiment $\alpha = 2.69$, $\beta = 1.50$, and $\gamma = 1.35$. The yields of the pro-

ducts were 0.377, 0.155, and 0.184 μM./sec. for the methanes, ethylenes, and ethanes respectively. Hence hydrogen atoms could have been generated by the reaction at a rate of $(0.69\times0.377) + (1.50\times1.55) - (0.65\times.184) = 0.37\mu$M./sec. Considerably more H-atoms can therefore be produced in the deuteration of the products than are required for the formation of C_2H_6 and C_2H_5D. This was found to be true in all cases.

However, any mechanism for the reaction must be able to account for these light ethanes along with the other products. In the case of the reaction of H-atoms with ethylene the following elementary reactions may be considered:

$$H + C_2H_4 \rightarrow C_2H_5 \quad [1]$$

$$C_2H_5 \rightarrow C_2H_4 + H \quad [2]$$

$$H + C_2H_5 \rightarrow C_2H_6^* \quad [3]$$

$$C_2H_6^* \rightarrow C_2H_5 + H \quad [4]$$

$$(M+)\ C_2H_6^* \rightarrow C_2H_6\ (+M) \quad [5]$$

$$C_2H_6^* \rightarrow C_2H_4 + H_2 \quad [6]$$

$$C_2H_6^* \rightarrow 2CH_3 \quad [7]$$

$$H + CH_3 \rightarrow CH_4^* \quad [8]$$

$$(M+)\ CH_4^* \rightarrow CH_4\ (+M) \quad [9]$$

$$2CH_3 \rightarrow C_2H_6^* \quad [10]$$

Corresponding reactions can occur with D-atoms.

Formation of Ethylenes

There are several possible explanations for the formation of the deutero-ethylenes. The primary step undoubtedly is

$$D + C_2H_4 \rightarrow C_2H_4D. \quad [1a]$$

Since the deuteroethyl radical probably possesses excess energy it may readily dissociate again:

$$C_2H_4D \rightarrow C_2H_3D + H. \quad [2a]$$

The more highly deuterated ethylenes could be formed from repetition of these two reactions. This mechanism suggests that the yield of deuteroethylenes might be pressure dependent. This was not the case over the pressure range studied.

Alternatively, the deuteroethyl radicals could undergo disproportionation (10). However, the very small butane yields indicated that disproportionation cannot be a major source of deuteroethylene.

The third possibility is that reaction [1*a*] is followed by:

$$D + C_2H_4D \rightarrow C_2H_3D + HD. \quad [6a]$$

However, the repetition of [1*a*] and [6*a*] does not provide an acceptable explanation for the formation of *all* the deuteroethylenes since this sequence does not produce any H-atoms. In some of the experiments the amount of H-atoms which could be derived in the formation of the other products was insufficient to account for the amounts of C_2H_6 and C_2H_5D. This objection

could be overcome if the deuteroethyl radical first underwent exchange reactions of the type

$$D + C_2H_4D \rightarrow C_2H_3D_2 + H \qquad [4a]$$

prior to forming ethylene by the counterpart of reaction [6*a*]. There is some evidence for [4*a*] from the study of the reaction of D-atoms produced by mercury photosensitization with ethane (23). Deuterobutanes were found which indicated exchange of ethyl radicals before recombination.

Little is known about the likelihood of reaction [6] (or [6*a*]). It is exothermic, but would appear to be less likely than reaction [4], [5], or [7] by the "Principle of Least Motion" (18). However, no unequivocal choice can be made between the first and third explanations for the formation of the deuteroethylenes.

Formation of Methanes and Ethanes

For reasons already indicated, appreciable quantities of ethane could not be formed by disproportionation of ethyl radicals. Moreover, normal disproportionation could not account for the formation of light ethanes. An unlikely "double disproportionation" of the type

$$C_2H_4D + C_2H_4D \rightarrow C_2H_6 + C_2H_2D_2$$

would be required. The remaining possible sources of ethane are reactions [5] and [10], both of which are preceded by reaction [3]. Methane formation, however, is also preceded by reaction [3]. The problem then arises of accounting for the fact that the methanes were always found to be highly deuterated while the ethanes were only slightly deuterated. A possible explanation can be found by considering the two most likely fates for the methyl radicals in the system:

$$H + CH_3 \rightarrow CH_4 \qquad [11]$$

$$CH_3 + CH_3 \rightarrow C_2H_6 \qquad [12]$$

The distribution of atoms in the reaction zone can be represented diagrammatically as:

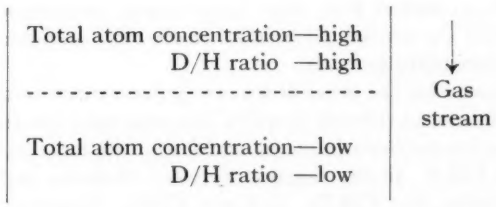

The total atom concentration decreases down the reaction tube as a result of both reaction and recombination. But the proportion of H-atoms in the gas stream will increase owing to the exchange of the D-atoms with ethylene and with free radicals.

Reaction [11] will be favored over reaction [12] in the upper part of the reaction zone where the atom concentration is highest. But since this is where the D/H atom ratio is also highest, the methanes will be highly deuterated.

Under the conditions of low atom concentration at the lower part of the reaction zone reaction [12] will occur more frequently than reaction [11]. But the ratio of H- to D-atoms has increased so that the ethanes will be less deuterated than the methanes.

This picture is in agreement with the observation (Table IV) that the yield of ethane decreases, and the yield of methane increases with increasing atom concentration. The reverse variation of yields with increasing ethylene concentration is likewise consistent with this explanation.

The large increase in methane formation with pressure (Fig. 6) may be attributed to the effect of the deuterium molecule acting as the third body in reaction [9]. The third body requirement is probably more stringent in this reaction than in reaction [10]. The reason for the increase in deuterium number of the ethanes with pressure is not apparent. It conceivably could be due to excited ethyl radicals formed in reaction [1*a*] reacting with D_2.

The experiments in which the atom detector was kept in the reaction chamber also suggested that the methanes are formed very near the ethylene inlet tube while the ethanes are formed lower in the reaction zone. Thus the methanes were unaffected by the presence of the detector while the deuteration of the ethanes was increased.

Although this scheme is qualitatively in accord with the experimental observations, no account has yet been taken of the possibility that the reaction rates of atoms and radicals may depend on their isotopic composition. If the rates were independent of isotopic composition the deuterium distribution for any given product should be controlled by simple probability, and depend solely on the relative amounts of H- and D-atoms available for reaction. For example, the plot between the amount of each deuteroethane against the number of deuterium atoms in the molecule should give a simple probability curve, the maximum of which should correspond to the deuterium number. The heterogeneous reaction between ethylene and molecular deuterium over a heated nickel catalyst (14, 25) produced deuteroethanes which fitted a simple probability curve with a maximum at $C_2H_4D_2$. Keii, however, has pointed out (13) that this agreement may have been largely fortuitous. In the present investigation the less deuterated products were more abundant than would be expected on probability grounds.

Further evidence for the dependence of reaction rate on isotopic constitution was obtained from experiments in which H-atoms were reacted with ethylene-d_4. In the reaction between D-atoms and C_2H_4, the most abundant methane produced was CD_3H. In the reaction between H-atoms and C_2D_4 the most abundant methane was CH_2D_2, and not CDH_3. Similarly, although C_2H_6 was the ethane formed in greatest amount in most of the $D+C_2H_4$ experiments, C_2D_6 was *not* the most abundant ethane formed under similar conditions in the reaction of H with C_2D_4. Owing to the large number of steps required to form some of the products, even a small difference in reaction rates of isotopically different species could account for the differences in the isotopic distributions of the products.

Because of the complexity of the reaction no decision could be reached as to what extent the deuterium distribution was due to the earlier explanation based on the flow pattern in the reaction zone, and to what extent it was due to differences in reaction rates between variously deuterated intermediates.

REFERENCES

1. AMDUR, I. J. Am. Chem. Soc. 57: 856. 1935.
2. BERLIE, M. R. and LEROY, D. J. J. Chem. Phys. 20: 200. 1952.
3. BERLIE, M. R. and LEROY, D. J. Discussions Faraday Soc. 14: 50. 1953.
4. CALLEAR, A. B. and ROBB, J. C. Trans. Faraday Soc. 51: 638. 1955.
5. DARWENT, B. DE B. and ROBERTS, R. Discussions Faraday Soc. 14: 55. 1953.
6. DIBELER, V. H. *et al.* J. Research Natl. Bur. Standards, 53: 107. 1954.
7. DINGLE, J. R. and LEROY, D. J. J. Chem. Phys. 18: 1632. 1950.
8. FRANCIS, A. W. and LUCASIEWICZ, S. J. Ind. Eng. Chem. Anal. Ed. 17: 703. 1945.
9. GROSSE, A. V. *et al.* Science, 113: 1. 1951.
10. IVIN, K. J. and STEACIE, E. W. R. Proc. Roy. Soc. (London), A, 208: 25. 1951.
11. KAPLAN, L. J. Am. Chem. Soc. 76: 1448. 1954.
12. KAUFMAN, S. and LIBBY, W. F. Phys. Rev. 93: 1337. 1954.
13. KEII, T. J. Chem. Phys. 23: 210. 1955.
14. MARKHAM, M. C., WALL, M. C., and LAIDLER, K. J. J. Chem. Phys. 20: 1331. 1952.
15. MELVILLE, H. W. and ROBB, J. C. Proc. Roy. Soc. (London), A, 196: 494. 1949.
16. MOORE, W. J. and TAYLOR, H. S. J. Chem. Phys. 8: 504. 1940.
17. POOLE, H. G. Proc. Roy. Soc. (London), A, 163: 424. 1937.
18. RICE, F. O. and TELLER, E. J. Chem. Phys. 6: 489. 1938.
19. SCHIFF, H. I. Discussions Faraday Soc. 14: 121. 1953.
20. SCHISSLER, D. O., THOMPSON, S. O., and TURKEVITCH, J. Discussions Faraday Soc. 10: 46. 1951.
21. SCHULER, K. E. and LAIDLER, K. J. J. Chem. Phys. 17: 1212. 1949.
22. SMITH, W. V. J. Chem. Phys. 11: 110. 1943.
23. STEACIE, E. W. R., ALEXANDER, W. A., and PHILLIPS, N. W. F. Can. J. Research, B, 16: 314. 1938.
24. TURKEVITCH, J., SCHISSLER, D. O., and IRSA, P. J. Phys. Chem. 55: 1078. 1951.
25. WILSON, J. N. *et al.* Ind. Eng. Chem. 45: 1480. 1953.

THE REACTIONS OF ACTIVE NITROGEN WITH ALKYL CHLORIDES[1]

By B. Dunford,[2] H. G. V. Evans,[2] and C. A. Winkler

ABSTRACT

The reactions of active nitrogen with methyl, ethyl, vinyl, propyl, and isopropyl chlorides yielded hydrogen cyanide and hydrogen chloride as the main products. Small amounts of cyanogen and a polymer were formed from all the halides, and all except methyl chloride also yielded small amounts of C_2 and C_3 hydrocarbons. The observed changes in amounts of products recovered with different reactant flow rates were characteristic of a fast reaction in which complete consumption of either reactant occurs when the other is present in excess. Mechanisms for the reactions are suggested on the basis that relatively long-lived complexes are formed in the initial attack of a nitrogen atom on the alkyl chloride.

INTRODUCTION

A number of reactions of active nitrogen, produced in a condensed electrical discharge, have been studied in this laboratory. Emphasis has been placed largely, though not exclusively, on the reactions with hydrocarbons (2, 3, 9, 11, 13, 14, 17, 18, 19). Hydrogen cyanide is the main nitrogen-containing product of these reactions, which implies that the reactions with saturated hydrocarbons involve direct attack at a completely shielded carbon atom. They are much faster than would be expected from the principle of least motion enunciated by Rice and Teller (15).

In an attempt to elucidate further the mechanism of the reactions, it appeared desirable to investigate the effect of a chlorine substituent on the reactivity. Accordingly, the reactions of active nitrogen with methyl, ethyl, vinyl, propyl, and isopropyl chlorides have been studied.

EXPERIMENTAL

The reactions were studied with conventional fast-flow techniques (11). Active nitrogen was produced by a condensed discharge and mixed with the halides in a reaction vessel that was sufficiently far from the discharge tube to prevent back diffusion into the discharge. The flow and activation of the nitrogen were kept constant in experiments with a given halide and the effects of change in flow rate of the halide determined. The reaction vessel could be surrounded by a furnace to study the effect of temperature. Condensable products were trapped with the usual arrangement of liquid air traps, and were analyzed by low temperature fractionation (12) and with a mass spectrometer.[3] The hydrogen cyanide, cyanogen, and hydrogen chloride produced in the reactions were estimated by titration (16, 20). The hydrogen produced in the reaction with methyl chloride was determined mass spectrometrically on samples of the gas issuing from the vacuum pump.

[1]*Manuscript received March 28, 1956.*
Contribution from the Physical Chemistry Laboratory, McGill University, Montreal, Quebec, with financial assistance from the National Research Council of Canada.
[2]*Holders of National Research Council Studentships and Fellowships.*
[3]*The authors are indebted to Dr. H. I. Schiff, of this department, for the mass spectrometer analyses.*

RESULTS

All the reactions produced a peach-colored flame of fairly high luminosity, which was confined to the upper part of the reaction vessel at the higher flow rates.

The main products of all the reactions were hydrogen cyanide and hydrogen chloride; small amounts of cyanogen were also formed. In all the reactions, significant amounts of a brown polymer were formed on the walls of the reaction vessel but not in the traps. This polymer was quite inert, and had properties somewhat resembling those of paracyanogen. Its composition varied appreciably with the different alkyl chlorides and to a lesser extent with different flow rates of a given alkyl chloride. It contained nearly equal amounts of carbon and nitrogen (on a mole basis) together with smaller amounts of chlorine and hydrogen.

The formation of polymer on the walls of the reaction vessel made it difficult to obtain reproducible results at higher flow rates. (The concentration of active nitrogen is very sensitive to wall conditions, and the polymer itself was probably formed by a wall reaction.)

Methyl Chloride

The rates of production of hydrogen cyanide, hydrogen chloride, and hydrogen, and the rate of consumption of methyl chloride, all varied linearly with methyl chloride flow rate up to a flow rate of about 3×10^{-6} mole/sec., and were independent of temperature in this linear region (Fig. 1). In this

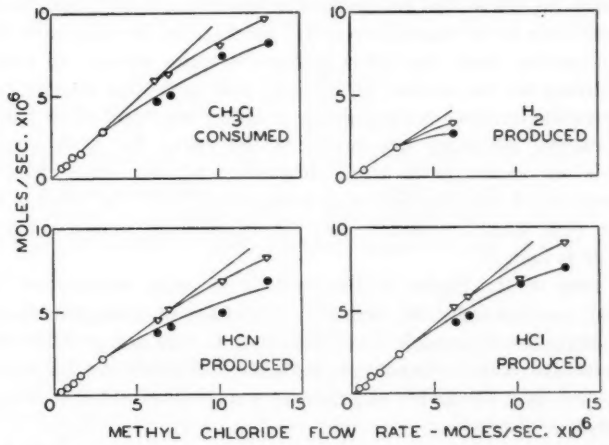

FIG. 1. Relations between methyl chloride flow rate and rates of methyl chloride consumption and product formation.

region, only 89% of the methyl chloride was consumed, independently of flow rate or temperature. At higher flow rates the yields of products approached a limiting value which was the greater, the higher the temperature.

The curves in Fig. 1 have only qualitative significance, since deposition of polymer changed the surface condition of the thermocouple wells at the center

and top of the reaction vessel and the thermocouple readings were therefore only a rough measure of the reaction temperature. Quite marked changes in the readings were observed both during an experiment and in successive experiments. In addition, the reaction was sufficiently exothermic to create marked temperature gradients in the reaction vessel. The temperatures at the center of the reaction vessel have therefore been recorded, rather arbitrarily, as "low" and "high" corresponding roughly to 100° and 300°C. respectively.

The amount of cyanogen formed was quite erratic, but it was always less than 3% of the methyl chloride consumed. A careful search failed to reveal the presence of any cyanogen chloride, methane, or ethane in the products.

Ethyl, Vinyl, and Propyl Chlorides

In these reactions, small amounts of hydrocarbons were formed as secondary products. Vinyl chloride gave only acetylene, ethyl chloride gave a mixture of C_2 hydrocarbons, and the propyl chlorides gave mixtures of C_2 and C_3 hydrocarbons. The composition of these products did not change significantly with flow rate in the limited range where samples sufficiently large for analysis could be recovered. Typical values are: for ethyl chloride, 94% ethylene, 5% acetylene, 1% ethane; for *n*-propyl chloride, 34% propylene, 41% ethylene, 17% acetylene, 6% propane, 2% ethane; for isopropyl chloride, 42% propylene, 33% ethylene, 18% acetylene, 6% propane, 1% ethane.

Figs. 2 and 3 show the changes in amounts of products recovered with different reactant flow rates. The different limiting yields with the various reactants may be attributed to changes in operating conditions, particularly the wall conditions in the reaction vessel. The shape of the curves for hydrogen cyanide production from the alkyl halides is quite similar to that of the analogous curves for the olefins (9, 17, 18), and is typical of a fast reaction in which there is complete consumption of either reactant when the other is present in excess. Although the break in the curve for hydrogen cyanide production is not as sharp for vinyl chloride as for the other chlorides, the general character of the reaction and comparison with the similar behavior of acetylene (19) leave no doubt that the reaction of active nitrogen with vinyl chloride is fast.

The reactions of the higher halides were even more exothermic than the reaction with methyl chloride, and the difficulties of temperature measurement were aggravated to such an extent that it was not possible to obtain meaningful results. A few experiments with ethyl chloride in a heated reaction vessel indicated that the yields of products were independent of temperature within experimental error.

DISCUSSION

There is some evidence that active nitrogen contains more than one chemically reactive species (7, 8, 14). However, considerations outlined in a further paper (4) suggest that one species, probably atomic nitrogen, is responsible for most of the reaction observed with the hydrocarbons and related compounds, and it is on this basis that the present results will be discussed.

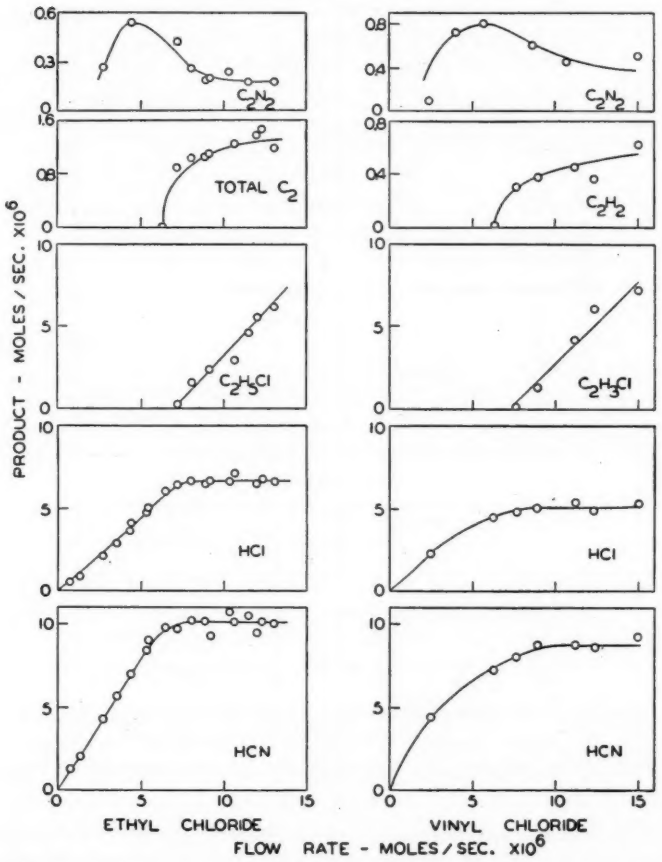

FIG. 2. Relations between rates of product formation and flow rates of ethyl and vinyl chlorides.

The observed initial linear variation in yield of hydrogen cyanide with methyl chloride flow rate, and its temperature independence, appear to be possible only for a fast reaction. It can be estimated from the experimental conditions that this behavior must correspond to a collision yield greater than about 5×10^{-5}. Similar results would probably be obtained for the higher halides, but the low flow rate region was not investigated as thoroughly for these reactions.

The recovery of methyl chloride at low flow rates might be attributed mainly to decomposition of nitrogen atom – methyl chloride complexes back to methyl chloride and nitrogen on the cold surface of the trap, although some channelling of methyl chloride in the flow through the reaction vessel might have occurred. Competition between a fast reaction of nitrogen atoms with methyl chloride and fast recombination of nitrogen atoms catalyzed by methyl

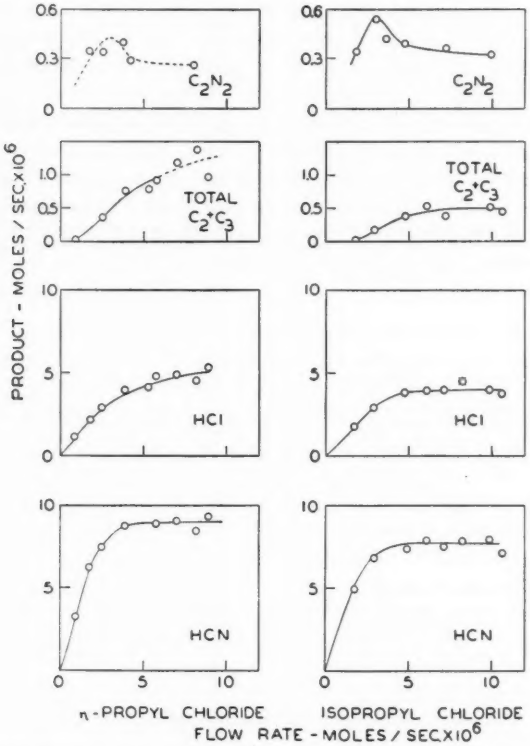

FIG. 3. Relations between rates of product formation and flow rates of propyl and isopropyl chlorides.

chloride or one of the reaction products can explain the observation that the yields were independent of temperature at low flow rates and increased with temperature at high flow rates. Similar, but more pronounced effects have been found in the reaction of methyl cyanide with active nitrogen where the temperature measurements were more trustworthy (5). A mathematical treatment of the problem is in preparation.

The features of the methyl chloride reaction outlined above suggest that a relatively long-lived methyl chloride – nitrogen atom complex was formed. The assumption that such complexes are formed in the reactions of the higher halides appears to be necessary to explain the formation of the secondary products. Further, the close similarity of the reactions of the higher halides to those of the unsaturated hydrocarbons suggests the possibility that hydrogen chloride is eliminated during formation of the complex, to yield a nitrogen atom complex with the corresponding unsaturated hydrocarbon. This is more fully discussed in the subsequent paper (4) on the basis of which it is possible to suggest the following mechanisms for the formation of the products obtained from the various active nitrogen – alkyl chloride reactions:

Methyl Chloride

$$CH_3Cl + N \rightarrow N.CH_3Cl \rightarrow HCN + HCl + H$$
$$H + H \rightarrow H_2$$

Ethyl Chloride

$$C_2H_5Cl + N \rightarrow N.C_2H_5Cl \rightarrow HCl + N.C_2H_4$$
$$N.C_2H_4 \rightarrow HCN + CH_3$$
$$CH_3 + N \rightarrow HCN + 2H$$
$$N + N.C_2H_4 \rightarrow N_2 + C_2H_4$$
$$N + N.C_2H_4 \rightarrow N_2 + C_2H_4^* \text{ (possibly } \dot{C}H_2\dot{C}H_2^*)$$
$$C_2H_4^* \rightarrow H_2 + C_2H_2^* \text{ (possibly } \dot{C}H{=}\dot{C}H^*)$$

Propyl Chloride

$$C_3H_7Cl + N \rightarrow N.C_3H_7Cl \rightarrow HCl + N.C_3H_6$$
$$N.C_3H_6 \rightarrow HCN + C_2H_4 + H$$
$$N.C_3H_6 \rightarrow N_2 + C_3H_6$$
$$N + N.C_3H_6 \rightarrow N_2 + C_3H_6^* \text{ (possibly } CH_3{-}\dot{C}H{-}\dot{C}H_2^*)$$
$$C_3H_6^* \rightarrow CH_3{-}CH^{*}{:} + CH_2$$
$$CH_3{-}CH^{*}{:} \rightarrow C_2H_4$$
$$CH_3{-}CH^{*}{:} \rightarrow C_2H_2 + H_2$$

Vinyl Chloride

$$CH_2CHCl + N \rightarrow N.CH_2CHCl \rightarrow HCl + N.C_2H_2$$
$$N.C_2H_2 + N \rightarrow N_2 + C_2H_2$$
$$N + N.C_2H_2 \rightarrow 2HCN$$

It will be noted that the formation of the secondary hydrocarbon products is accompanied by recombination of two nitrogen atoms. This recombination appears to be the only source of sufficient energy to form these products and, for their formation in significant amounts, it is obviously necessary that a relatively long-lived complex should be formed. Thus, the higher halides might be expected to show the same change in yields with temperature at higher flow rates that was observed for methyl chloride. In spite of experimental difficulties, there was some indication that the effect was less marked for the higher halides. This might indicate a lower activation energy for these reactions. On the other hand, the spontaneous decomposition of complexes containing more than one carbon atom would make available carbon-containing intermediates that should react very rapidly with nitrogen atoms (1) and the direct reaction should be favored over the recombination.

The cyanogen produced in the alkyl chloride reactions was probably formed by the combination of two cyanogen radicals. The recombination of two nitrogen atoms makes available some 225 kcal. of energy, and there is a quite high probability that a substantial part of this energy is transferred from the newly forming N_2 molecule to the internal degrees of freedom of the rest of the complex (4). This can bring about dissociation into very reactive fragments. For methyl chloride, for example, reactions of the following type are all exothermic:

$$N + N.CH_3Cl \rightarrow N_2 + CH_2Cl + H$$
$$N + N.CH_3Cl \rightarrow N_2 + HCl + CH + H_2$$
$$N + N.CH_3Cl \rightarrow N_2 + CH_2 + H + Cl.$$

It seems rather likely that cyanogen radicals will be formed by reaction of such fragments with still another nitrogen atom, e.g.

$$N + CH_2 \rightarrow CN + H_2$$
$$N + CH \rightarrow CN + H.$$

These reactions are sufficiently exothermic to give the electronically excited cyanogen radicals that are responsible for emission of the reaction flames (4). For the higher halides it is possible that some cyanogen was formed directly by such reactions as

$$N + N.C_2H_4 \rightarrow (CN)_2 + 2H_2.$$

However, this type of reaction involves a great deal of rearrangement, and more likely are reactions such as

$$N + N.C_2H_4 \rightarrow N + 2CH_2$$
$$N + CH_2 \rightarrow CN + H_2$$
$$2CN \rightarrow (CN)_2.$$

The fact that cyanogen production passes through a maximum at low chloride flow rates seems to be good evidence that more than two atoms of nitrogen are involved in its formation. If only two nitrogen atoms were involved, cyanogen production from the ethyl chloride reaction should be similar to the ethylene production, at least at high flow rates where the amount of ethylene reacting with nitrogen atoms can be neglected.

According to the mechanism suggested above, the production of unsaturated hydrocarbons should pass through a maximum as the chloride flow rate is increased. The chloride flow rate at which this maximum should occur will depend upon the relative rates of the reactions of the chlorides and the unsaturated hydrocarbons with nitrogen atoms. Apparently, the maximum yields were not attained in the region studied and this, together with the observation that little or no unsaturated hydrocarbons were recovered at low flow rates, gives some indication that nitrogen atoms react faster with the unsaturated hydrocarbons than with the alkyl chlorides.

The presence of highly reactive intermediate species in the reactions of the halides with nitrogen atoms, and particularly the presence of free CN radicals, probably accounts for the formation of polymer by a wall reaction involving mainly CN radicals with smaller amounts of the other intermediates. This would mean that recombination of two nitrogen atoms was necessary for polymer formation, in agreement with the observation that the polymer was formed near the top of the reaction vessel, especially at higher flow rates. It would also account for the differences in composition of the polymer from the different reactions.

The mechanisms outlined above involve production of hydrogen atoms, and the small amounts of saturated hydrocarbons formed in the reactions of the higher halides probably resulted mainly from hydrogenation of the correspond-

ing olefin. Failure to detect methane as a product indicates that the concentration of atomic hydrogen was low in all the reactions. Hydrogen chloride (10) and methyl cyanide (6) are efficient recombination catalysts for hydrogen atoms. It seems quite possible that alkyl halides would behave like methyl cyanide in this respect, and in any event there was probably enough hydrogen chloride formed in the reactions to keep the concentration of hydrogen atoms at a low value.

The occurrence of secondary reactions involving more than one nitrogen atom makes it necessary to be cautious in drawing conclusions about the rate of the primary reaction, particularly since many of the products of these secondary reactions are known to react fast with nitrogen atoms. However, it seems likely (4) that the main energy barrier for the reactions is surmounted when the complex is formed. This conclusion would have to be modified if the secondary reactions formed products capable of reacting with alkyl chlorides to set up a chain reaction. For the methyl chloride reaction, hydrogen and chlorine atoms are possible chain carriers. However, the absence of any detectable amounts of methane, ethane, chlorine, cyanogen chloride, or ethylene chloride in the products makes it seem unlikely that there was an important contribution from chain reactions carried by hydrogen or chlorine atoms. It is possible to write a reaction scheme for a chain carried by CN radicals:

$$N + CH_3Cl \rightarrow N.CH_3Cl$$
$$N + N.CH_3Cl \rightarrow N_2 + CH_2Cl + H$$
$$N + CH_2Cl \rightarrow CN + HCl + H$$
$$CN + CH_3Cl \rightarrow HCN + CH_2Cl.$$

The third reaction is exothermic and should be very fast (4), but it is doubtful that the last reaction would be fast enough to be effective as a chain carrier. Absence of a significant contribution from a chain reaction is also indicated by the reactions of the higher halides. In these, the recovery of unsaturated hydrocarbons with the same number of carbon atoms as the parent halide provides good evidence that the main path of the reaction was not hydrogen or chlorine atom abstraction followed by nitrogen atom attack on the resulting radical.

It appears probable, from the foregoing discussion, that the reactions of nitrogen atoms with alkyl chlorides involve direct attack at a shielded carbon atom without requiring a high activation energy.

REFERENCES

1. ARMSTRONG, D. A. and WINKLER, C. A. Can. J. Chem. 33: 1649. 1955.
2. BACK, R. A. and WINKLER, C. A. Can. J. Chem. 32: 718. 1954.
3. BLADES, H. and WINKLER, C. A. Can. J. Chem. 29: 1022. 1951.
4. EVANS, H. G. V., FREEMAN, G. R., and WINKLER, C. A. Can. J. Chem. In press.
5. FORST, W. and WINKLER, C. A. J. Phys. Chem. In press.
6. FORST, W. and WINKLER, C. A. Can. J. Chem. 33: 1814. 1955.
7. FREEMAN, G. R. and WINKLER, C. A. J. Phys. Chem. 59: 371. 1955.
8. FREEMAN, G. R. and WINKLER, C. A. Can. J. Chem. 33: 692. 1955.
9. GESSER, H., LUNER, C., and WINKLER, C. A. Can. J. Chem. 31: 346. 1953.
10. GLASSTONE, S., LAIDLER, K. J., and EYRING, H. The theory of rate processes. McGraw-Hill Book Company, Inc., New York. 1941.

11. GREENBLATT, J. and WINKLER, C. A. Can. J. Research, B, 27: 721. 1949.
12. LEROY, D. J. Can. J. Research, B, 28: 492. 1950.
13. ONYSZCHUK, M., BREITMAN, L., and WINKLER, C. A. Can. J. Chem. 32: 351. 1954.
14. ONYSZCHUK, M. and WINKLER, C. A. J. Phys. Chem. 59: 368. 1955.
15. RICE, F. O. and TELLER, E. J. Chem. Phys. 6: 489. 1938.
16. SCOTT, W. W. Standard methods of chemical analysis. D. Van Nostrand Company, Inc., New York. 1920.
17. TRICK, G. S. and WINKLER, C. A. Can. J. Chem. 30: 915. 1952.
18. VERSTEEG, J. and WINKLER, C. A. Can. J. Chem. 31: 1. 1953.
19. VERSTEEG, J. and WINKLER, C. A. Can. J. Chem. 31: 129. 1953.
20. WALLIS, T. Ann. 345: 353. 1906.

THE VIBRATIONAL SPECTRA OF ACETALDEHYDE AND ACETALDEHYDE-d_1 [1]

By J. C. Evans[2] and H. J. Bernstein

ABSTRACT

The Raman spectra of liquid CH_3CHO and CH_3CDO were obtained photoelectrically and depolarization ratios measured. Infrared spectra of the vapors and solids were also obtained. A vibrational assignment is given and the spectra correlated. The vibrational spectra of the acetyl halides reported in the literature are also correlated.

Several infrared and Raman investigations of acetaldehyde and acetaldehyde-d_4 have been made but complete agreement as to the vibrational assignments has not been reached (3, 4, 6, 7, 8, 9, 12, 14). Pitzer and Weltner's reassignment (9) is consistent with the thermodynamic data but has not been definitely established. The reported depolarization ratios of some of the Raman bands (4) are inconsistent with this assignment and, recently, a different assignment for the low lying bands has been proposed (6).

The most promising source of further relevant information seemed to be the vibrational spectrum of acetaldehyde-d_1 (CH_3CDO) and an investigation of the Raman and infrared spectra of this molecule has been made. The Raman spectrum in the liquid phase and the infrared spectra in the vapor and solid phases have been examined. Similar studies were made on acetaldehyde.

The vibrational assignment for acetaldehyde which is indicated by these results is very similar to that made by Pitzer and Weltner; the revisions are mainly in the higher wave number region and have negligible effect upon the calculated thermodynamic functions.

The spectra of the related molecules, the acetyl halides, may now be correlated with some success.

EXPERIMENTAL

Acetaldehyde (Eastman Kodak) was refractionated. Acetaldehyde-d_1 was prepared and fractionally distilled by Dr. L. C. Leitch.

A White grating spectrometer with photoelectric recording (16) was used to obtain the Raman spectra of the two compounds in the liquid phase. Depolarization ratios were measured (2) and corrected for convergence error (10). The infrared spectra were obtained with a Perkin Elmer Model 12C (double pass) spectrometer with LiF, CaF_2, NaCl, and KBr optics. A low temperature cell of the type described by Wagner and Hornig (15) was used to measure the infrared spectra of the solids.

The spectra are illustrated in Figs. 1 to 4 and the data are collected in Tables I and II.

[1]*Manuscript received April 16, 1956.*
Contribution from the Division of Pure Chemistry, National Research Council, Ottawa, Canada. Issued as N.R.C. No. 3998.
[2]*National Research Council Postdoctorate Research Fellow 1953–55.*

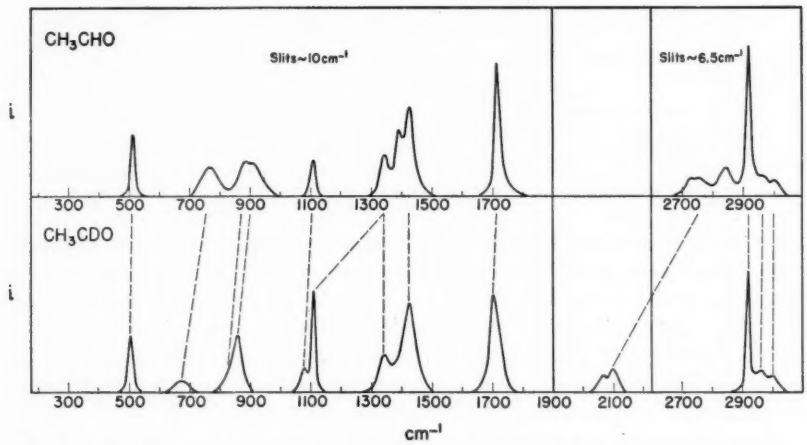

FIG. 1. The Raman spectra of CH_3CHO and CH_3CDO in the liquid phase. Intensity scales are arbitrary and are not strictly comparable. Above 1900 cm.$^{-1}$, the intensity scales are reduced by a factor of five. Excitation by 4358 Å Hg.

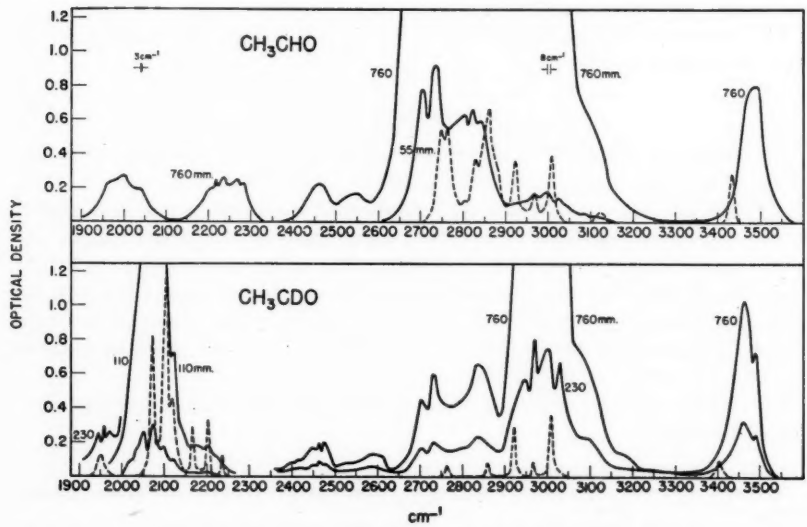

FIG. 2. The infrared spectra of CH_3CHO and CH_3CDO, 3600-1900 cm.$^{-1}$.
Vapor spectra: cell length =.10 cm.; temperature 20° C. Vapor pressures are given on the curves.
Solid spectra: broken lines. Films of unknown thicknesses at −180° C.

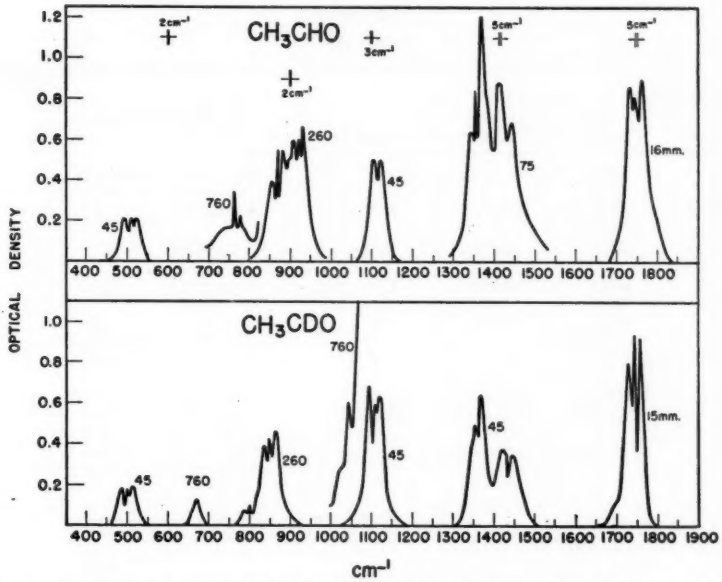

FIG. 3. The infrared spectra of CH_3CHO and CH_3CDO. Vapor spectra between 1900 and 450 cm.$^{-1}$. Vapor pressures are given on the curves. 10 cm. cell at 20° C.

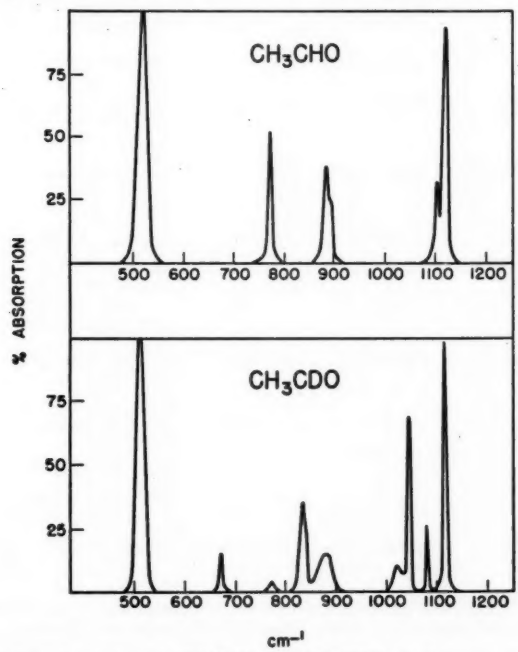

FIG. 4. The infrared spectra of CH_3CHO and CH_3CDO. Solid spectra 1200–450 cm.$^{-1}$. Films of unknown thickness at −180° C.

TABLE I

CH_3CHO

Infrared		Raman		Assignment
Vapor	Solid	liquid	$\rho_{corr.}$	
3485	3432			$2\times1743 = 3486$ (A')
~3120	3125			$1743+1400 = 3143$ (A')
3024	3007	3001	0.87	a''; $\nu(CH_3)$
2996				
2967	2967	2964	~0.76	a' ; $\nu(CH_3)$
	2920	2917	0.10	a' ; $\nu(CH_3)$
2840	2876			a' ; $\nu(CH)$
2822	2859	2843	0.22	
2804	2827 sh			$2\times1400 = 2800$ (A')
				$2\times1352 = 2704$ (A')
2736	2762	2751	0.31	and other combinations of
2704	2749	2731	0.36	1352, 1400, and 1430 cm.$^{-1}$
2550				$1743+(830) = 2573$ (A'')
2464				$1352+1111 = 2463$ (A')
2282				$919+1352 = 2271$ (A')
2268				
2236				
2218				$2\times1111 = 2222$ (A')
2206				
2040				$919+1111 = 2030$ (A')
2000				
1960				
1790 sh				$2\times919 = 1838$ (A')
		~1740 sh	?	$919+(830)$
1761				
1743		1714	0.33	a'; $\nu(C{=}O)$
1732				
1441	1422	1426	~0.8	a' and a''; def. (CH_3)
~1420				
~1410				
	~1390	1391	~0.65	a'; C—H rocking
~1390				
1369				
1352	1349	1342	~0.8	a'; def. (CH_3)
1341				
1122	1120	1109	0.34	a'; ν(C—C)
1104				
	1103			$888+$tors. (~230 cm.$^{-1}$)
930				
919	888 sh	911	0.45	a'; CH_3 rocking
909				
880				
867	883	885	p. or dp. (?)	a''; CH_3 rocking
853				
777				A''; $509+$tors. (?)
763	772	767	0.87	a''; C—H wagging
521				
509	517	512	0.40	a'; δC—C=O
493				

In Tables I and II estimated positions are used for the coupled modes in determining the wave numbers of overtones and combination tones. These estimated values are bracketed.

TABLE II
CH_3CDO

Infrared		Raman		Assignment
Vapor	Solid	liquid	$\rho_{corr.}$	
3490				
	3405			$2\times1743 = 3486$ (A')
3462				
3173				$1743+1431 = 3174$ (A' and/or A'')
3096				$1743+1353 = 3096$ (A')
3028	3008	2998	~0.86	a''; $\nu(CH_3)$
3000				
2970	2968	2965	~0.76	a' ; $\nu(CH_3)$
2946				
	2921	2917	0.13	a' ; $\nu(CH_3)$
2840	2859			$2\times1431 = 2862$ (A' and/or A'')
2733	2764			$1353+1431 = 2784$ (A' and/or A'')
2704				$2\times1353 = 2706$ (A')
2600				$1743+(890) = 2633$ (A')
2528				$1431+1109 = 2540$ (A', A'')
2476				
2465				$1353+1109 = 2462$ (A')
2450				
2416				
				$1743+668 = 2411$ (A'')
2400				
2222	2234			$1431+802 = 2233$ (A' and/or A'')
2200	2202			$2\times1109 = 2218$ (A')
2175	2165			$1346+833 = 2179$ (A'')
2148				$(1040)+1109 = 2149$ (A')
	2117 sh			$1116+2\times513 = 2139$ (A')
2120				Fermi doublet
	2103	2097	0.35	
2096				$2\times(1040)$
2071				a'; ν(C—D)
	2071	2069	0.36	
2050				
2036				
				$1353+668 = 2021$ (A'')
2018				
1970				
1958	1950			$1109+(890) = 1999$ (A')
1945				
		1714 sh	?	$(810)+(890) = 1700$ (A'')
1757				
1743	1690	1702	0.21	a'; ν(C=O)
1730				
1442				
	1417	1426	0.80	a'; a''; CH_3 def.
1420				
1366				
1353	1346	1343	0.68	a'; CH_3 def.
~1345				
1244 v.v.w.				$2\times668 = 1236$ (A')
1192 v.v.w.				?
1118				
1109	1116	1111	0.12	a'; C—D rocking
1094				
Overlapped	1081	1080	0.50	a'; ν(C—C)
1043 v.w.	1040			833+tors. (?)
1025				
	1023			$2\times513 = 1026$ (A')

TABLE II (*Concluded*)

Infrared		Raman		Assignment
Vapor	Solid	liquid	$\rho_{corr.}$	
924 v.v.w. 913				668+tors. (?)
865 849 837	~880	858	0.46	a'; CH_3 rocking
816 802 799	833	~820 (overlapped)	?	a''; CH_3 rocking
	770			?
668	672	674	~0.86	a''; C—D wagging
513 500 487	513	505	0.36	a'; δC—C=O

DISCUSSION OF RESULTS

Following previous authors, symmetry C_s is assumed for both molecules. Each molecule should have ten a' and five a'' fundamental modes of vibration. All modes should be infrared and Raman active, the Raman bands arising from the a' modes being polarized and those from the a'' modes being depolarized. Moments of inertia were calculated* and the structures expected for the principal types of infrared bands were determined according to Badger and Zumwalt (1), some extrapolation of their results being necessary in this case. The a'' modes should give rise to bands with strong central peaks (*C* type) while the a' modes should give rise to hybrid bands, i.e. bands which consist of doublets with or without a weak central peak. The separation of the doublets was calculated, using the symmetric rotator formulae (5), to be ~27–28 cm.$^{-1}$ for both CH_3CHO and CH_3CDO. The symmetric top approximation is not a very good one in these cases but several doublets of approximately this separation were observed.

The C—H Stretching Modes

Comparison of the spectra of the two molecules in the 3000 cm.$^{-1}$ region gives immediately those bands which arise from the aldehyde CH group and the overtone and combination tone levels which are in Fermi resonance with it. The infrared spectra of the vapors show overlapping bands which are not readily identified individually but the solid spectra and the Raman spectra of the liquids are more clearly resolved. The depolarization ratios in the Raman spectra distinguish between the a' and a'' asymmetric CH_3 stretching modes at 2965 and 3001 cm.$^{-1}$ respectively. Previous assignments in this region are markedly different.

**Dimensions used in calculating the moments of inertia were: C—H=C—D = 1.09 Å; C—C = 1.50 Å; C=O = 1.22 Å; angle CHO = 120°; CH_3 angles tetrahedral (13).*

C—D Stretching Mode

Strong Fermi resonance between the fundamental and an overtone or combination tone is evident from the appearance of two almost equally intense, similarly polarized bands in the Raman spectrum of liquid CH_3CDO. The infrared spectrum of the solid shows similar features with further overtone or combination bands in the vicinity, but a reduction in the extent of the resonance is indicated by the infrared spectrum of the vapor. A band with doublet structure of separation $\sim$21 cm.$^{-1}$ is the pronounced feature present. The identity of the level which resonates with the fundamental ν(CD) will be discussed in conjunction with the assignment of the modes in the 1000 cm.$^{-1}$ region.

Region below 1800 cm.$^{-1}$

The new data did not warrant any major change in Pitzer and Weltner's assignment of the fundamentals which lie in this region, but they did provide support in some instances and confirmation in others. Fig. 1, giving the Raman spectra of the two liquids, shows that the in-plane aldehyde C—H rocking mode is at 1391 cm.$^{-1}$, and in CH_3CDO it is at 1111 cm.$^{-1}$. In the infrared spectra of the vapors, the bands overlap but it is apparent that the most pronounced difference between the two spectra in the CH_3 deformation region is at $\sim$1410 cm.$^{-1}$. The aldehyde group CH rocking mode is therefore identified.

The out-of-plane wagging modes of the aldehyde C—H and C—D groups may confidently be assigned to the two depolarized Raman bands at 767 and 674 cm.$^{-1}$ respectively. Both bands are very weak in the infrared but both have the expected *C* type structure. It has been suggested recently that this C—H mode in CH_3CHO coincides with the skeletal bending mode near 500 cm.$^{-1}$, part of the evidence for this being the reported depolarization ratio of 6/7 for the Raman band (4). However, this band, which was hardly affected by deuterium substitution at the aldehyde C—H group, was observed here to be polarized in both molecules.

The remaining bands, in the 800–1200 cm.$^{-1}$ region, may be readily correlated in the two molecules but for an understanding of the differences between the spectra it is necessary to postulate coupling of the various vibrational modes.

The *C* type bands at 867 cm.$^{-1}$ in CH_3CHO and at 802 cm.$^{-1}$ in CH_3CDO arise from the one a'' mode which is expected in this region, a CH_3 rocking mode. The corresponding Raman bands should be depolarized but in both cases overlapping with adjacent polarized bands prevented this from being confirmed. The unexpectedly large difference in position of this band in CH_3CHO and CH_3CDO ($\sim$65 cm.$^{-1}$) may be explained in the following manner. In CH_3CHO coupling of the two a'' modes, C—H wagging and CH_3 rocking, which are both close to 800 cm.$^{-1}$, forces the two energy levels apart, one increasing in wave number and the other decreasing. In CH_3CDO the coupling is removed and the apparent shift in the CH_3 rocking mode is appreciably more than the shift expected for an uncoupled mode of this kind. Two

modes remain to be assigned in this region, the C—C stretching and the CH_3 rocking modes, both being a' modes. The situation is further complicated in CH_3CDO by the presence of the a' mode, C—D rocking in this region. In CH_3CHO there are two bands, the higher of which at 1109 cm.$^{-1}$ in the Raman spectrum has been assigned by Pitzer and Weltner to the ν(C—C) mode. This high value was favored because of the measured, short C—C bond (13). The other band, at 911 cm.$^{-1}$ (Raman), is then the CH_3 rocking mode.

At first sight, comparison of the spectra of CH_3CHO and CH_3CDO would indicate a reversal of this assignment since the band at 911 cm.$^{-1}$ in CH_3CHO is at 858 cm.$^{-1}$ in CH_3CDO and the band at 1109 cm.$^{-1}$ in CH_3CHO is at 1080 cm.$^{-1}$ in CH_3CDO, that is, we have the surprising result that deuterium substitution has a greater effect upon the CH_3 rocking mode than upon the C—C stretching mode. However, if because of this apparent anomaly, the assignments were reversed, a further important feature of the spectrum of CH_3CDO, the Fermi doublet at ~2080 cm.$^{-1}$, would still remain unexplained. Since it is not possible to find a suitable overtone or combination of the observed bands in CH_3CDO to account for this doublet, it must be assumed that the overtone of a perturbed fundamental is involved. A plausible suggestion is that the 1109 cm.$^{-1}$ band in CH_3CHO arises from ν(C—C) and that on deuterium substitution it would fall to ~1050 cm.$^{-1}$. However, interaction with the a' CH_3 rocking mode gives rise to two levels at 1080 cm.$^{-1}$ and 858 cm.$^{-1}$, and thus the unexpectedly large change in the CH_3 rocking mode is explained. An equally plausible explanation is that the main interaction is between the C—D rocking mode and the CH_3 rocking mode, the band at ~2080 cm.$^{-1}$ being then the first overtone of the C—D rocking mode, which, if uncoupled, would lie at ~1050 cm.$^{-1}$. It is noteworthy that in CH_3CHO, ν(C—H) is in strong Fermi resonance with two overtones or combination bands, one of which is very probably the overtone of the C—H rocking mode. However, the assignments of overtone and combination bands in Table II are based on the first explanation, although no serious difficulty would be encountered in using the alternative explanation.

Product rule ratios were calculated* assuming negligible interaction between the torsional modes and the other a'' modes. Theoretical and observed

TABLE III

Species	Theoretical ratio	Observed ratio
a'	1.91	1.89
a''	1.20	1.22*

*The observed ratio is, of course, dependent upon the uncertainties in estimating the position of the unresolved band 825 cm.$^{-1}$

*Moments of inertia used were:
CH_3CHO: $I_A = 16.6$; $I_B = 78.8$; $I_C = 90.1 \times 10^{-40}$ gm. cm.^{2}
CH_3CDO: $I_A = 20.8$; $I_B = 79.0$; $I_C = 94.4 \times 10^{-40}$ gm. cm.^{2}

ratios are collected in Table III. The contribution made by the torsional modes has been factorized out of the theoretical value for the a'' modes (9).

It may be seen from Tables I and II that the interpretation of several weak features required combination with the unobserved torsional mode. Further, in the infrared spectrum of solid CH_3CDO very weak features at 770 and 2117 cm.$^{-1}$, and in the vapor at 1192 cm.$^{-1}$, remain unexplained.

Solid Spectra

Most bands are at different positions in the solid and vapor spectra, some being at higher wave numbers in the solid and others at lower wave numbers. These changes provide an indication of the mechanism of intermolecular interaction between acetaldehyde molecules. The most significant are the changes undergone by the bands arising from the stretching modes of the carbonyl group and the aldehyde C—H and C—D groups. ν(C—H) and ν(C—D) are at higher wave numbers in the solid spectra indicating that hydrogen bonding between the C—H or C—D and the C=O groups is not involved in the interaction. It appears that the interaction is similar to that occurring in formaldehyde (11) and that similar arguments may be invoked to explain the changes in ν(C—H), ν(C—D), and the other vibrational modes with phase change, complicated, however, by the fact that interaction between vibrational modes is present in CH_3CDO.

There is also a difficulty in assigning the strong band at 1040 cm.$^{-1}$ in solid CH_3CDO. Its considerable intensity suggests that it might be a fundamental. However this would lead into a very much more complicated interpretation of the Raman bands and the vapor spectrum than that already given.

TABLE IV

ASSIGNMENT OF RAMAN SPECTRA OF $CH_3—\overset{O}{\overset{\|}{C}}—X$

	X = H	D	F	Cl	Br	I
	νCH_3 2964	2965		2994 p	2991	(3001)
	νCH_3 2917	2917	2940	2938 p	2929	2924
	2843	2097				
	νC—X 2751		815	594 p	555 p	540
	2731	2069				
	νC=O 1714	1702	1840	1802 p	1812 p	1793
	δCH_3 1426	1426	1428	1422 0.9	1418 0.85	1418
a'	δC—X 1391	1111	434 or 590	352 p or 438 p	304 p or 338 p	261 or 285
	δCH_3 1342	1343	1376	1361 p	1352 0.96	1350
	δCH_3 911	858	(1004)	957 p	(938) d?	(904)
	νCC 1109	1080	1106	1100 p	1084 p	1067
	δCCO 512	505	590 or 434	438 p or 352 p	338 or 304	285 or 261
	νCH_3 3001	2998	3038	3018 d	3015	
a''	δCH_3 1426	1426	1428	1422 0.9	1418 0.85	1418
	δCH_3 885	~825		(1032) p?	(988)	(943)
	δCX 767	674	(208)	(260) p?		

Brackets indicate tentative assignments.
Bands definitely polarized or depolarized are marked p *and* d *respectively.*
Numerical values of depolarization ratios are given for some bands where ambiguities might arise, and also question marks.

Vibrational Assignment for Molecules $CH_3C\begin{matrix}O\\ \diagdown\\ X\end{matrix}$

The vibrational assignment for CH_3CHO and CH_3CDO is of great assistance in understanding the spectra of the acid halides for which X is F, Cl, Br, and I. In the case of acetyl chloride the Raman spectrum with depolarization ratios was obtained with the photoelectric instrument previously mentioned. For the fluoride (12), bromide (12), and iodide (7), however, the data were taken from the literature and were in all cases Raman data only. Our results for acetyl chloride are in good agreement with those of Reference 12 with the exceptions that the band at 260 cm.$^{-1}$ is not reported in Reference 12 and that the band at 957 cm.$^{-1}$ was found here to be polarized. In Table IV the spectra of these molecules in the liquid phase are assigned, where possible, according to the schematic representation given in column 1.

REFERENCES

1. BADGER, R. M. and ZUMWALT, L. R. J. Chem. Phys. 6: 711. 1938.
2. EDSALL, J. T. and WILSON, E. B., Jr. J. Chem. Phys. 6: 124. 1938.
3. GERDING, H. and LECOMTE, J. Rec. trav. chim. 58: 614. 1939.
4. GERDING, H., NIJVELD, W. J., and RIJNDERS, G. W. A. Rec. trav. chim. 60: 25. 1941.
5. GERHARD, S. L. and DENNISON, D. M. Phys. Rev. 43: 197. 1933.
6. HADNI, M. A. Compt. rend. 238: 2150. 1954.
7. KOHLRAUSCH, K. W. F. Ramanspektren. J. W. Edwards, Ann Arbor, Mich. 1945. p. 283.
8. MORRIS, J. C. J. Chem. Phys. 11: 230. 1943.
9. PITZER, K. S. and WELTNER, W. J. Am. Chem. Soc. 71: 2842. 1949.
10. RANK, D. H. and KAGARISE, R. E. J. Opt. Soc. Amer. 40: 89. 1950.
11. SCHNEIDER, W. G. and BERNSTEIN, H. J. Trans. Faraday Soc. 52: 13. 1956.
12. SEEWAN-ALBERT, H. and KAHOVEC, L. Acta Phys. Austriaca, 1: 352. 1948.
13. STEVENSON, D. P., BURNHAM, H. D., and SCHOMAKER, V. J. Am. Chem. Soc. 61: 2922. 1939.
14. THOMPSON, H. W. and HARRIS, G. P. Trans. Faraday Soc. 38: 37. 1942.
15. WAGNER, E. L. and HORNIG, D. F. J. Chem. Phys. 18: 298. 1950.
16. WHITE, J. U., ALPERT, N. L., and DEBELL, A. G. J. Opt. Soc. Amer. 45: 154. 1955.

HYDROLYSIS AND HYDRAZINOLYSIS OF ESTERS OF N,N-DIMETHYLDITHIOCARBAMIC ACID

A METHOD FOR THE PREPARATION OF MERCAPTANS[1]

By Marshall Kulka

ABSTRACT

A method has been developed for the preparation of mercaptans from alkyl and aralkyl chlorides. This consists of the condensation of sodium N,N-dimethyldithiocarbamate with halides followed by alkaline hydrolysis or hydrazinolysis of the resulting N,N-dimethyldithiocarbamates (IV). In the hydrazinolysis of IV, an insoluble solid by-product was formed which was identified as 3-hydrazino-4-amino-5-mercapto-4,1,2-triazole. Although this method was found to have wide scope a few failures were encountered. Nitro-derivatives of IV were sensitive to alkali or hydrazine and yielded only tars on attempted degradation. β-Phenoxyethyl N,N-dimethyldithiocarbamates (IX) were found to possess a labile alkyl–oxygen bond so that in the presence of alkali or hydrazine only the corresponding phenols were formed. The labile nature of the alkyl–oxygen bond ceased abruptly when the alkyl chain of IX was increased so that 3-*p*-chlorophenoxypropyl and 4-*p*-chlorophenoxybutyl mercaptans could be prepared in high yields.

In connection with our search for new insecticides a variety of mercaptans were required as intermediates. Of the most useful methods for the preparation of mercaptans even the thiourea method (21) is limited in scope. While thiourea reacts readily with alkyl and aralkyl bromides to form the isothiuronium salts, the reaction with many chlorides is extremely slow or does not proceed at all. Furthermore no nitrobenzyl mercaptans can be prepared by this method. The purpose of this investigation was to find a method for the preparation of mercaptans which would supplement the thiourea method.

v. Braun (5) observed that some aralkyl dithiocarbamates (I), which could be easily obtained from the corresponding aralkyl chlorides, when heated alone or with alkali gave the corresponding mercaptans (II) in high yields. One objection to the use of dithiocarbamates (I) as a source of mercaptans is the

$$\underset{\text{I}}{RS_2CNH_2} \longrightarrow \underset{\text{II}}{RSH} + HSCN$$

fact that they (I) are not stable enough to be purified by distillation. The esters of N,N-dimethyldithiocarbamic acid on the other hand may be distilled without decomposition and therefore they were adopted for degradation studies.

It was found that sodium N,N-dimethyldithiocarbamate (III), which is readily obtained from carbon disulphide, dimethylamine, and sodium hydroxide, reacts easily with chlorides including *p*-nitrobenzyl chloride, aryloxyalkyl chlorides, and *p*-nitrochlorobenzene, compounds which do not react with thiourea under normal conditions. The resulting N,N-dimethyldithiocarbamates (IV) which were obtained in high yields (Table I) were not only

[1]*Manuscript received April 4, 1956.*
Contribution from the Dominion Rubber Company Limited Research Laboratories, Guelph, Ontario.

thermally stable but also exhibited considerable resistance to hydrolysis. Prolonged heating with aqueous acids or in acetic hydrochloric acid solution did not produce any appreciable change while heating with aqueous alkali caused only partial hydrolysis. However when IV was heated under reflux for five hours or longer with five moles of aqueous-alcoholic alkali, the mercaptide (V) was formed in high yield together with sodium sulphide, sodium carbonate, water, and dimethylamine. A variety of mercaptans were successfully prepared (Table II) from the corresponding chlorides by this two stage

$$\underset{\text{III}}{RCl} + NaS_2CN(CH_3)_2 \longrightarrow \underset{\text{IV}}{RS_2CN(CH_3)_2} + NaCl$$

$$\underset{\text{IV}}{IV} + 5NaOH \longrightarrow \underset{\text{V}}{RSNa} + Na_2S + Na_2CO_3 + 2H_2O + NH(CH_3)_2$$

method and a few failures were encountered. *p*-Nitrobenzyl N,N-dimethyldithiocarbamate (IV, R = *p*-$NO_2C_6H_4CH_2$) like *p*-nitrobenzyl isothiuronium chloride is sensitive to alkali and attempted hydrolysis yielded only tar. Also *p*-xylylene bis-N,N-dimethyldithiocarbamate, *p*-$(CH_3)_2NCS_2CH_2C_6H_4CH_2S_2CN(CH_3)_2$, remained unchanged after prolonged heating with excess alkali.

Another method of degradation of IV, namely hydrazinolysis, was investigated. When benzyl N,N-dimethyldithiocarbamate (IV, R = $C_6H_5CH_2$) was heated under reflux with excess hydrazine hydrate in ethanol, an 82% yield of benzyl mercaptan (II, R = $C_6H_5CH_2$) was obtained. In addition a highly insoluble white compound precipitated from the reaction mixture and proved to be 3-hydrazino-4-amino-5-mercapto-4,1,2-triazole (VIII). This (VIII) must

$$\underset{\text{IV}}{RS_2CN(CH_3)_2} + H_2NNH_2 \longrightarrow \underset{\text{II}}{RSH} + \underset{\text{VI}}{H_2NNHCSN(CH_3)_2}$$

$$\underset{\text{VI}}{VI} + H_2NNH_2 \longrightarrow \underset{\text{VII}}{H_2NNHCSNHNH_2} + NH(CH_3)_2$$

$$2\ \underset{\text{VII}}{VII} \longrightarrow \underset{\text{VIII}}{\text{(triazole)}} + H_2NNH_2 + H_2S$$

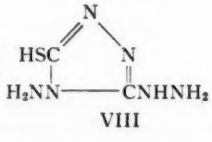

be formed from the thiosemicarbazide (VI) which with hydrazine could produce thiocarbohydrazide (VII) and dimethylamine. Two moles of VII or alternatively one mole of VI and one mole of VII could undergo cyclization to form VIII. That this is the mechanism for the formation of VIII is indicated by the fact that authentic samples of diethyl xanthate or thiocarbohydrazide (19, 20) when heated with hydrazine in ethanol formed VIII.

It is noteworthy that where alkaline hydrolysis failed, hydrazinolysis succeeded in the case of *p*-xylylene bis-N,N-dimethyldithiocarbamate. *p*-Xylylene dimercaptan was obtained in 77% yield after prolonged treatment with hydrazine. However, attempted hydrazinolysis of *p*-nitrobenzyl and *p*-nitrophenyl

N,N-dimethyldithiocarbamates like attempted alkaline hydrolysis yielded only resinous materials.

In view of the known anomalous reactions of some phenoxyalkyl halides it was necessary to investigate the conversion of these halides to the phenoxyalkyl mercaptans. Gordon (10) and Lyle, Dewitt, and Pattison (16) observed that 2-phenoxyethyl halides did not produce the Grignard reagents in the presence of magnesium and ether. Instead the alkyl–oxygen bond was severed and phenol was formed. On the other hand phenoxyalkyl halides with alkyl chain greater than three carbon atoms behaved normally in respect to Grignard formation (16). Also, abnormal results were obtained in the reaction of 2-phenoxyethyl bromide with sodium cyanide but not in the case of 3-phenoxypropyl bromide which yielded γ-phenoxybutyronitrile (10). Crane and Rydon (6) have found that compounds of the type $C_6H_5OCH_2CH_2\overset{+}{S}R_2$, but not of type $C_6H_5OCH_2CH_2SR$, are split by dilute alkali to give initially $R_2\overset{+}{S}CH{=}CH_2$ and sodium phenoxide.

In this investigation all phenoxyalkyl halides reacted normally with III to give the corresponding phenoxyalkyl dimethyldithiocarbamates (Table I). However when the latter were subjected to alkaline hydrolysis or hydrazinolysis it was soon found that 2-phenoxyethyl N,N-dimethyldithiocarbamates (IX) gave no mercaptans. Instead the alkyl–oxygen bond of IX was severed and the corresponding phenol (X) was obtained in high yield. The

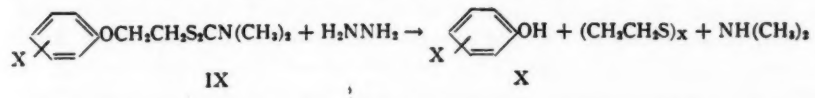

IX X

same results were obtained when β-*p*-*t*-butylphenoxyethyl bromide was treated with thiourea and the resulting isothiuronium salt heated with aqueous alkali. The sulphur–alkyl bond in the compound obtained by substituting sulphur for the oxygen atom in IX is also labile in nature. Thus the reaction of β-*p*-chlorophenylmercaptoethyl N,N-dimethyldithiocarbamate with hydrazine in ethanol gave *p*-chlorothiophenol in 50% yield.

It was expected that steric hindrance might play a part in retarding the cleavage of the alkyl–oxygen bond in IX. Therefore β-(2,4-dichlorophenoxy) ethyl and β-(2-*t*-butyl-4-methylphenoxy)ethyl N,N-dimethyldithiocarbamates were prepared and then subjected to hydrazinolysis. The products of the reactions were 2,4-dichlorophenol and 2-*t*-butyl-4-methylphenol respectively showing that the ortho bulky groups do not strengthen the alkyl–oxygen bond.

The weak nature of the alkyl–oxygen bond of IX ends abruptly when the length of the alkyl chain is increased. Thus 3-*p*-chlorophenoxypropyl and 4-*p*-chlorophenoxybutyl mercaptans were prepared in 85 and 87% yields by the hydrazinolysis of the corresponding phenoxyalkyl N,N-dimethyldithiocarbamates. There is also a difference in the light stability of IX and its higher homologues. The phenoxypropyl and phenoxybutyl N,N-dimethyldithiocarbamates remain unchanged on standing while IX turns pink or red very quickly on exposure to light.

It has been already reported (14) that when *o*-(2-chloroethoxy)benzyl chlorides (XI) are treated with thiourea and the resulting *o*-(2-chloroethoxy) benzylisothiuronium chlorides subjected to alkaline cleavage, no mer-

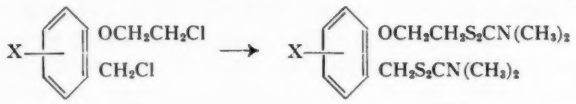

XI XII

captans are formed because simultaneous cyclization occurs to give the seven-membered ring compounds the 2,3-dihydrobenzo(*f*)-1,4-oxathiepins. With sodium dimethyldithiocarbamate (III), 2-(2-chloroethoxy)-4-methylbenzyl chloride (XI, X = 4-CH_3) yielded the bis-dithiocarbamate (XII) but alkaline cleavage of this did not yield a dimercaptan nor 7-methyl-2,3-dihydrobenzo(*f*)-1,4-oxathiepin. Instead a complex mixture was formed whose components were not identified.

EXPERIMENTAL

Sodium N,N-Dimethyldithiocarbamate

To stirred 40% dimethylamine (340 ml.) was added dropwise first carbon disulphide (185 ml.) and then sodium hydroxide (120 gm.) in water (300 ml.), the reaction temperature being kept at 10–15° by cooling. The reaction mixture was stirred at room temperature for two hours and then concentrated *in vacuo* to about half the original volume and allowed to cool. The precipitate was filtered, washed with a little cold acetone, and air-dried. The yield from three successive crops was 361 gm. This product, which is a hydrate melting at 106–108°, was pure enough to be used in the preparation of the N,N-dimethyldithiocarbamic esters.

Preparation of the N,N-Dimethyldithiocarbamates (Table I)

To a solution of sodium N,N-dimethyldithiocarbamate (0.3 mole) in acetone (400 ml.) was added the halide (0.25 mole), and the reaction mixture was heated under reflux for periods depending upon the reactivity of the halide. With alkyl bromides and benzyl chlorides the reaction was exothermic and required little heating. Three hours' refluxing time was required in the case of the phenoxyalkyl chlorides, and in the extreme case of *p*-nitrochlorobenzene several days were required. The precipitated sodium halide was filtered, the acetone was distilled off from the filtrate, and the residue was either distilled or crystallized from methanol.

Hydrolysis of N,N-Dimethyldithiocarbamates to Mercaptans (Table II)

This is exemplified by the hydrolysis of benzyl N,N-dimethyldithiocarbamate to benzyl mercaptan. To a solution of sodium hydroxide (15 gm.) in water (30 ml.) was added benzyl N,N-dimethyldithiocarbamate (7) (15 gm.) and ethanol (150 ml.), and the reaction mixture was heated under reflux for five hours. Dimethylamine was given off through the condenser and could be caught in a dry ice trap, and sodium carbonate precipitated from the reaction mixture. The ethanol was removed and the residue acidified. Carbon dioxide and hydrogen sulphide were liberated. The precipitated mercaptan was ex-

TABLE I

THE PREPARATION OF N,N-DIMETHYLDITHIOCARBAMATES $RS_2CN(CH_3)_2$ FROM THE CORRESPONDING HALIDES, RX

$RS_2CN(CH_3)_2$ R =	Halide used X =	Reaction time	M.p., °C.	% Yield	Empirical formula	Analyses			
						Calc.		Found	
						C	H	C	H
$C_6H_5CH_2$ (7)	Cl	15 min.	40–41	82					
p-$ClC_6H_4CH_2$	Cl	15 min.	54–55	82	$C_{10}H_{12}NClS_2$	48.88	4.89	48.96	4.79
2,4-$DiClC_6H_3CH_2$	Cl	15 min.	82–83	94	$C_{10}H_{11}NCl_2S_2$	42.86	3.93	43.32	3.94
3,4-$DiClC_6H_3CH_2$	Cl	15 min.	75–76	95	$C_{10}H_{11}NCl_2S_2$	42.86	3.93	43.11	4.04
2,4-$DiCH_3C_6H_3CH_2$	Cl (13)	15 min.	B.p. 219–222 (10 mm.)	80	$C_{12}H_{17}NS_2$	60.25	7.11	60.26	7.05
p-$NO_2C_6H_4CH_2$	Cl	15 min.	106–107	95	$C_{10}H_{12}O_2N_2S_2$	46.88	4.69	47.20	4.48
3-NO_2-4-$CH_3OC_6H_3CH_2$	Cl	15 min.	102–103	82	$C_{11}H_{14}N_2O_3S_2$	46.15	4.90	46.07	4.91
p-$NO_2C_6H_4$	Cl	10 days	156–157	20	$C_9H_{10}N_2O_2S_2$	44.63	4.13	45.16	4.10
2,4-$DiNO_2C_6H_4$	Cl	15 min.	152–153	84	$C_9H_9N_3O_4S_2$	37.62	3.14	37.70	3.00
$C_6H_5CH_2CH_2$	Cl	3 hr.	45–46	92	$C_{11}H_{15}NS_2$	58.66	6.67	58.85	6.53
$CH_3(CH_2)_{10}CH_2$	Br	30 min.	39–40	76	$C_{15}H_{31}NS_2$	62.28	10.73	62.11	10.66
$CH_3(CH_2)_{14}CH_2$	Br	30 min.	48–49	78	$C_{19}H_{39}NS_2$	66.09	11.31	66.06	11.14
$CH_3(CH_2)_4CH_2$	Br	30 min.	B.p. 167–168 (10 mm.)	86	$C_9H_{19}NS_2$	52.69	9.27	52.96	9.48
p-$(CH_3)_3CC_6H_4OCH_2CH_2$	Cl	4 hr.	61–62	90	$C_{15}H_{23}NOS_2$	60.61	7.74	60.80	7.60
p-$CH_3C_6H_4OCH_2CH_2$	Cl	3 hr.	64–65	88	$C_{12}H_{17}NOS_2$	56.47	6.66	56.55	6.58
p-$ClC_6H_4OCH_2CH_2$	Cl	3 hr.	73–74	90	$C_{11}H_{14}NOClS_2$	47.91	5.08	47.88	4.96
2,4-$DiClC_6H_3OCH_2CH_2$	Cl	3 hr.	73–74	98	$C_{11}H_{13}NOCl_2S_2$	42.58	4.19	42.40	4.26
2-$(CH_3)_3C$-4-$CH_3C_6H_3OCH_2CH_2$	Cl (14)	3 hr.	78–79	96	$C_{16}H_{25}NOS_2$	61.73	8.04	61.83	7.94
p-$ClC_6H_4O(CH_2)_2$	Br (9)	1 hr.	92–93	82	$C_{12}H_{16}NOClS_2$	49.74	5.53	50.06	5.25
p-$ClC_6H_4O(CH_2)_4$	Cl	3 hr.	64–65	85	$C_{13}H_{18}NOClS_2$	51.40	5.93	51.58	5.71
p-$[(CH_3)_2NCS_2CH_2]_2C_6H_4$	Cl	15 min.	178–179	96	$C_{14}H_{20}N_2S_4$	48.84	5.81	48.96	5.79
$[(CH_3)_2NCS_2CH_2CH_2]_2S$	Cl	15 min.	111–112	80	$C_{10}H_{20}N_2S_5$	36.59	6.10	36.87	6.01
2-$[(CH_3)_2NCS_2CH_2]$-4-$CH_3C_6H_3OCH_2CH_2S_2CN(CH_3)_2$	Cl (14)	3 hr.	114–115	87	$C_{16}H_{24}N_2OS_4$	49.48	6.18	49.64	6.07
p-$ClC_6H_4CH_2SCH_2CH_2$	Cl*	1 hr.	50–51	90	$C_{12}H_{16}NClS_3$	47.14	5.22	47.38	5.14
p-$ClC_6H_4SCH_2CH_2$	Br*	15 min.	96–97	98	$C_{11}H_{14}NClS_3$	45.29	4.80	45.26	4.71

**These were prepared from p-chlorobenzyl mercaptan and ethylene dichloride and from p-chlorothiophenol and ethylene dibromide respectively by the method of Patterson and du Vigneaud (18).*

tracted with benzene, the extract washed with water, and the solvent removed. The residue distilled at 77–79° at 12 mm. pressure yielding a colorless odiferous liquid (7.2 gm. or 86%) of *benzyl mercaptan.*

Hydrazinolysis of N,N-Dimethyldithiocarbamates to Mercaptans (Table II)

This is exemplified by the hydrazinolysis of 3-*p*-chlorophenoxypropyl N,N-dimethyldithiocarbamate to *3-p-chlorophenoxypropyl mercaptan.* A solution of 3-*p*-chlorophenoxypropyl N,N-dimethyldithiocarbamate (12 gm.), 85% hydrazine hydrate (20 ml.), and ethanol (80 ml.) was heated under reflux for 30 hr. Dimethylamine was given off through the condenser and a white solid precipitated from the reaction mixture. The white solid (1.1 gm.) was filtered, washed with methanol, water, methanol, and hot benzene, and dried. It melted at 233–235° with decomposition and did not depress the melting point of 3-hydrazino-4-amino-5-mercapto-4,1,2-triazole (20). The filtrate was taken to dryness *in vacuo.* The residue was treated with water and extracted with benzene. The extract was washed with water and the solvent removed. The residue distilled at 153–155° at 10 mm. pressure as a colorless liquid with odor not too objectionable. The yield was 7.2 gm. or 85%, $n_D^{24} = 1.5620$. Anal. calc. for $C_9H_{11}OClS$: C, 53.33; H, 5.43. Found: C, 53.37, 53.37; H, 5.41, 5.14.

TABLE II

THE PREPARATION OF MERCAPTANS, RSH, FROM THE CORRESPONDING N,N-DIMETHYLDITHIOCARBAMATES, $RS_2CN(CH_3)_2$, BY HYDROLYSIS (METHOD A) AND BY HYDRAZINOLYSIS (METHOD B)

Mercaptan, R =	Method of prep.	B.p.	n_D^{20}	% Yield
$C_6H_5CH_2$ (8)	A		1.5730	86
	B	73 (10 mm.)		82
p-$ClC_6H_4CH_2$ (15)	A	105 (10 mm.)		95
2,4-$DiClC_6H_3CH_2$ (4)	A	123–125 (10 mm.)	1.6000	88
3,4-$DiClC_6H_3CH_2$ (15, 4)	A	132–134 (11 mm.)	1.6015	93
2,4-$Di(CH_3)C_6H_3CH_2$ (13)	A[a]	100–102 (10 mm.)	1.5610	70
$C_6H_5CH_2CH_2$ (5, 12)	A	95– 98 (12 mm.)		66
$CH_3(CH_2)_4CH_2$ (2)	A*	155–160		61
$CH_3(CH_2)_{10}CH_2$ (21)	A*	134–135 (10 mm.)	1.4575	86
$CH_3(CH_2)_{14}CH_2$	A*	182–188 (10 mm.)		65
p-$ClC_6H_4O(CH_2)_3$	B[b]	153–155 (10 mm.)	1.5620	85
p-$ClC_6H_4O(CH_2)_4$	B[c]	170–172 (10 mm.)	1.5550	87
p-$SHCH_2C_6H_4CH_2SH$ (1)	B†	M.p. 44–45		77

**The reaction time required was 24 hr. instead of 5.*

†*The reaction time required was three days instead of 30 hr. This compound was also prepared in 86% yield by the thiourea method.*

ANALYSES

[a]*Calc. for $C_9H_{12}S$: C, 71.05; H, 7.89. Found: C, 71.01; H, 7.78.*

[b]*Calc. for $C_9H_{11}OClS$: C, 53.33; H, 5.43. Found: C, 53.37; H, 5.41.*

[c]*Calc. for $C_{10}H_{13}OClS$: C, 55.43; H, 6.00. Found: C, 55.41; H, 5.85.*

Preparation of Sulphides

This is exemplified by the preparation of *3-p-chlorophenoxypropyl p-chlorobenzyl sulphide.*

To a solution of potassium hydroxide (0.7 gm.) in methanol (40 ml.) was added *p*-chlorobenzyl chloride (2.0 gm.) and 3-*p*-chlorophenoxypropyl mercaptan (2.3 gm.), and the resulting solution was heated under reflux for 10 min. The precipitated potassium chloride was filtered, the methanol removed from the filtrate, and the residue distilled. The colorless liquid (3.2 gm.)

which boiled at 257° at 10 mm. pressure solidified on cooling. The cake was pulverized, washed with methanol, and dried. The white product melted at 37–38° alone or in admixture with the compound prepared from *p*-chlorobenzyl mercaptan and 3-*p*-chlorophenoxypropyl bromide. Anal. calc. for $C_{16}H_{16}OCl_2S$: C, 58.72; H, 4.89. Found: C, 58.72, 58.78; H, 4.64, 4.95.

The above method was also used for the preparation of the following sulphides:

Bis-p-chlorobenzyl sulphide from *p*-chlorobenzyl mercaptan and *p*-chlorobenzyl chloride in 80% yield. It melted at 42–43°; literature (17) 41°.

Benzyl 3-nitro-4-methoxybenzyl sulphide from benzyl mercaptan and 3-nitro-4-methoxybenzyl chloride in 78% yield, m.p. 55–56°. Anal. calc. for $C_{15}H_{15}NO_3S$: C, 62.30; H, 5.19. Found: C, 62.30; H, 5.20.

p-Chlorobenzyl β-p-t-butylphenoxyethyl sulphide from *p*-chlorobenzyl mercaptan and β-*p*-*t*-butylphenoxyethyl bromide in 90% yield, b.p. 250° (10 mm.). Anal. calc. for $C_{19}H_{23}OClS$: C, 68.17; H, 6.88. Found: C, 68.07; H, 6.86.

p-Chlorobenzyl n-dodecyl sulphide from *n*-dodecyl mercaptan and *p*-chlorobenzyl chloride in 80% yield, b.p. 235–236° (10 mm.), $n_D^{20} = 1.5155$. Anal. calc. for $C_{19}H_{31}ClS$: C, 69.82; H, 9.50. Found: C, 69.89; H, 9.35.

Hydrazinolysis of β-2,4-Dichlorophenoxyethyl N,N-Dimethyldithiocarbamate to 2,4-Dichlorophenol

A reaction mixture of β-2,4-dichlorophenoxyethyl N,N-dimethyldithiocarbamate (20 gm.), 85% hydrazine hydrate (20 ml.), and ethanol (100 ml.) was heated under reflux for 30 hr. The white precipitate was filtered from the cooled reaction mixture and the filtrate taken to dryness *in vacuo*. The residue was treated with water and extracted with benzene. The benzene extract was washed with water and the solvent removed. The residue distilled at 89–93° at 10 mm. pressure and the distillate (9 gm. or 86%) which solidified melted at 38–40° alone or in admixture with 2,4-dichlorophenol. The white precipitate was extracted with boiling benzene leaving a benzene-insoluble product (1.5 gm.) which melted at 233–235° with decomposition and did not depress the melting point of 3-hydrazino-4-amino-5-mercapto-4,1,2-triazole (20). The benzene extract was concentrated and cooled. A white amorphous malodorous substance (0.4 gm., m.p. 80–90°) precipitated which gave analyses agreeing with those of ethylene sulphide polymer.

In the same way *β-p-chlorophenoxyethyl*, *β-p-t-butylphenoxyethyl*, *β-p-tolyloxyethyl*, and *β-(2-t-butyl-4-methylphenoxy)ethyl N,N-dimethyldithiocarbamates* hydrazinolyzed to *p-chlorophenol*, *p-t-butylphenol*, *p-cresol*, and *2-t-butyl-4-methylphenol* respectively.

Alkaline Cleavage of β-p-t-Butylphenoxyethyl Bromide and N,N-Dimethyldithiocarbamate

A solution of β-*p*-*t*-butylphenoxyethyl bromide (55 gm.), thiourea (20 gm.), and ethanol (200 ml.) was heated under reflux for 24 hr. To this was added sodium hydroxide (20 gm.) in water (100 ml.) and the resulting reaction mixture was heated under reflux for 5 hr. The cooled reaction mixture was diluted with water, acidified, and extracted with benzene. The benzene extract was washed with water, the solvent removed, and the residue distilled. There

was obtained an alkali-soluble distillate (22 gm.), b.p. 120–125° (11 mm.), which when crystallized from benzene melted at 98–100° either alone or in admixture with *p-t*-butylphenol. This phenol was also obtained when *β-p-t*-butylphenoxyethyl N,N-dimethyldithiocarbamate was heated with alcoholic alkali as above.

3-Hydrazino-4-amino-5-mercapto-4,1,2-triazole

A reaction mixture of thiocarbohydrazide (2 gm.) (11), ethanol (10 ml.), and 85% hydrazine hydrate (5 ml.) was heated under reflux for 24 hr. The white precipitate was filtered, washed with methanol, water, methanol, and hot benzene in that order. The white powder (0.85 gm.) melted at 233–235° with decomposition. Stollé and Bowles (20) give a melting–decomposition point of 228°. A similar prolonged treatment of diethyl xanthate also gave 3-hydrazino-4-amino-5-mercapto-4,1,2-triazole.

4-p-Chlorophenoxybutyl Chloride

A reaction mixture of *p*-chlorophenol (65 gm.), 1,4-dichlorobutane (100 ml.), a solution of potassium hydroxide (30 gm.) in water (100 ml.), and benzene (200 ml.) was heated under reflux for three days. The organic layer was separated, washed with aqueous alkali and with water, and the solvent and excess 1,4-dichlorobutane were removed *in vacuo*. The residue distilled at 159–162° (10 mm.) as a colorless liquid, $n_D^{22} = 1.5340$, yield 45 gm. Anal. calc. for $C_{10}H_{12}OCl_2$: C, 54.80; H, 5.48. Found: C, 54.35, 54.71; H, 5.26, 5.39.

The residue from the distillation when crystallized from benzene–methanol yielded 21 gm. of white prisms of *1,4-bis-p-chlorophenoxybutane*, m.p. 107–108°. Anal. calc. for $C_{16}H_{16}O_2Cl_2$: C, 61.64; H, 5.14. Found: C, 61.74; H, 5.12.

ACKNOWLEDGMENT

The microanalyses were provided by Gisela von Stritzky.

REFERENCES

1. AUTENRIETH, W. and BEUTTEL, F. Ber. 42: 4349. 1909.
2. BACKER, H. J., TERPSTRA, P., and DYSTRA, N. D. Rec. trav. chim. 51: 1166. 1932. Chem. Abstr. 27: 491. 1933.
3. BEZZI, S. and LANZA, P. Gazz. chim. ital. 80: 180. 1950. Chem. Abstr. 45: 3798. 1951.
4. BOENIGK, J. W., CHRISTIAN, J. E., and JENKINS, G. L. Am. Pharm. Assoc. 38: 357. 1949. Chem. Abstr. 44: 1443. 1950.
5. v. BRAUN, J. Ber. 45: 1563. 1912.
6. CRANE, C. W. and RYDON, H. N. J. Chem. Soc. 766. 1947.
7. DAVIES, W. H. and SEXTON, W. A. Biochem. J. 40: 331. 1946. Chem. Abstr. 41: 405. 1941.
8. FARLOW, M. W. and SIGNAIGO, F. K. U.S. Patent No. 2,402,613. 1946. Chem. Abstr. 40: 5758. 1946.
9. GAGNON, P. E., BOIVIN, J. L., and GIGUÈRE, J. Can. J. Research, B, 28: 352. 1950.
10. GORDON, M. J. Chem. Soc. 1931. 1951.
11. GUHA, P. C. and DE, S. C. J. Chem. Soc. 125: 1215. 1924.
12. HEWEIHI, Z. Chem. Ber. 86: 781. 1953.
13. KULKA, M. Can. J. Research, B, 23: 106. 1945.
14. KULKA, M. Can. J. Chem. 33: 1442. 1955.
15. LEWIS, T. R. and ARCHER, S. J. Am. Chem. Soc. 73: 2109. 1951.
16. LYLE, R. E., DEWITT, E. J., and PATTISON, I. C. J. Org. Chem. 21: 61. 1956.
17. OVERBERGER, C. G., LIGTHELM, S. P., and SWIRE, E. A. J. Am. Chem. Soc. 72: 2856. 1950.
18. PATTERSON, W. I. and DU VIGNEAUD, V. J. Biol. Chem. 111: 393. 1935. Chem. Abstr. 30: 80. 1936.
19. SCOTT, E. S. and AUDRIETH, L. F. J. Org. Chem. 19: 1231. 1954.
20. STOLLÉ, R. and BOWLES, P. E. Ber. 41: 1099. 1908.
21. URQUHART, G. G., GATES, J. W., and CONNOR, R. Org. Syntheses, Coll. Vol. 3: 363. 1955.

THE APPLICATION OF INTERPOLATION THEORY TO DATA ON THE ADSORPTION OF NITROGEN, OXYGEN, AND ARGON ON RUTILE[1]

By J. M. Honig and L. H. Reyerson[2]

ABSTRACT

The interpolation theory has been applied to data on the adsorption of nitrogen, oxygen, and argon on rutile at 77° K. It has been demonstrated that the oxygen and argon data cannot be interpreted on the basis of the Langmuir model, modified by the introduction of surface heterogeneity effects. The interpolation theory verifies, however, that the distribution of adsorption energies among surface sites, obtained by inversion of the nitrogen isotherm, is physically significant, and that nitrogen is suitable for BET surface area calculations.

INTRODUCTION

The inadequacy of the Langmuir model in the interpretation of gas adsorption phenomena is well known. Nevertheless, a variant of this model, the BET multilayer adsorption theory, has found widespread use in the estimation of surface areas, though it is recognized that the results cannot be completely reliable. Attempts have been made to improve on the Langmuir model by taking account of the energy heterogeneity of the surface (2, 3, 10, 11, 12, 13, 17, 20, 21, 22, 23). While this is a step in the right direction, the results are still unsatisfactory because lateral interactions are left out of consideration. On the other hand, a reasonably rigorous treatment of both effects (12) or even a rather specialized approach along these lines (1, 8, 9) leads to complicated equations. In practice one is therefore often forced to return to the use of the BET equation in the analysis of gas adsorption isotherms.

In order to have confidence in the results of such a simple approach, one must determine how well the data conform to the restrictive assumptions of the Langmuir or BET model. Thermodynamic considerations (see for example (4, 5, 16)) have been quite helpful for this purpose. Recently a new approach has been cited in the literature (14, 15) in which it was shown that all data conforming to the Langmuir model, the BET model, or to a theory dealing with surface heterogeneity effects must lie within well-defined limits on a plot of surface coverage versus pressure. Details for the construction of these limits by use of the so-called interpolation theory (18) have been provided. Such an analysis should aid in deciding whether the simple adsorption theories are applicable to a given adsorbate–adsorbent system. For, if a given set of datum points is found to fall outside the interpolation limits, then the Langmuir model and the various modifications which include surface heterogeneity effects are hopelessly inadequate. In such cases it is obviously not justifiable to use the

[1]*Manuscript received April 12, 1956.*

Contribution from the Department of Chemistry, Purdue University, Lafayette, Indiana, and the Department of Chemistry, University of Minnesota, Minneapolis 14. Presented in part before the Division of Colloid Chemistry at the 128th Meeting of the American Chemical Society, at Minneapolis, September 11–16, 1955.

[2]*One of us (LHR) gratefully acknowledges funds received from the graduate school in partial support of this work. Both authors are indebted to Mr. Chi Chang for performing the calculations on which Figs. 1, 2, and 3 are based.*

isotherm data to compute a distribution of adsorption energies among surface sites, and even the BET method of determining at what point on the isotherms monolayer coverage is complete is open to criticism.

The purpose of the present article is to provide examples showing how the interpolation procedure operates. The method will be utilized to settle a problem raised by Honig and Reyerson (13) in connection with a study on the adsorption of nitrogen, oxygen, and argon on rutile.

THE INTERPOLATION THEORY

Any adsorbent–adsorbate system which conforms to the modified Langmuir theory is characterized by an adsorption isotherm of the form (11):

$$[1] \qquad \frac{n}{n_m} \equiv \theta(p, T) = \int_{\epsilon_0}^{\epsilon_m} \frac{dF(\epsilon)}{1+(\beta(\epsilon, T)/p)e^{-\epsilon/kT}}$$

where n and n_m are the number of adsorbate molecules held on the surface at a pressure p and at monolayer coverage respectively, θ is the fraction of the surface covered at pressure p and temperature T, $dF(\epsilon) \equiv f(\epsilon)d\epsilon$ is the fraction of sites associated with adsorption energies in the range ϵ to $\epsilon+d\epsilon$, ϵ_0 and ϵ_m are respectively the minimum and maximum values of ϵ encountered on the surface, and β is a quantity defined by:

$$[2] \qquad \beta(\epsilon, T) = (2\pi mkT/h^2)^{3/2}kT\, j_g(T)/j_s(\epsilon, T)$$

where m is the mass of the adsorbate particles, while j_g and j_s represent the partition functions of the particles in the gas and in the adsorbed phases respectively. Note that the latter quantity depends on ϵ (7, 11, 12).

Eq. [1] represents a one-to-one correspondence between θ and F. Rosenbloom (18) has developed a theory in which he proves that one can select two distribution functions $F_a(\epsilon)$ and $F_b(\epsilon)$ such that the corresponding equations $\theta_a(p, T)$ and $\theta_b(p, T)$ form the limits, mentioned in the introduction, within which the data must fall if eq. [1] is to apply. For details of the construction of the extremal isotherms the reader is referred to the original publication (14).

In what follows it suffices to note that the bounding isotherms θ_a and θ_b are adjusted to a given set of experimental data by the arbitrary selection of a set of reference points through which the functions θ_a and θ_b are required to pass. One then observes whether the remaining experimental points lie within the region which is bounded by the functions θ_a and θ_b. This gives an indication as to the applicability of the Langmuir model or of models combining the Langmuir postulates with the concept of surface heterogeneity. For, it is evident from the remarks that if any points fall outside this region, this is a clear indication that eq. [1] cannot be used in the interpretation of the data.

The calculations cited below were based on the use of the following relations:

$$[3] \qquad \theta_a(p, T) = \frac{(\theta_2-\theta_1)p+[\theta_1p_2(1-\theta_2)-\theta_2p_1(1-\theta_1)]}{(\theta_2-\theta_1)p+[p_2(1-\theta_2)-p_1(1-\theta_1)]},$$

$$[4] \qquad \theta_b(p, T) = \frac{\theta_1\theta_2(p_1-p_2)}{p_1p_2(\theta_2-\theta_1)/p+(\theta_2p_1-\theta_1p_2)}.$$

These equations require the selection of two reference points (θ_1, p_1) and (θ_2, p_2) from among the data. It was shown in (14) that [3] and [4] result upon simplification of the expression for the "third-order" limiting isotherms. Being approximate, they bound a wider region in the θ vs. p diagram than the exact functions, and thus less precise information is obtained. On the other hand, no unknown parameters are involved, and the calculations are relatively simple.

One should note that the quantity n_m cancels from both sides of [4] when θ is replaced by n/n_m. On the other hand, the value of n_m must be specified for use in [3]. It has been verified, however, that the dependence of θ_a on n_m is not marked. It has also been established that none of the conclusions reached below would be invalidated by the selection of n_m values which differ radically from the set adopted below.

APPLICATION TO NITROGEN, OXYGEN, ARGON ADSORPTION ISOTHERMS

The interpolation theory will now be applied to the adsorption on nitrogen, oxygen, and argon observed at 77° K. (13). The isotherms are drawn as dotted lines through the experimental points in Figs. 1, 2, and 3. Two sets of extremal isotherms are entered as heavy curves on each figure. The reference data used in the computation of each set are listed in the captions of the diagrams. The areas bounded by each set of extremals are shaded and are labelled A and B respectively. The low pressure region of Fig. 1 has been expanded in the inset

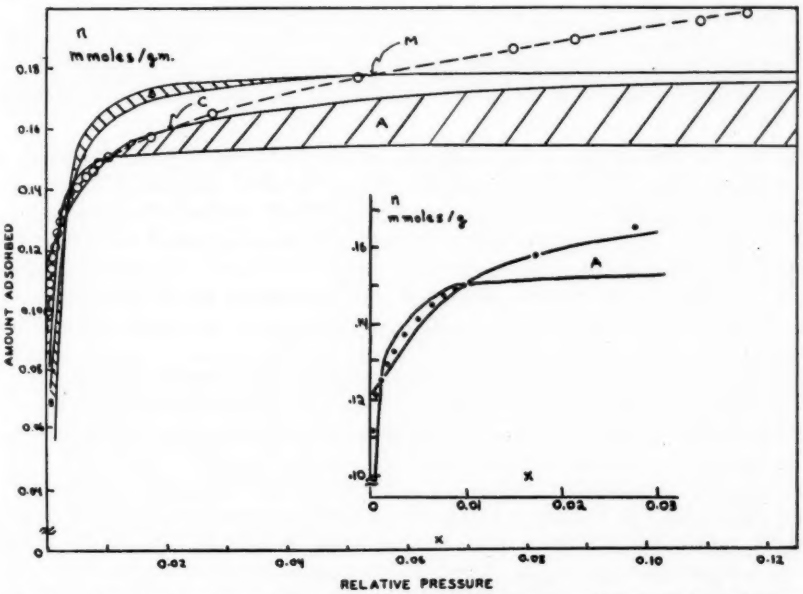

FIG. 1. Limiting isotherms for the adsorption of nitrogen on rutile at 77° K. Reference points for Area A: $n_1 = 0.125$ mmoles/gm.; $p_1 = 0.13$ cm. Hg; $n_2 = 0.149$ mmoles/gm.; $p_2 = 0.78$ cm. Hg. Reference points for Area B: $n_1 = 0.137$ mmoles/gm.; $p_1 = 0.29$ cm. Hg; $n_2 = 0.177$ mmoles/gm.; $p_2 = 4.12$ cm. Hg; $n_m = 0.179$ mmoles/gm. Open circles are experimental points, connected by dotted line; shaded regions are areas bounded by extremal isotherms.

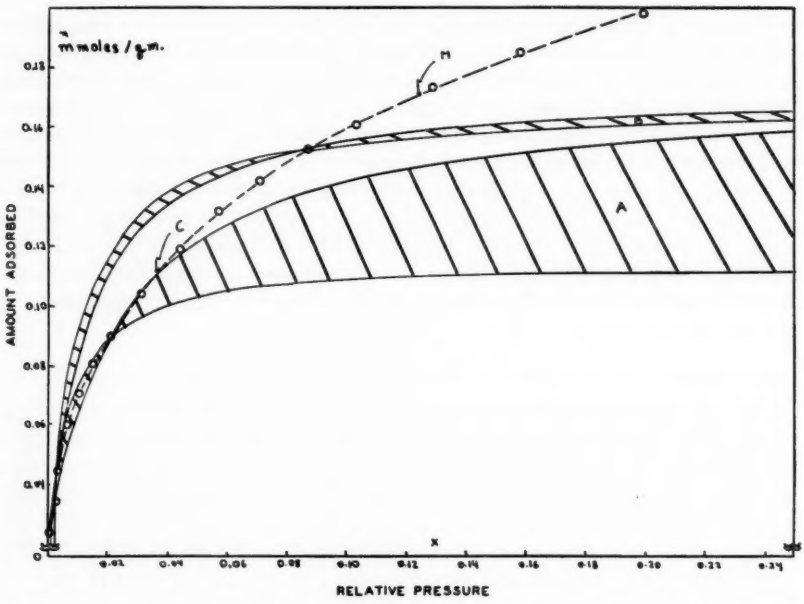

FIG. 2. Limiting isotherms for the adsorption of oxygen on rutile at 77° K. Reference points for Area A: $n_1 = 0.0346$ mmoles/gm.; $p_1 = 0.040$ cm. Hg; $n_2 = 0.0901$ mmoles/gm.; $p_2 = 0.34$ cm. Hg. Reference points for Area B: $n_1 = 0.0346$ mmoles/gm.; $p_1 = 0.040$ cm. Hg; $n_2 = 0.142$ mmoles/gm.; $p_2 = 1.13$ cm. Hg; $n_m = 0.171$ mmoles/gm. Open circles are experimental points, connected by dotted line; shaded regions are areas bounded by extremal isotherms.

to Fig. 1. The values of n_m were taken from Table II of (13). Attention is directed to the interlacing structure of θ_a and θ_b, which alternately form lower and upper bounds in the intervals marked off by the reference points p_1 and p_2.

Inspection of the graphs shows that the low pressure points fall within the bounds prescribed by the third-order theory. However, in every case there exists a point labelled C beyond which all experimental points fall outside the area A. These findings can be qualitatively related to the results of the BET theory which predicts the onset of multilayer formation beyond the point labelled M on each isotherm.[3] The formation of higher layers clearly violates the Langmuir postulate which excludes the case of multilayer adsorption. It is therefore necessary for the high pressure points to fall above the upper limit prescribed for the first layer by the interpolation theory.

Further examination indicates, however, that the isotherms cross the theoretical limits at a point C below the point M where monolayer coverage is essentially complete. Thus, for argon the point C occurs at $n = 0.10$ mmoles ($\theta = 0.62$), and for oxygen, at $n = 0.11$ mmoles ($\theta = 0.64$). On the other hand, the nitrogen isotherm remains within the limiting bounds up to $n = 0.16$ mmoles ($\theta = 0.90$).

[3]*The presence of multilayer condensation is clearly established by unpublished work of the authors in the partial pressure range* $0.1 \leqslant p/p_0 \leqslant 0.9$. *All three adsorbates yield type II isotherms in the BET classification.*

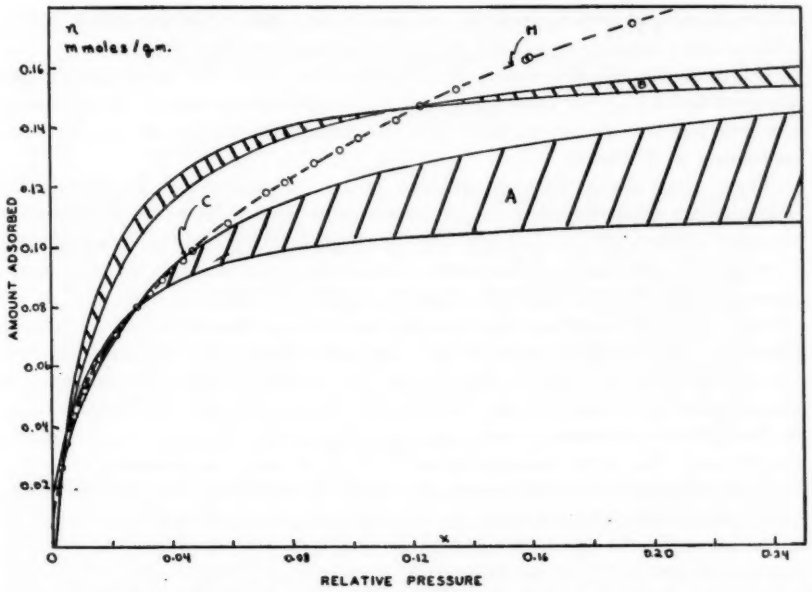

FIG. 3. Limiting isotherms for the adsorption of argon on rutile at 77° K. Reference points for Area A: $n_1 = 0.0264$ mmoles/gm.; $p_1 = 0.08$ cm. Hg; $n_2 = 0.0808$ mmoles/gm.; $p_2 = 0.69$ cm. Hg. Reference points for Area B: $n_1 = 0.0264$ mmoles/gm.; $p_1 = 0.08$ cm. Hg; $n_2 = 0.142$ mmoles/gm.; $p_2 = 2.32$ cm. Hg; $n_m = 0.164$ mmoles/gm. Open circles are experimental points, connected by dotted line; shaded regions are areas bounded by extremal isotherms.

These findings can be checked by the selection of other reference points. It has been verified that when these are chosen from the data below the point C, the isotherm is always found to cross the third-order limiting curve near point C. However, if one of the reference points is selected from the data falling above point C, the limiting curves bound an area B which does not coincide with the experimental points except near (θ_1, p_1) and (θ_2, p_2).

DISCUSSION OF RESULTS

The results indicate that all adsorption data remain within their extremal bounds at low surface coverage, provided that the reference points are selected, in conformity with the simplifying assumptions of the interpolation theory, from the region below point C.

However, while the nitrogen isotherm remains within its prescribed bounds until monolayer coverage is almost complete, the oxygen and argon isotherms deviate from their prescribed limits much sooner. Evidently the system nitrogen: rutile conforms more closely to the modified Langmuir model than the other two systems. This behavior can probably be explained on the basis of a statement by Drain (6). Nitrogen possesses a quadrupole moment of appreciable magnitude, which contributes to the physical binding of nitrogen molecules to the surface. In oxygen or argon this contribution is absent, and the binding energy to the surface is appreciably lower. As a result, factors such as lateral

interactions and surface mobility, which are ignored in the Langmuir model, play a more significant role for oxygen or argon than for nitrogen.

Undoubtedly the experimental conditions are such that even for nitrogen the modified Langmuir model is a poor approximation to reality. Nevertheless, the interpolation theory at least does not invalidate the use of the inversion technique in this case.

These conclusions settle a problem raised by Honig and Reyerson (13). The authors showed that if the inversion procedure of Sips (19) is applied to the data plotted in Figs. 1–3, one obtains three different distribution functions. In particular, the rutile surface seemed to present an abundance of high energy sites toward nitrogen, but not toward oxygen or argon. Presumably, if the concept of energy heterogeneity has physical reality, the distribution functions obtained with the three gases on the same solid should have been similar. The interpolation theory now indicates that the restrictive assumptions basic to the inversion procedure do not hold for the oxygen or argon isotherms. Hence, in the light of information now available, the energy distributions calculated in (13) from the latter two isotherms have no physical significance.

Perhaps one of the most interesting results is that the interpolation theory confirms the suitability of using nitrogen gas for surface area measurements of rutile according to the BET procedure. The selection of oxygen or argon as the adsorbate at 77° K. by Brunauer, Emmett, and Teller would obviously have been much less satisfactory for surface area studies. The interpolation method also indicates that the magnitude for n_m obtained by the BET method must be approximately correct. For, it may be assumed that the failure of the nitrogen datum points to lie within the area A of Fig. 1 is due primarily to the onset of multilayer formation. Hence, the fact that the points C and M agree within 10% lends credence to the BET results.

REFERENCES

1. Champion, W. M. and Halsey, G. D. J. Am. Chem. Soc. 76: 974. 1954.
2. Cremer, E. J. chim. phys. 46: 411. 1949.
3. Cremer, E. and Flügge, S. Z. physik. Chem. B, 41: 453. 1938.
4. de Boer, J. H. The dynamical character of adsorption. The Clarendon Press, Oxford. 1953.
5. de Boer, J. H. and Kruyer, S. Koninkl. Ned. Akad. Wetenschap. Proc., B, 55: 451. 1952; B, 56: 67. 1953.
6. Drain, L. E. Trans. Faraday Soc. 49: 650. 1953.
7. Drain, L. E. and Morrison, J. A. Trans. Faraday Soc. 48: 316. 1952; 49: 654. 1953.
8. Halsey, G. D. J. Chem. Phys. 16: 931. 1948.
9. Halsey, G. D. J. Am. Chem. Soc. 73: 2693. 1951; 74: 1082. 1952.
10. Halsey, G. D. and Taylor, H. S. J. Chem. Phys. 15: 624. 1947.
11. Hill, T. L. J. Chem. Phys. 17: 762. 1949.
12. Honig, J. M. and Hill, E. L. J. Chem. Phys. 22: 851. 1954.
13. Honig, J. M. and Reyerson, L. H. J. Phys. Chem. 56: 140. 1952.
14. Honig, J. M. and Rosenbloom, P. C. Can. J. Chem. 33: 193. 1955.
15. Honig, J. M. and Rosenbloom, P. C. J. Chem. Phys. 23: 2179. 1955; 24: 510. 1956.
16. Kemball, C. Advances in Catalysis, 2: 333. 1950.
17. Roginskii, S. Doklady Akad. Nauk S.S.S.R. 45: 61, 194. 1944.
18. Rosenbloom, P. C. Bull. Soc. Math. France. In press.
19. Sips, R. J. Chem. Phys. 16: 490. 1948; 18: 1024. 1950.
20. Temkin, M. and Levich, V. Zhur. Fiz. Khim. 20: 1441. 1946.
21. Todes, O. M. and Bondareva, A. K. Zhur. Priklad. Khim. 21: 693. 1948.
22. Tompkins, F. C. Trans. Faraday Soc. 46: 569. 1950.
23. Zeldowitsh, J. Acta Physicochim. U.R.S.S. 1: 961. 1934.

THE ENTROPIES OF IONS IN AQUEOUS SOLUTION

I. DEPENDENCE ON CHARGE AND RADIUS[1]

By K. J. Laidler

ABSTRACT

Empirical equations recently proposed for the entropies of ions in aqueous solution involve a linear dependence on the first power of the valency z and, in some cases, an inverse dependence on the square of a modified radius. Such relationships have no fundamental validity since the entropies are related arbitrarily to a zero value for the proton. It is shown that the entropy changes for reactions of various ionic types indicate that the entropy must depend on z^2, as proposed by Born on the basis of simple electrostatic theory. When the entropies of monatomic ions are related to the absolute scale, in which the proton has a value of -5.5 e.u., they are found to vary linearly with z^2/r_u, where r_u is the univalent radius defined by Pauling. The slope is found to be close to that predicted by the Born equation, and the non-electrostatic part of the entropy is shown to correspond to the movement of the ion in a free volume of 0.73 cu. Å.

INTRODUCTION

Recently several workers (12, 9, 3, 4, 6) have proposed empirical equations which accurately relate the conventional partial molal entropies of ions in aqueous solution to parameters such as the valency, z, the effective radius, r_e, and, in the case of complex ions, the number of ligands. The prototype of such equations is that of Powell and Latimer (12) who show that the entropies of monatomic ions are accurately represented by the formula

$$[1] \qquad \bar{S}^\circ = (3/2)\, R \ln(\text{at.wt.}) + 37 - 270\, z/r_e^2$$

where the effective radius r_e is the crystal radius plus 2.0 Å in the case of cations and 1.0 Å in the case of anions. The discussion that follows will relate explicitly to the Powell–Latimer scheme but the arguments are applicable, *mutatis mutandis*, to all of the others.

DEPENDENCE OF ENTROPY ON CHARGE

Although it is undoubtedly the case that the equations permit accurate estimates to be made of the entropies of ions of various kinds, they unfortunately do not correctly represent the manner in which entropies depend upon charge and radius. That this is the case becomes apparent from a consideration of the following points:

(1) The entropies employed in the empirical equations are arbitrarily related to the value of zero for the proton. Gurney (8) has recently obtained convincing evidence that the absolute entropy of the proton is actually -5.5 e.u., and if this is the case the entropies of ions of various types must all be modified by the subtraction of $5.5z$ in the case of cations and the addition of $5.5z$ in the case of anions. With these changes Powell and Latimer's straight line plot splits into several parallel straight lines, and a different dependence of $\bar{S}^\circ$ on z is clearly called for.

[1]*Manuscript received April 24, 1956.*
Contribution from the Department of Chemistry, University of Ottawa, Ottawa, Canada.

(2) Born (2) has proposed that the free energies and entropies of ions are the values given by simple electrostatic theory for a conducting sphere of charge ze and radius r. The resulting expressions, and the numerical values corresponding to ions in aqueous solution at 25° C., are

$$[2] \qquad F^\circ_{el} = z^2e^2/2r\,D = 2.05\,z^2/r \text{ kcal. per mole,}$$

$$[3] \qquad S^\circ_{el} = (z^2e^2/2r\,D)\,(\delta \ln D/\delta T) = 9.42\,z^2/r \text{ cal. per degree.}$$

(In using the above numerical coefficients, the value of r must be in Å.) On the basis of Eq. [3] one would expect a linear dependence of $\bar{S}^\circ$ on z^2/r, rather than upon z/r_e^2 as found by Powell and Latimer. This is not, of course, a compelling argument, since Born's assumption that ions behave like conducting spheres may not be justified. However it will now be shown that there is strong *experimental* evidence in favor of a dependence on z^2.

(3) Since the variation of entropy with charge is much more important than the variation with size (and this is especially true of the absolute entropies) one can, to a rough approximation, ignore size effects and see how entropy changes in complete reactions depend on the charges on the ions. Thus if one considers a reaction

$$A^{z_A} + B^{z_B} \rightleftarrows C^{z_C} + D^{z_D}$$

the entropy change, if the individual entropies depend on z^2, will be related to the quantity

$$z_C^2 + z_D^2 - z_A^2 - z_B^2$$

which may be written as $\sum z^2$. If on the other hand the entropies depend on z the entropy change will be related to

$$z_C + z_D - z_A - z_B$$

which will be written as $\sum z$. There are a number of reactions for which $\sum z^2$ and $\sum z$ differ in sign, and these should provide a means of differentiating between the two possibilities; apart from this, one can see whether trends in ΔS can be correlated with $\sum z^2$ or with $\sum z$.

The results for a number of reactions are shown in Table I. The ΔS values were mostly calculated using the $\bar{S}^\circ$ values listed by Latimer; these $\bar{S}^\circ$ values are all conventional ones, based on $\bar{S}_{H^+}^\circ = 0.0$, but the values of ΔS are absolute and do not depend on this convention. Only a selection of possible examples can be given, but those chosen are typical and show the general trends. It is clear that there is a close correlation between ΔS and $\sum z^2$, but none at all between ΔS and $\sum z$. Fig. 1 shows a plot of ΔS against $\sum z^2$. If attempts were made to predict ΔS on the basis of $\sum z$, the wrong sign would be obtained in many cases (e.g. reactions 11 to 14). One could, however, make rough estimates of ΔS by multiplying $\sum z^2$ by about 10.

This close correlation between ΔS and $\sum z^2$, covering a wide range of reaction types, and the lack of correlation with $\sum z$, strongly indicates that entropy is a function of z^2 and not of z. If the relationships proposed by Powell and

TABLE I

ENTROPY CHANGES FOR REACTIONS OF VARIOUS IONIC TYPES

Reaction	$\sum z$	$\sum z^2$	ΔS (e.u.)	Ref.
1. $C_6H_5OH + OH^- \rightarrow C_6H_5O^- + H_2O$	0	0	− 8.2	10
2. $C_6H_5NH_2 + H_3O^+ \rightarrow C_6H_5NH_3^+ + H_2O$	0	0	1.4	10
3. $2H_2O \rightarrow H_3O^+ + OH^-$	2	2	− 18.7	9, 10
4. $NH_4OH \rightarrow NH_4^+ + OH^-$	2	2	− 18.9	9
5. $H_2CO_3 + H_2O \rightarrow H_3O^+ + HCO_3^-$	2	2	− 22.9	9
6. $HSO_4^- + H_2O \rightarrow H_3O^+ + SO_4^{2-}$	2	4	− 26.3	9
7. $HCO_3^- + H_2O \rightarrow H_3O^+ + CO_3^{2-}$	2	4	− 35.0	9
8. $HPO_4^= + H_2O \rightarrow H_3O^+ + PO_4^{3-}$	2	6	− 43.0	9
9. $UOH^{3+} \rightarrow U^{4+} + OH^-$	2	8	− 52.0	1
10. $ClO_4^- + 2H^+ + 2Fe^{2+} \rightarrow ClO_3^- + H_2O + 2Fe^{3+}$	0	8	− 73.5	9
11. $MnO_4^- + 5Fe^{2+} + 8H^+ \rightarrow Mn^{2+} + 5Fe^{3+} + 4H_2O$	−2	20	−213.6	9
12. $Cr_2O_7^{2-} + 3Tl^+ + 14H^+ \rightarrow 2Cr^{3+} + 3Tl^{3+} + 7H_2O$	−4	24	−248.6	9
13. $Cr_2O_7^{2-} + 6Fe^{2+} + 14H^+ \rightarrow 2Cr^{3+} + 6Fe^{3+} + 7H_2O$	−4	30	−339.2	9
14. $2MnO_4^- + 5Tl^+ + 16H^+ \rightarrow 2Mn^{2+} + 5Tl^{3+} + 8H_2O$	−4	30	−359.2	9

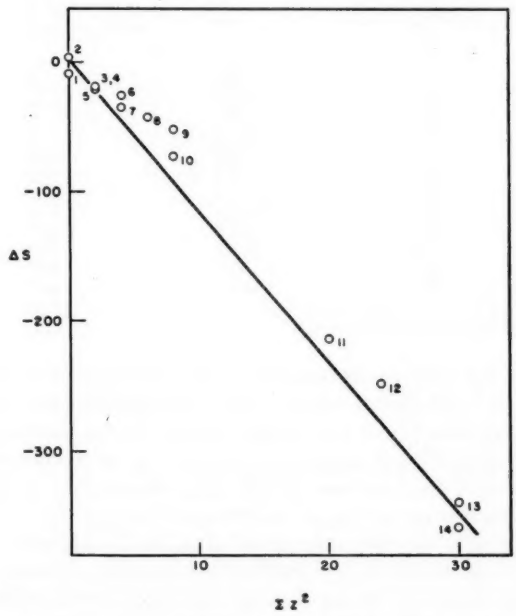

FIG. 1. Plot of entropy change against $\sum z^2$ for reactions of various ionic types. The numbers relate to the reactions listed in Table I.

Latimer were accepted as of fundamental significance it would be necessary to regard the correlations shown in Fig. 1 as purely coincidental, arising from fortuitous variations in ion radii. Such would appear to be extremely unlikely

A NEW EMPIRICAL EQUATION

In view of these conclusions it is clearly of interest to examine the absolute entropies of aqueous ions with a view to confirming their dependence on z^2 and to finding out how they vary with ion size.

Column 2 of Table II shows values for monatomic cations,* calculated from Latimer's values in the manner indicated above. In the next column the value $(3/2)R$ ln(at.wt.) has been subtracted from the absolute values. This procedure was found by Powell and Latimer to improve the correlation, and

TABLE II

ABSOLUTE ENTROPIES AND UNIVALENT RADII

Ion	$\bar{S}^\circ_{abs}$ ($H^+ = -5.5$)	$\bar{S}^\circ_{abs} - (3/2)\,R\ln$(at.wt.)	Univalent radius (Å)
Cs^+	26.3	11.8	1.69
Rb^+	24.2	9.0	1.48
K^+	19.0	8.1	1.33
Na^+	8.9	− 0.4	0.95
Ag^+	12.2	− 1.7	1.26
Li^+	− 2.1	− 7.9	0.60
Ra^{2+}	2	− 14.1	1.7*
Ba^{2+}	− 8	− 22.7	1.53
Hg^{2+}	− 16.4	− 32.2	1.25
Cd^{2+}	− 25.6	− 32.8	1.14
Sr^{2+}	− 20.4	− 33.7	1.32
Ca^{2+}	− 24.2	− 35.2	1.18
Mg^{2+}	− 39.2	− 48.7	0.82
Zn^{2+}	− 36.5	− 48.9	0.88
Tl^{3+}	− 58.5	− 74.3	1.15
In^{3+}	− 78.5	− 92.6	1.04
Al^{3+}	− 91.4	−101.2	0.72
Ga^{3+}	− 99.5	−112.1	0.81
U^{4+}	−100	−116.3	1.6*
Pu^{4+}	−109	−125.3	1.3*

Estimated by extrapolation.

was found to do the same in the present study; its theoretical justification is considered below. Column 4 shows the "univalent" radii r_u given by Pauling (11); these were found empirically to give better correlation than the ordinary crystal radii. This is understandable in view of the fact that the univalent radii represent the true sizes of the ions, whereas the crystal radii are reduced to various degrees owing to electrostatic attractions.

In order to confirm the dependence of $\bar{S}^\circ_{abs}$ on z^2 one may plot $\bar{S}^\circ_{abs} - (3/2)\,R\ln$(at.wt.) against $1/r_u$ and find by interpolation the entropies corresponding to some arbitrary radius. Taking 1.3 Å as the radius, the entropies obtained are as follows: $z = 1$, 7.5 e.u.; $z = 2$, −27.0 e.u.; $z = 3$, −68 e.u.; and $z = 4$, −126 e.u. These values are shown plotted against both z and z^2 in Fig. 2. The linear dependence on z^2 is clearly established.

Since Eq. [3] predicts a dependence of entropy on z^2/r, it is natural to test such a dependence first. Fig. 3 shows a plot of $\bar{S}^\circ_{abs} - (3/2)\,R\ln$(at.wt.) against z^2/r_u. The linearity shown in this plot is as good as could be expected;

Anions are not considered in this paper, since the range of values is not sufficiently great to permit a test of the dependence on z and r.

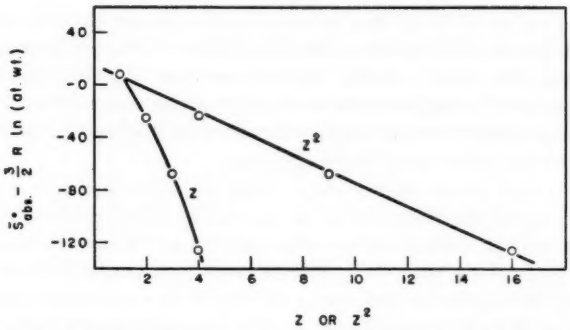

FIG. 2. Plot of $\bar{S}^\circ_{abs} - (3/2)\, R \ln(\text{at.wt.})$ against z (the valency) and z^2, the entropies corresponding to a univalent radius of 1.3 Å. This plot establishes the fact that entropy varies linearly with z^2 and not with z.

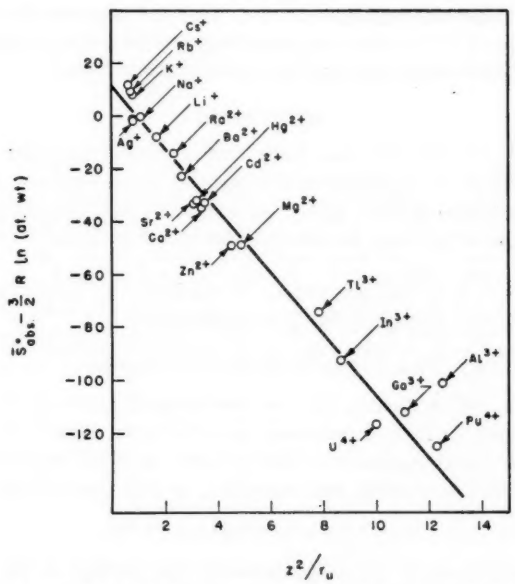

FIG. 3. Plot of $\bar{S}^\circ_{abs} - (3/2)\, R \ln(\text{at.wt.})$ against z^2/r_u, where z is the valency and r_u the univalent radius.

some improvement could be realized by adding a small constant value to all of the radii, but is hardly worth while in view of uncertainties in the univalent radii. It may be noted that small errors in the radii are highly magnified when z is large; an increase of 0.1 in the value for plutonium, for example, displaces the point by 0.9 to the left, and puts it to the left of the curve.

The only point that is seriously off the line is that for aluminum. This may well be due to an error in the radius, and it is of interest that Goldschmidt (7)

gave a crystal radius (0.83 Å) that is considerably greater than Pauling's value (0.5 Å). The use of a univalent radius calculated from Goldschmidt's value would displace the point to the left of the line. Apart from this case Goldschmidt's and Pauling's values are mainly in good agreement; for lithium, however, Goldschmidt's value is again larger than Pauling's, and the change would displace the point away from the line.

Attempts to find linear relationships using the crystal radii r_c rather than the univalent radii were not quite as successful. The addition of constant values to the crystal radii gave no advantage, and the use of functions like z^2/r_u^2, $z^2/(r_u+a)^2$, z^2/r_c^2, and $z^2/(r_c+a)^2$, showed no improvement over z^2/r_u.

It is therefore concluded that the function z^2/r_u is the most satisfactory simple function. The equation of the straight line, obtained by the method of least squares (neglecting aluminum), is

$$[4] \qquad \bar{S}^\circ_{abs} = (3/2)\ R \ln(\text{at.wt.}) + 10.2 - 11.6\ z^2/r_u.$$

The mean deviation in entropy is 4.8 e.u., and the mean deviation in $1/r_u$ is 0.16; at a radius of 1.2 Å this corresponds to a deviation in radius of about 0.12 Å, which is probably close to the actual uncertainty.

DISCUSSION

Several points of interest arise from this empirical equation. In the first place, the coefficient of the z^2/r_u term in Eq. [4] is not far from that given by Eq. [3]. It thus appears that as far as entropies are concerned the simple electrostatic picture is much nearer to the truth than had hitherto been suspected.

Other points relate to the significance of the term $(3/2)\ R \ln(\text{at.wt.})$ and to the intercept on the entropy axis. The contribution

$$[5] \qquad \bar{S}^\circ_{n.e.s.} = (3/2)\ R \ln(\text{at.wt.}) + 10.2$$

appearing in Eq. [4] is clearly the non-electrostatic part of the entropy. A very simple model (5) for a monatomic particle in the liquid phase regards it as having translational motion in a "free volume" v_f of the order of a molecular volume; the partition function corresponding to this type of motion is

$$[6] \qquad f = \{(2\pi mkT)^{3/2}/h^3\} v_f e^{-E_0/RT}$$

where E_0 is the difference in energy between the particle in the liquid phase and in the gas phase. If the ions are regarded as independent localized systems this partition function leads to the result that the entropy per mole is

$$[7] \qquad \bar{S}^\circ = R[3/2 + \ln\{(2\pi mkT)^{3/2} v_f/h^3\}].$$

This is equivalent to

$$[8] \qquad \bar{S}^\circ - (3/2)\ R \ln(\text{at.wt.}) = 3/2 + (3/2)\ R \ln\{(2\pi kT)/h^2N\} + R \ln v_f.$$

Insertion into this equation of the numerical values (with $T = 298.2°$ K.) gives rise to

$$[9] \qquad \bar{S}^\circ - (3/2)\ R \ln(\text{at.wt.}) = 2.91 + R \ln v_f$$

where v_f is the free volume in cu. Å.

In comparing this equation with Eq. [5] it is necessary to take into consideration the fact that Eq. [5] contains a "cratic" term (8) for the mixing of the ions with water; this term amounts to $R \ln(1000/55.5) = 7.9$ e.u. In order for Eqs. [5] and [9] to be equivalent it is therefore necessary that

$$10.2-7.9 = 2.9+R \ln v_f. \qquad [10]$$

This leads to a value for v_f of 0.73 cu. Å, which is entirely reasonable. The volume should, of course, be smaller than the volume of the actual cavities occupied by the ions, owing to the volumes of the ions themselves.

The general conclusions to which the present work leads are therefore as follows. The absolute entropy of a monatomic ion in solution can be regarded as made up of a non-electrostatic and an electrostatic term. The first of these corresponds to the free motion of the ion in a free volume of about 0.73 cu. Å, and the electrostatic term is represented approximately by Eq. [3], which is based on classical electrostatic theory. The view that entropies depend on z seems to be entirely without foundation.

Later papers will deal more explicitly with the entropies of polyatomic ions.

REFERENCES

1. BETTS, R. H. Can. J. Chem. 33: 1775. 1955.
2. BORN, M. Z. Physik, 1: 45. 1920.
3. COBBLE, J. W. J. Chem. Phys. 21: 1443, 1446, 1451. 1953.
4. CONNICK, R. E. and POWELL, R. E. J. Chem. Phys. 21: 2206. 1953.
5. EYRING, H. and HIRSCHFELDER, J. O. J. Phys. Chem. 41: 249. 1937.
6. GEORGE, P., HANANIA, G. I. H., and IRVINE, D. H. J. Chem. Phys. 22: 1616. 1954.
7. GOLDSCHMIDT, V. M. Skrifter Norske Videnskaps-Akad. Oslo, I. Mat. Naturv. Kl. 1926.
8. GURNEY, R. W. Ionic processes in solution. McGraw-Hill Book Company, Inc., New York. 1953.
9. LATIMER, W. M. Oxidation potentials. 2nd ed. Prentice-Hall, Inc., New York. 1952.
10. PAPEE, H. M., CANADY, W. J., and LAIDLER, K. J. To be published.
11. PAULING, L. The nature of the chemical bond. Cornell Univ. Press, Ithaca, N.Y. 1939.
12. POWELL, R. E. and LATIMER, W. M. J. Chem. Phys. 19: 1139. 1951.

THE ADSORPTION OF NITROGEN BY BROMINATED GRAPHITE AND CARBON BLACK[1]

By H. L. McDermot and J. C. Arnell

ABSTRACT

The adsorption of nitrogen has been measured at 78° K. for three artificial graphites and one carbon black, which have been brominated to saturation and then debrominated by heat-treatment under vacuum or in the presence of an inert gas over a range of temperatures. During the bromine removal, the graphites were heated to a maximum temperature of 1000° C. and the carbon black to a maximum of 1200° C. When the graphite of smallest area was brominated it did not return to its original area even after heat-treatment at 1000° C., whereas the graphite of largest area exceeded its original area when it was brominated and heated at 1000° C. The surface area of the brominated carbon black was restored to the original value when it was evacuated at 400° C. After evacuation at 600° C., the surface area was greater than that of the original carbon black, but fell to a value less than the original area when the sample was evacuated at 1200° C. These observations are believed to be in accord with the known structures of the graphites and the carbon black.

INTRODUCTION

It has been known for a long time that graphite sorbs copious quantities of bromine when simply exposed to the vapor at room temperature. In 1933, Frenzel (2) found that graphite took up 83.5% of its own weight of bromine from an atmosphere saturated with bromine vapor. This observation was confirmed by Rüdorff (7) who undertook a systematic investigation of the sorption of bromine by a variety of natural graphites. He found that they all sorbed very nearly 83% of their own weight irrespective of the size of the graphite crystals. From this observation together with the large bromine sorption he concluded that bromine was not simply adsorbed on the surface of the crystals. Microscopic observation of single crystals of graphite revealed an expansion along the *c*-axis of the crystal accompanying bromination. X-ray diffraction photographs of the brominated graphite showed only 001 lines whose position indicated an identity period of 10.4 Å compared to an identity period of 3.35 Å for the untreated graphite. All of these experimental observations were explained by postulating that the bromine was intercalated between the sheets of hexagonally arranged carbon atoms which comprise the graphite crystal. Since the amount of bromine sorbed was independent of the size of the graphite crystals, it follows that virtually all the bromine was held in this fashion.

Following the work of Rüdorff, little work was done on the subject of brominated graphites. In particular, with the exception of an important investigation by Hennig (4), no work was done on the properties of the product remaining after debromination of the graphite. This product, which is a graphite containing a small amount of firmly held bromine, has been called a "residue compound" by Hennig (4). He has shown that the composition of

[1]*Manuscript received April 23, 1956.*
Contribution from the Defence Research Chemical Laboratories, Ottawa, Canada. Also issued as D.R.C.L. Report No. 214.

these compounds is a function of the composition of the parent lamellar compounds and of the temperature to which the parent compound is heated during decomposition. Hennig measured the X-ray diffraction patterns of some of the residue compounds and found only a very slight increase in the c spacing of the graphite compared to that of the unbrominated graphite. He concluded from this that very little of the bromine of the residue compound was intercalated in the graphite. He suggests that it was trapped by crystal imperfections.

The work to be presented logically follows that done by Hennig. It is a systematic investigation of some of the adsorptive properties of residue compounds prepared from three artificial graphites and one carbon black. In particular, the surface area and hysteresis effects have been studied by measuring the adsorption of nitrogen at 78° K.

EXPERIMENTAL AND RESULTS

Three graphites and one carbon black were chosen for study. The graphites used were artificial graphites manufactured by Acheson Colloids Ltd. and have been described previously by McDermot and Arnell (5). For the purpose of this work, they have been designated as G-1, G-2, and G-3. The carbon black, designated as Spheron 9, was provided through the courtesy of the Godfrey L. Cabot Co. Some of its properties have been given by McDermot and Lawton (6). All the samples were brominated by exposure to saturated bromine vapor in the absence of air at room temperature. The surface areas of the graphites and of the carbon black prior to bromination and the approximate amounts of bromine sorbed by them are presented in Table I.

TABLE I

	Surface area, meters²/gm.	Weight of bromine sorbed, gm./gm.
G-1	45	0.6
G-2	96	—
G-3	18	0.6
Spheron 9	112	0.4

It will be noted that there is no correlation between the weights of bromine sorbed and the surface areas of the graphites. Moreover the amounts of bromine sorbed are considerably less than those reported by Rüdorff.

After bromination the residue compounds were prepared by evacuating the samples at a series of temperatures beginning at room temperature and continuing up to about 1000° C. After each period of heating the samples were cooled in liquid nitrogen and the nitrogen adsorption measured at 78° K. In some of the early experiments, equipment was not available for heating the samples to high temperatures *in vacuo* and therefore they were heated in a stream of inert gas. For completeness the adsorption of nitrogen was measured for one graphite while it was still saturated with bromine.

The results for G–3 are presented first because most of the work was done with this graphite. The surface areas corresponding to different heat treatments are listed in Table II for three series of experiments carried out on this graphite.

TABLE II

Run	Treatment	Br_2 retained, gm./gm.	Surface area, meters²/gm.
1	Saturated with Br_2	0.6	5.2
	Evacuation at 100° C.	—	10.5
	Evacuation at 300° C.	0.07	9.8
2	Evacuation at 25° C.	0.068	8.6
	Evacuation at 100° C.	0.064	9.9
	Evacuation at 300° C.	0.055	10.1
	Evacuation at 600° C.	0	9.6
	Evacuation at 1000° C.	0	11.8
3	Saturated with Br_2 to only 0.24 gm./gm.		
	Evacuation at 25° C.	0.03	7.9
	Untreated graphite	—	18.4

Some of the results from Run 1 are plotted in Fig. 1 along with the isotherms of the untreated graphite. The isotherm measured after the 300° C. evacuation is omitted because it was almost identical to that for the 100° C. evacuation. Fig. 2 depicts the isotherms measured after evacuation of the sample at room temperature and after heating it to 1000° C.

In a previous paper dealing with these graphites (5), McDermot and Arnell demonstrated the existence of two types of hysteresis in the low temperature isotherms. The first type of hysteresis, which was believed to be due to the porous nature of the graphites, manifested itself as a broad hysteresis loop extending from saturation down to a relative pressure of approximately 0.45. This type of hysteresis has been called "pore" hysteresis. The second type of hysteresis, which was termed "swelling hysteresis", was attributed to intercrystalline swelling and was seen as an inability of the desorption curve to rejoin the initial adsorption curve below a relative pressure of 0.45, where "pore" hysteresis was manifestly impossible.

Both of these hysteresis effects are evident in the isotherms for nitrogen adsorbed on G-3. In the case of the graphite saturated with bromine, the isotherm was found to be reversible over the whole range of relative pressures as might be expected if it is assumed that the pore space and the space responsible for swelling are completely filled with bromine at saturation. Both types of hysteresis are absent. As bromine is removed from the saturated graphite the pores empty and the hysteresis loop, characteristic of the pore structure, reappears in the samples which have been evacuated at temperatures as low as 25° C. This is shown by the isotherm in Fig. 2 (triangles) measured after evacuation at room temperature. Swelling type hysteresis only reappears in the later stages of debromination where evacuation at high temperatures was used. In the case of G-3, swelling hysteresis was observed only after the sample had been heated to 1000° C. as is shown by the squares in Fig. 2.

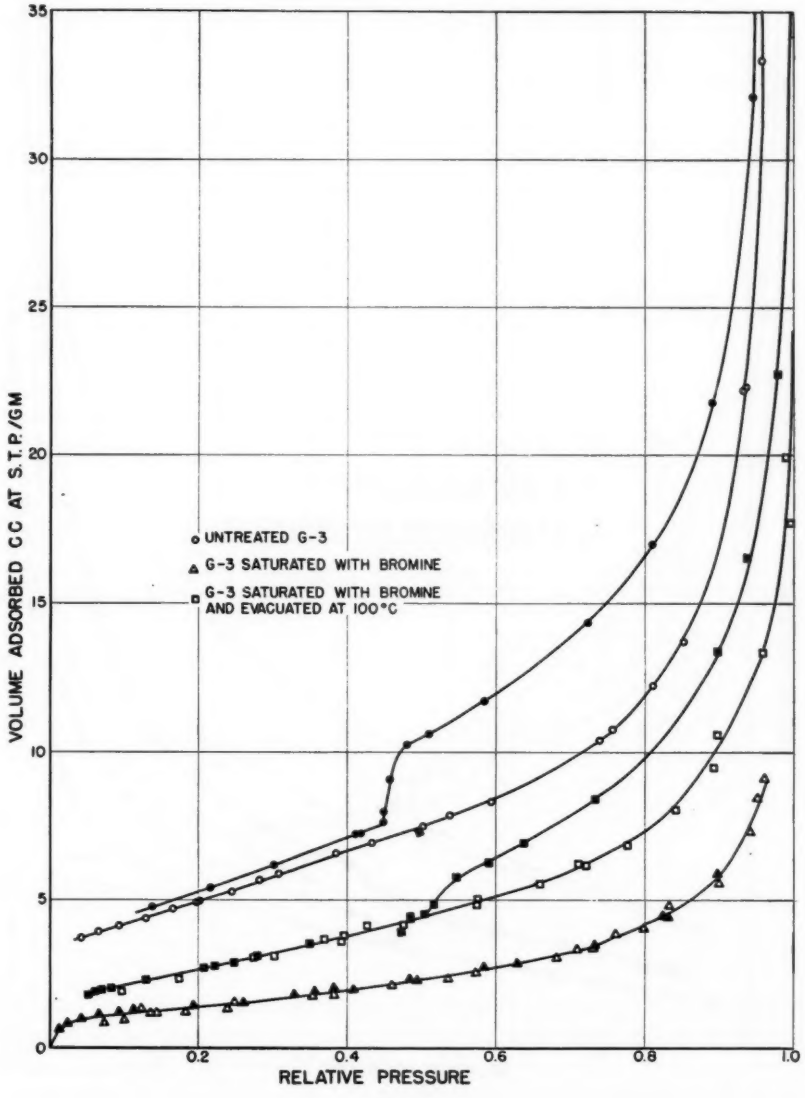

FIG. 1.

An experiment was conducted to ascertain the effect of partial bromination of a sample of G-3. The sample was brominated to a concentration of 0.24 gm. bromine/gm. graphite and then evacuated at room temperature to a bromine content of 0.033 gm./gm. The isotherm measured after this treatment is compared to one measured after room temperature evacuation of a fully bro-

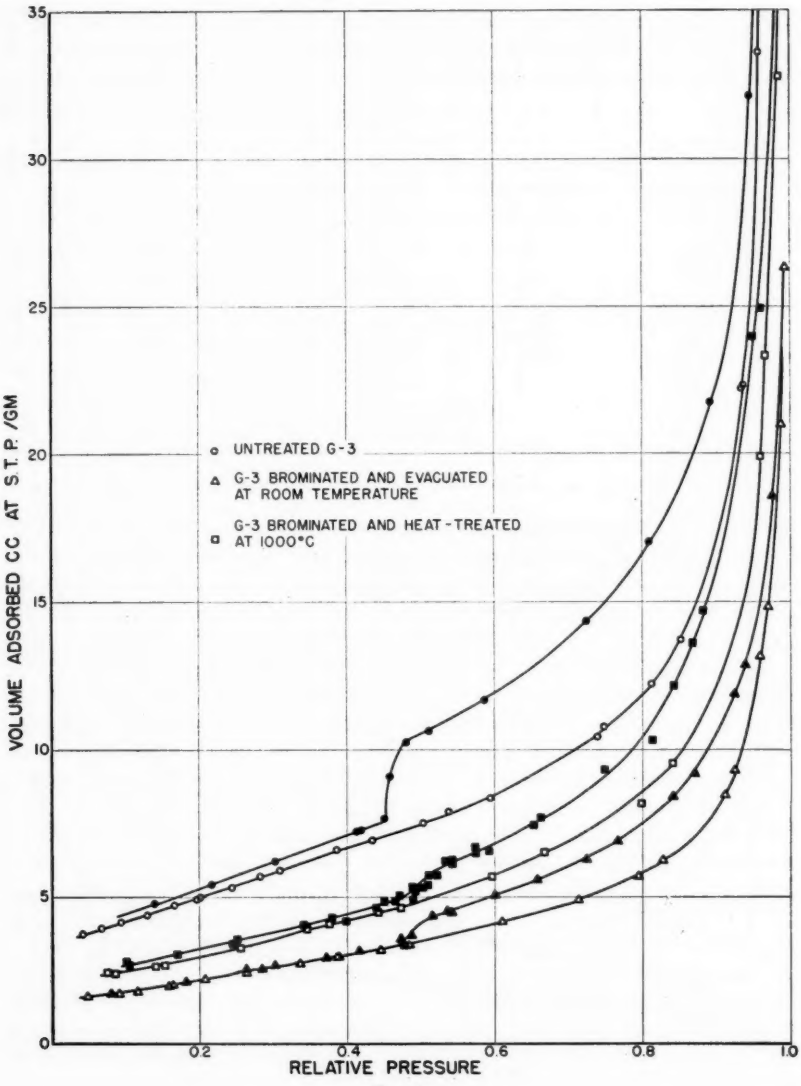

FIG. 2.

minated sample in Fig. 3. After evacuation at room temperature the bromine content of the saturated sample fell from 0.6 gm./gm. to 0.068 gm./gm. It is clear that the surface areas of the two samples are identical. It will be noted that the desorption curve obtained after evacuation of the partially brominated graphite is slightly higher than that measured after evacuation of the fully brominated sample. This is believed to be due to the fact that during

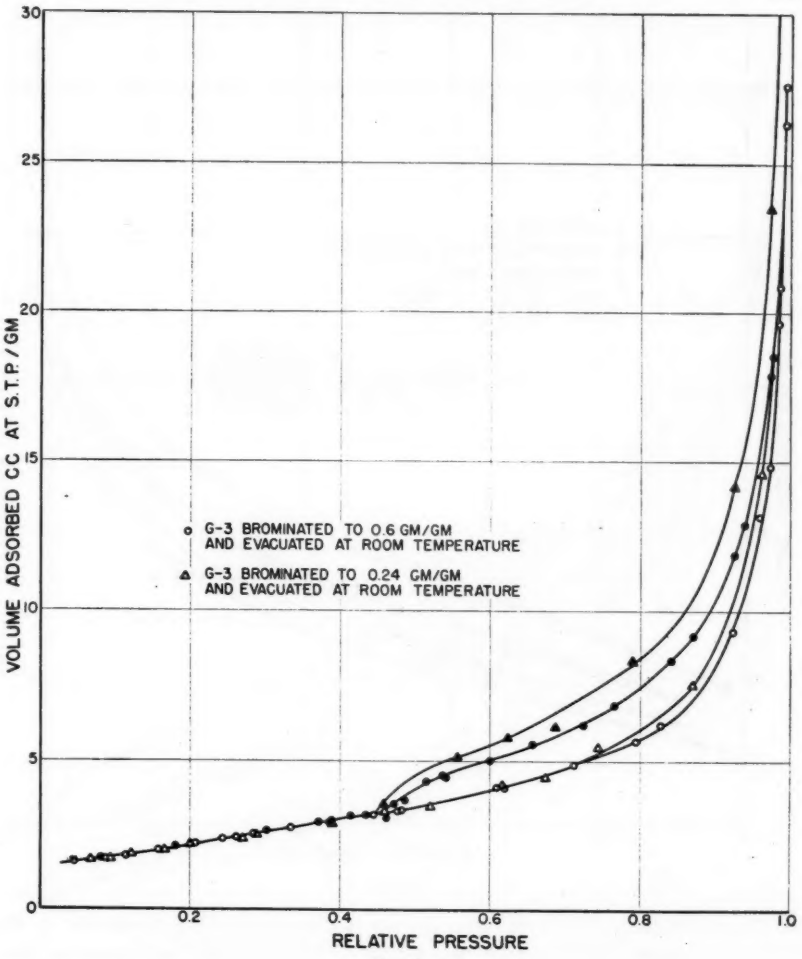

FIG. 3.

nitrogen adsorption a somewhat higher degree of saturation was reached in the former case than in the latter, rather than because of any difference in pore structure between the two samples.

The effect of bromination on G-1 is illustrated by the isotherms shown in Fig. 4. The isotherms were measured with a sample of G-1 which had been saturated with bromine, evacuated successively at room temperature and 200° C., and then heat-treated at 500° C. and 1000° C. For the sake of clarity the desorption points at the higher pressures are omitted because this part of the isotherm is similar in shape for all of the graphites and is illustrated by the isotherm following the 200° C. evacuation. The lower desorption points are included because they again point out that the so-called swelling hysteresis,

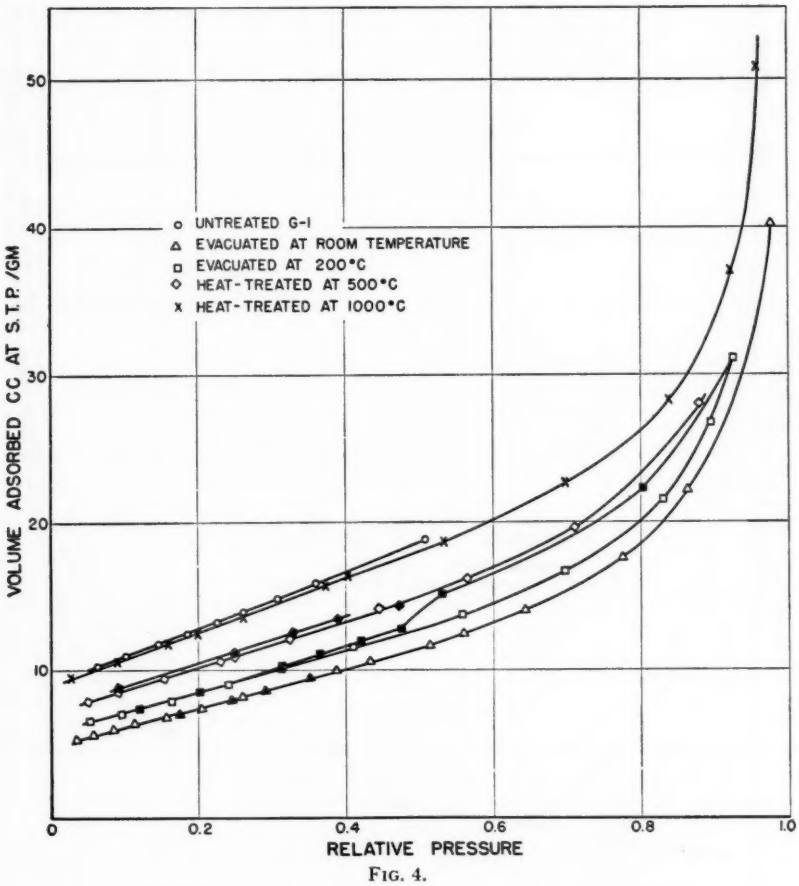

FIG. 4.

which is absent in the room temperature isotherm, becomes apparent in the 500° C. isotherm. It should be noted that unlike G-3, the surface area does return to almost its original value after the 1000° C. heating. The surface area corresponding to the various treatments along with the quantity of bromine retained by the graphite is given in Table III.

TABLE III

Treatment temperature, °C.	Br_2 retained, gm./gm.	Surface area, meters²/gm.
25	0.03	27
200	0	32
500	0	37
1000	0	44
Untreated graphite		46

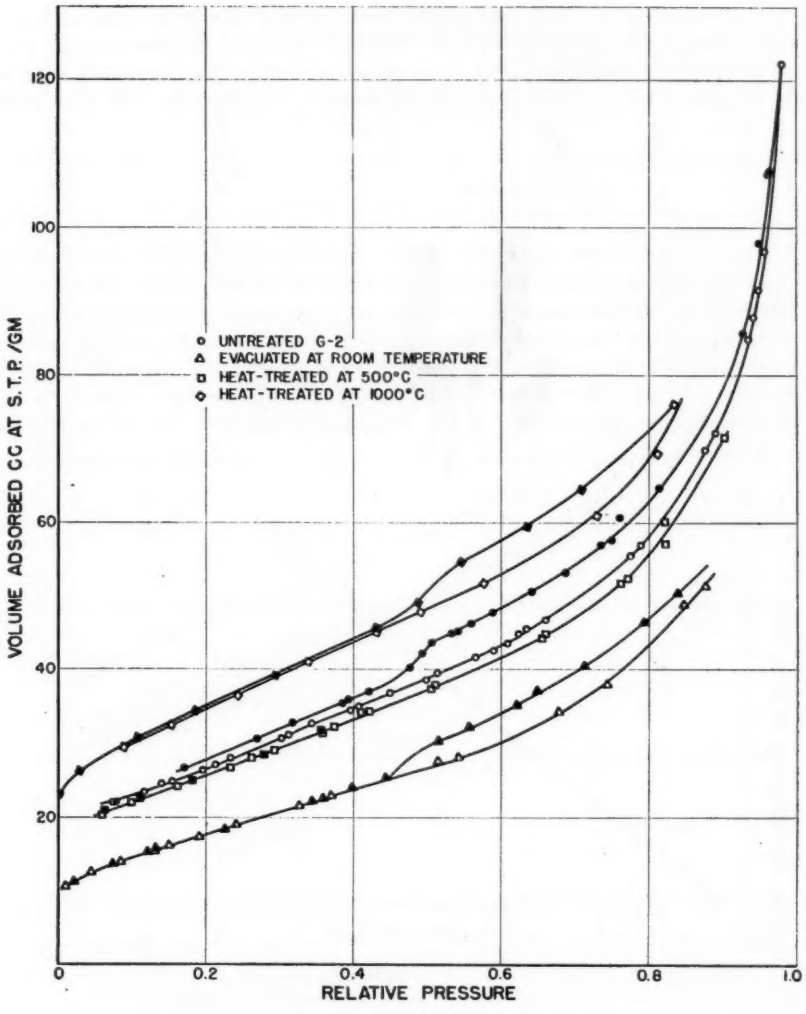

FIG. 5.

Isotherms were measured with a sample of G-2 which had been saturated with bromine, evacuated at room temperature, and then heat-treated at 500° C. and 1000° C. These isotherms along with that for the untreated graphite are presented in Fig. 5. For clarity many of the desorption points have been omitted. The most remarkable feature of these isotherms is the increase in surface area observed after the 1000° C. heat-treatment over that of the untreated graphite. This is also brought out in Table IV which gives the surface areas corresponding to different heat-treatments.

TABLE IV

Treatment temperature, °C.	Br_2 retained, gm./gm.	Surface area, meters²/gm.
25	0.09	70
500	0	92
1000	0	121
Untreated graphite		96

The increase in area over that of the original graphite which was observed after the 1000° treatment was quite different from the behavior of the graphites with smaller surface areas. Accordingly an experiment was done to ascertain that the increase was indeed characteristic of the brominated graphite and not of the graphite. A sample of G-2 was heated to 1000° C. for the same length of time as was used for the brominated compound. The isotherm was measured for this sample and is shown in Fig. 6 along with that for the untreated G-2.

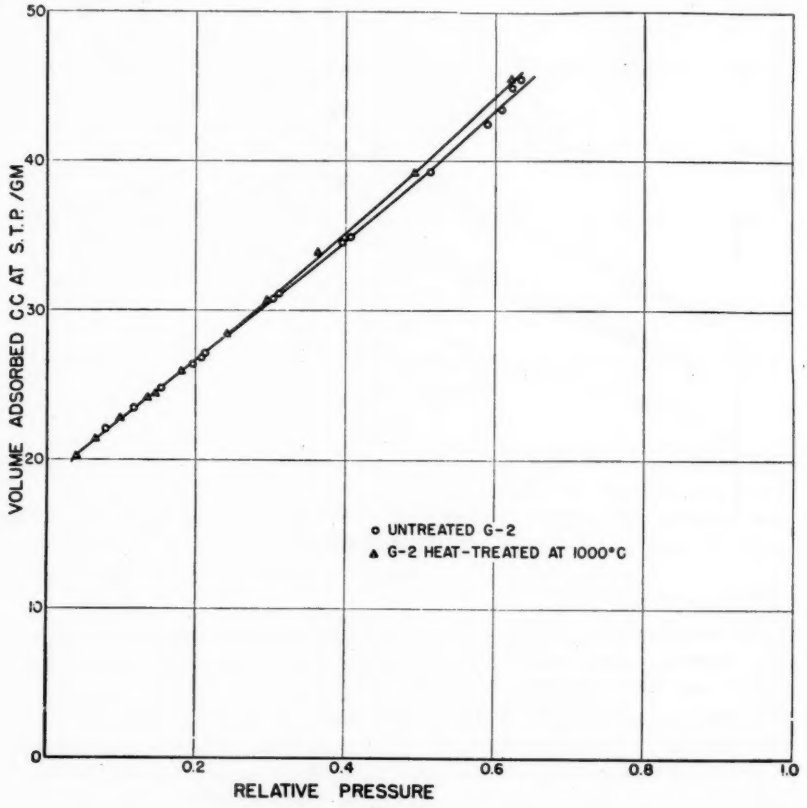

FIG. 6.

It can be seen that there is little difference between the two isotherms.

Isotherms were measured for a sample of Spheron 9 which was brominated, evacuated successively at room temperature, 200°, and 400°, and then heat-treated at 600° and 1200° C. Representative isotherms are shown in Fig. 7

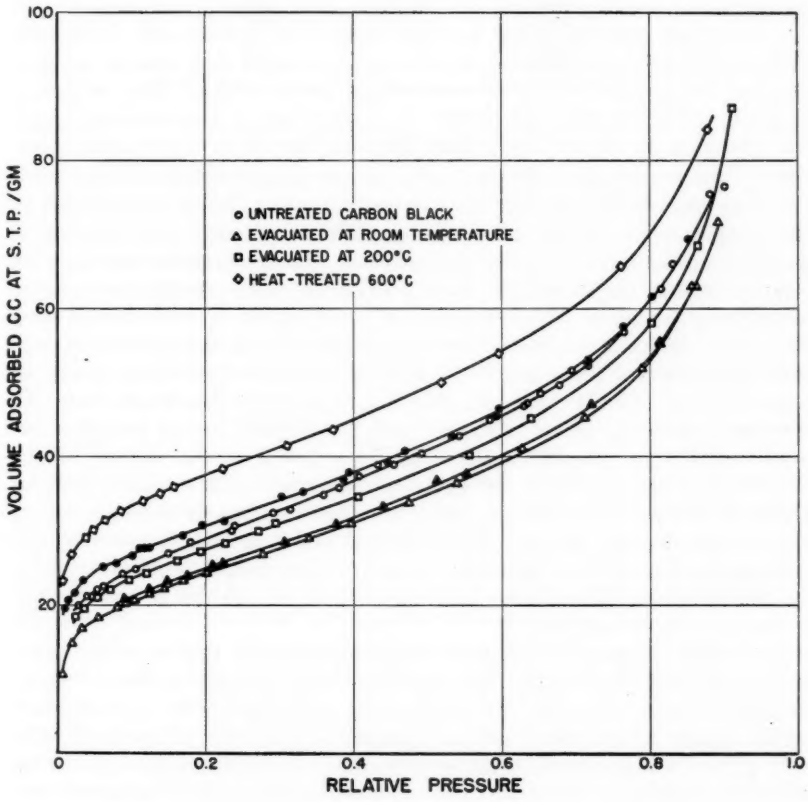

FIG. 7.

along with the isotherm of the untreated carbon black. All of the isotherms exhibited swelling hysteresis but this is only shown for one of the isotherms to avoid a confusion of points. It will be noted that this is the first carbon whose isotherms after room temperature evacuation have shown this type of hysteresis. The surface areas corresponding to various temperatures along with the amounts of bromine retained by the Spheron are given in Table V.

The table shows that the surface area increased to more than its original value at 600° C. and then with further heating to 1200° C. dropped to below its original value.

TABLE V

Temperature, °C.	Br_2 retained, gm./gm.	Surface area, meters²/gm.
25	0.345	89
200	0.091	98
400	0.026	102
600	0	131
1200	0	94
Untreated	—	104

DISCUSSION

In the initial stages of debromination all the graphites behaved the same way. The adsorptive behavior of a fully brominated graphite is illustrated by the isotherm shown in Fig. 1 for a sample of G-3 saturated with bromine. It is clear from the lack of hysteresis in this case that the bromine has filled the pores as well as the interstitial spaces which are believed to be responsible for swelling hysteresis. When the sample is evacuated at room temperature most of the bromine is removed, the surface area increases considerably, and part of the pore volume is emptied as is shown by restoration of the hysteresis loop. However, in all the graphites, the lower parts of the isotherms were still reversible after evacuation at room temperature showing that bromine continued to block the adsorption sites that were responsible for swelling hysteresis. McDermot and Arnell (5) have suggested that this so-called swelling hysteresis is due to a process of intercrystalline swelling. It is reasonable to suppose that the area between the crystallites responsible for this swelling was occupied by bromine and was thus denied to the nitrogen molecules. Hence the absence of swelling hysteresis and the cause for the loss of some of the surface area of the sample.

In the case of Spheron 9 the surface area measured by the low temperature nitrogen adsorption method is not the area of the crystallites, but of agglomerates of many crystallites. Moreover the crystallites of the carbon black are not regular crystals such as those of graphite but are more correctly parallel layer groups in which the orientation is random in an axis perpendicular to the layers of carbon atoms (1). Spheron 9 is not porous but it does display swelling type hysteresis (6). It is interesting to note in this connection that although the carbon black loses a considerable fraction of its original surface area on bromination and subsequent evacuation at room temperature, swelling hysteresis is still present in contrast to the behavior of the graphites. This point is shown very clearly by the isotherm outlined by the triangles in Fig. 7. Such behavior is remarkable because after evacuation at room temperature the carbon black retains more bromine than any of the graphites. McDermot and Lawton (6) have proposed that intercrystalline swelling is also responsible for the hysteresis effects that they have observed to accompany the adsorption of nitrogen by Spheron 9. Since the crystallites of the carbon black are compacted into agglomerates it is possible that spaces responsible for swelling hysteresis are of such a size that they may be penetrated by nitrogen molecules,

but not by the much larger bromine molecules. Hence, swelling hysteresis appears for the sample after evacuation at room temperature despite the fact that a relatively large amount of bromine is retained by the carbon black.

It is of particular interest to examine in some detail the behavior of the graphites after evacuation at 1000° C. The graphite of lowest surface area G-3 loses area when it is brominated and never regains it entirely even when heated to 1000° C. By contrast G-2, which has the highest surface area, shows an increase in area with respect to its original area when it is brominated and heated to 1000° C. G-1, whose surface area lies between the other two, just reaches its surface area after heating to 1000° C. The behavior of the graphites would thus appear to be related to the surface area of the starting material. Wilson and McDermot (8) have taken X-ray diffraction photographs of two of the Acheson graphites, of which one was G-3, and showed that the line broadening is consistent with their nitrogen surface areas. Hence the surface area can be taken to be a measure of the crystallite dimensions, in which case G-3 has the largest crystallites and G-2 the smallest. Viewed in these terms it is clear that the loss in surface area on bromination and subsequent removal of bromine at high temperatures such as was observed for G-3 can only be explained by the filling of cracks or crevices by bromine or by crystallite growth. The first explanation would be expected to apply at low debromination temperatures because the bromine would be held by strong adsorptive forces which prevail in such fissures. However, it is reasonable to expect that a temperature of 1000° C. would suffice to drive off physically adsorbed bromine. Hence the loss of surface area after the high temperature treatment is likely due to crystallite growth resulting from the bromine and the high temperature treatments. In the case of G-2, the area of the brominated graphite which has been treated at 1000° C. is greater than that of the untreated graphite. By the same reasoning it must be assumed that the new surface area has been produced by a decrease in the average crystallite size due to an activation process resulting from the bromine and the heat-treatment. It has been proved experimentally that crystallite growth does not occur when G-2 is heated to 1000° C. (see Fig. 6); therefore, the activation process is not opposed by a tendency toward crystallite growth. Hence the difference in behavior between the graphites must be due to different susceptibilities towards crystallite growth and towards activation by bromine. Furthermore it would appear that these susceptibilities are related to the crystallite dimensions because it is only in this respect that the graphites differ appreciably from one to another.

It was observed that heat-treatment of brominated Spheron 9 at 600° C. produced a carbon black of much higher surface area than the original Spheron. This may have been caused by bromine activation at 600° C. which opened up new surface area for nitrogen adsorption. Further heating at 1200° C. diminished the area to a value slightly less than that of the parent carbon black. In this instance, it is likely that the heat-treatment caused some crystal growth with a consequent loss of surface area.

No attempt has been made in the course of this work to investigate the fully brominated compound in any detail. All of our attention has been focused on

the residue compounds left after the evacuation of a brominated carbon. However it is noteworthy that contrary to the findings of Rüdorff (7), carbons of different crystallite dimensions sorbed different quantities of bromine. Rüdorff (7) and Frenzel (2) found that all their graphites sorbed 0.80 to 0.83 gm. of bromine/gm. of carbon. Goldsmith (3) reports a saturation value of 0.70 gm./gm. The values given in this paper range from 0.4 to 0.6 gm./gm. and do not bear any simple relationship to the area of the carbon. Thus it would appear that the quantity of bromine sorbed depends on the specific carbons and cannot be explained by any single process such as intercalation of bromine between the carbon planes. For example, in the graphites studied here, a part of the bromine was held in the pore structure and part was adsorbed on the surface. Judging by the ease with which most of the bromine could be removed, a large part was probably held by simple condensation between the particles. This idea is borne out by the observation that the powdered graphite, which was a free-flowing powder, became semisolid when saturated with bromine. This would be expected if the particles were stuck together by condensed liquid.

One experiment was done which showed that within the limits investigated the degree of bromination did not effect the surface area of the residue compound. A sample of G-3 which was only partially brominated yielded the same surface area after room temperature evacuation as a sample which had been saturated with bromine and then evacuated at room temperature, notwithstanding the fact that the quantities of bromine held by the two residue compounds were different. This is in accord with the notion that most of the bromine is held rather superficially and the only part that effects the surface area is that which is adsorbed or condensed between the crystallites.

REFERENCES

1. Biscoe, J. and Warren, B. E. J. Appl. Phys. 13: 364. 1942.
2. Frenzel, A. Dissertation Tech. Hochschule, Berlin. 1933.
3. Goldsmith, M. J. Chem. Phys. 18: 523. 1950.
4. Hennig, G. J. Chem. Phys. 20: 1438. 1952.
5. McDermot, H. L. and Arnell, J. C. Can. J. Chem. 33: 913. 1955.
6. McDermot, H. L. and Lawton, B. E. Can. J. Chem. 34: 769. 1956.
7. Rüdorff, W. Z. anorg. Chem. 245: 383. 1941.
8. Wilson, L. G. and McDermot, H. L. Unpublished.

INTENSITY IN THE RAMAN EFFECT

V. THE EFFECT OF INTERMOLECULAR INTERACTION ON THE RAMAN SPECTRUM OF CARBON DISULPHIDE[1]

By J. C. Evans[2] and H. J. Bernstein

ABSTRACT

The Raman spectrum of CS_2 has been obtained photoelectrically for the liquid and solutions of varying concentrations in cyclopentane, and depolarization ratios and intensities measured. The intensity of the forbidden bands ν_2 and ν_3 relative to that of the Raman active band ν_1 decreases rapidly with dilution. The bands are present because of intermolecular interaction which probably occurs between the C atom of one molecule of CS_2 and only one of the S atoms of the other.

The Raman spectrum of liquid CO_2 has been investigated recently (9) and the doubly degenerate bending mode ν_2 and the antisymmetric stretching mode ν_3 which are forbidden by selection rules have been observed as weak bands along with the allowed totally symmetrical stretching mode ν_1. Although depolarization ratios of the forbidden bands were not measured it was argued from the band contours (9) in the liquid that ν_2 is depolarized and ν_3 polarized. These data have been interpreted on the basis of strong intermolecular interaction in liquid CO_2 which distorts the molecule along its length so that the center of symmetry is essentially destroyed (9).

One might expect a closely parallel situation with regard to spectral details and the effects of intermolecular interaction for carbon disulphide. In this paper we have investigated the Raman spectrum of CS_2, liquid and in solutions of cyclopentane, in order to establish—(i) that the presence of the forbidden bands in the Raman spectrum is indeed due to the environment and (ii) the effect of the interaction on the shape of the molecule.

The Raman spectrum of CS_2 (5), depolarization ratios (2), and relative intensities (6) have been obtained some years ago and the discussion of its spectrum and the effect of Fermi interaction given by Placzek (7) on the basis of these older data. Newer data have been compiled by Herzberg (4) and the positions of the bands given there are confirmed by our investigation to within ± 1 cm.$^{-1}$. For purposes of calculating resonance interaction constants the more accurately measured data quoted by Herzberg have been used. The depolarization ratios of the forbidden bands ν_2 and ν_3 have been measured confirming Bhagavantam's result (2) for ν_2 and ν_3 (polarized). For purposes of comparing frequencies the infrared spectrum of the liquid was also obtained.

EXPERIMENTAL

The Raman spectra were photoelectrically recorded on a White grating Raman spectrometer (10) using λ4358 as the exciting line. Depolarization ratios (ρ_{obs}) were measured by wrapping polaroid film around the Raman tube,

[1]*Manuscript received April 9, 1956.*
Contribution from the Division of Pure Chemistry, National Research Council, Ottawa, Canada. Issued as N.R.C. No. 4018.
[2]*N.R.C. Postdoctorate Research Fellow 1953–55.*

first with its axis parallel to the tube and then at right angles, and these ratios corrected for convergence (8) to give ρ_{corr}. Integrated intensities were measured relative to the 458 cm.$^{-1}$ band of CCl_4 obtained under identical instrumental and optical conditions and were corrected for the spectral sensitivity of the photomultiplier $\sigma_{\Delta\lambda}$ and for convergence error according to [1]

$$[1] \qquad I_{true} = \left[\frac{I_{obs}(1+\rho_{corr})}{1+\rho_{obs}} \times \sigma_{\Delta\lambda} \Big/ \left\{ \frac{I_{obs}(1+\rho_{corr})}{1+\rho_{obs}} \times \sigma_{\Delta\lambda} \right\}_{458 cm.^{-1}} \right] \times 100$$

where 100 is taken as the true integrated intensity of the 458 cm.$^{-1}$ band in CCl_4.

When bands overlapped, no attempt to resolve them by curve analysis was made, the measured intensity being taken as the area under the contour. This is indicated by bracketing bands in the tables. The Raman spectra of three solutions of CS_2 in cyclopentane were also measured in which the ratio of the volume of CS_2 to the total volume was 0.65, 0.49, and 0.36. The infrared spectrum was obtained with a Perkin Elmer 12C double pass spectrometer using CsBr, KBr, and NaCl optics. The results for CS_2 liquid are given in Table I and the Raman spectrum shown in Fig. 1.

TABLE I
LIQUID CS_2

Assignment[a]	$\Delta\nu$[b]	Raman $\Delta\nu$	Raman ρ_{obs}	Raman ρ_{corr}	Raman I_{true}[d]	Infrared ν
ν_2		390	0.7$_9$	0.6$_3$[c]	9.7$_3$	393 s.
ν_1'	648.3	648	0.4$_1$	0.2$_5$	488	
ν_1	656.5	655				654 w.
$2\nu_2$	796.0	797	0.4$_0$	0.2$_5$	94.2	789 v.w.
$2\nu_2'$	804.9	804				809 v.w.
ν_3		1515	0.7$_9$	0.6$_3$	6.9$_4$	Not measured

[a] *ν_1' and $2\nu_2'$ are satellite lines corresponding to the transitions (11'0), (03'0) ← (01'0).*
[b] *Data from Herzberg, Ref. 4.*
[c] *Measured by Bhagavantam to be 0.8 (Indian J. Phys. 7: 83. 1932).*
[d] *The 458 cm.$^{-1}$ band of CCl_4 is 100.*

Rough decomposition of the overlapped doublets at ~650 and 800 cm.$^{-1}$ indicates that the band at 648 cm.$^{-1}$ contributes about one-third of the total intensity and 804 cm.$^{-1}$ contributes about two-fifths of the intensity in its doublet. The ratio of the areas under the doublets is then

$$I_{800}/I_{650} = 94.2/488 = 0.193$$

and a rough estimate of $I_{2\nu_2}/I_{\nu_1}$ is 0.17$_4$. These ratios are to be compared with 0.32 obtained photographically by Pienkowski (6).

The intensities of the doublets at 650, 800 cm.$^{-1}$ and the forbidden band at 390 cm.$^{-1}$ have been measured as functions of concentration and the results shown in Figs. 2, 3, and 4, respectively. It should be mentioned that depolar-

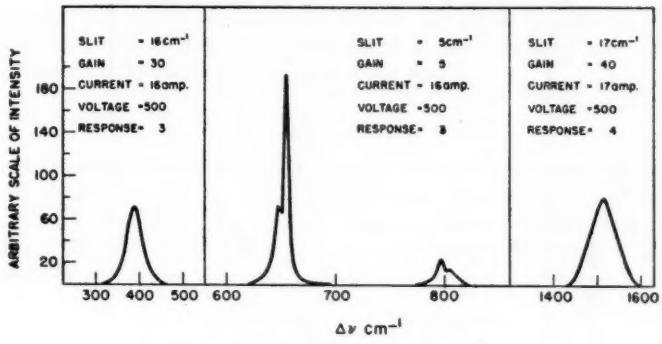

FIG. 1. Raman spectrum of liquid CS_2.

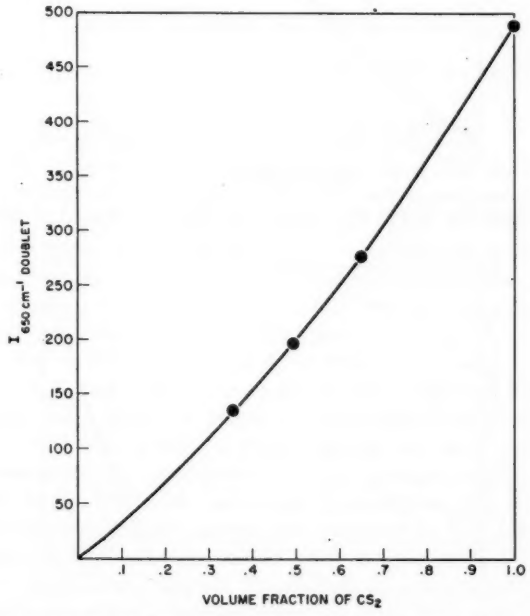

FIG. 2. Raman intensity of 650 cm.$^{-1}$ doublet of CS_2 as a function of concentration in cyclopentane.

ization ratios of the doublets and frequencies did not change within experimental error as a function of concentration, nor did the contours of the doublets at 650 and 800 cm.$^{-1}$. The ν_2 band position changed slightly as a function of concentration (from 390 cm.$^{-1}$ in CS_2 to 387 cm.$^{-1}$ in dilute solution) whereas the depolarization ratio was too uncertain to indicate whether or not changes in it took place. The depolarization ratio under most favorable conditions was very difficult to measure for the 390 cm.$^{-1}$ band because of overlapping (at

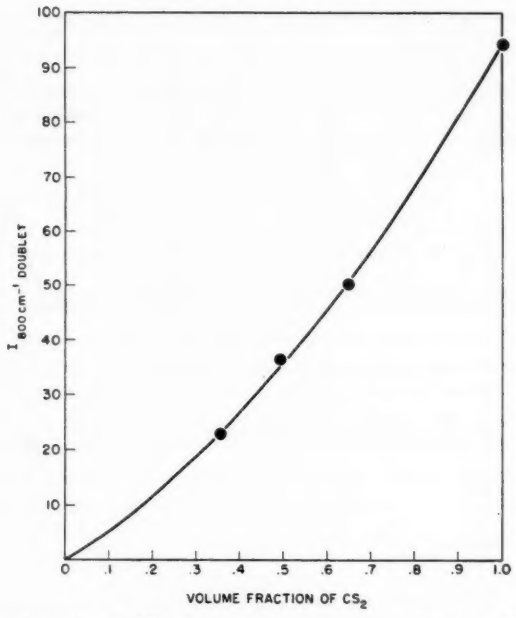

FIG. 3. Raman intensity of 800 cm.$^{-1}$ doublet of CS_2 as a function of concentration in cyclopentane.

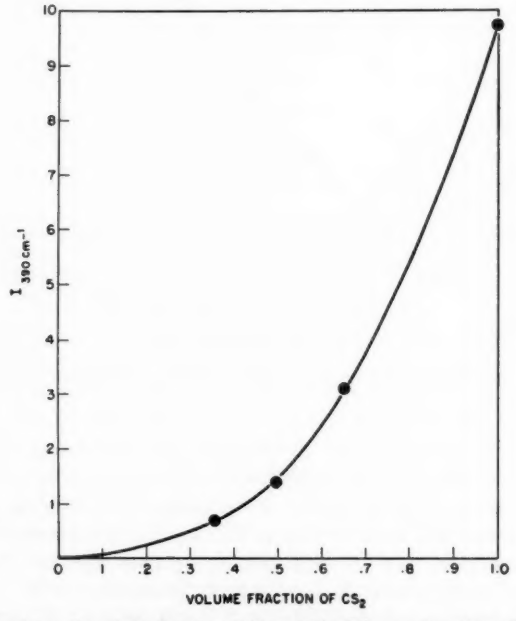

FIG. 4. Raman intensity of the band at 390 cm.$^{-1}$ in CS_2 as a function of concentration in cyclopentane.

wide slits) with either the exciting line or the band at 650 cm.$^{-1}$ or both. The uncertainty in the quoted depolarization ratio may be as much as 0.15 for ν_2 whereas it is about 0.03 for the other bands.

DISCUSSION

From Placzek's formulae (7) for the separation of the main resonating components ν_1 and $2\nu_2$, viz. $X_1 = \sqrt{(\delta^2+4w^2)}$, and that for the satellites (ν_1' and $2\nu_2'$), viz. $X_2 = \sqrt{(\delta^2+8w^2)}$, we find, using the more accurate data quoted by Herzberg, that $\delta = 120.0$ cm.$^{-1}$ and $w = 35.6$ cm.$^{-1}$ for liquid CS_2. Further, according to the theory for resonance (5),

$$\frac{I_{2\nu_2}}{I_{\nu_1}} = \left(\frac{\sqrt{X_1-\delta}\,\alpha_1-\sqrt{X_1+\delta}\,\alpha_2}{\sqrt{X_1+\delta}\,\alpha_1+\sqrt{X_1-\delta}\,\alpha_2}\right)^2$$

where α_1 and α_2 are the polarizability derivatives for the transitions

$$(10°0) \leftarrow (00°0) \text{ and } (02°0) \leftarrow (00°0)$$

respectively. If $\alpha_2/\alpha_1 \ll 1$, which is usually true for the ratio of overtone to fundamental,

$$I_{2\nu_2}/I_{\nu_1} \approx (X_1-\delta)/(X_1+\delta) = 0.075_3.$$

The calculated value for this intensity ratio is about half the observed value. Using the approximate value for $I_{2\nu_2}/I_{\nu_1}$ obtained experimentally (0.17_4) and solving for α_2/α_1 gives -0.128 for this ratio. Since the uncertainty in the experimental intensity ratio is large, it is not even possible to say that the sign of the calculated ratio α_2/α_1 is correct. The negative sign would imply of course that either α_2 or α_1 was negative. Since the sum of the unperturbed levels $\nu_1°+2\nu°$ is the same as $\nu_1+2\nu_2 = 1452.5$ cm.$^{-1}$, and $2\nu_2°-\nu_1° = 120.0$ cm.$^{-1}$, we find that $2\nu_2° = 786.2$ cm.$^{-1}$ and $\nu_1° = 666.2$ cm.$^{-1}$ for liquid CS_2.

From Figs. 2, 3, and 4 we see that the bands at 650 and 800 cm.$^{-1}$ do not deviate as markedly from the linear concentration dependence as does the band at 390 cm.$^{-1}$. The deviation from linearity can arise not only from the effects of intermolecular interaction but also because of the dependence of the intensity on the refractive index and the reflection loss (1). If account is taken of these factors and the corrections indicated in Ref. 1 made, the result that the most marked intensity fall-off with concentration is experienced by the 390 cm.$^{-1}$ band is not altered. This would be expected if the presence of this band is due to intermolecular interaction. It is interesting to compare also the relative intensities of these bands as a function of concentration (see Table II).

It is evident from Table II that the relative intensity of the allowed doublets at 650 and 800 cm.$^{-1}$ remains approximately constant whereas the relative intensity of the 390 cm.$^{-1}$ band approaches zero with dilution. This is direct evidence that this band arises primarily from the action of the intermolecular force field. Buchheim (3) has shown that the ratio of the intensity of this forbidden band to that of the allowed band ν_1 should be proportional to the square of the field strength. If we assume a coulombic field between interacting CS molecules, and that the distance between interacting molecules is

TABLE II

Solution, vol. fraction of CS_2	Relative intensity*		
	390 cm.$^{-1}$	650 cm.$^{-1}$ doublet	800 cm.$^{-1}$ doublet
1.0	2.0_0	100	19.3
0.65	1.1_1	100	18.1
0.49	0.69	100	18.6
0.36	0.50	100	17.0

**The fourth power scattering term and the temperature dependent exponential term have not been included in the intensity.*

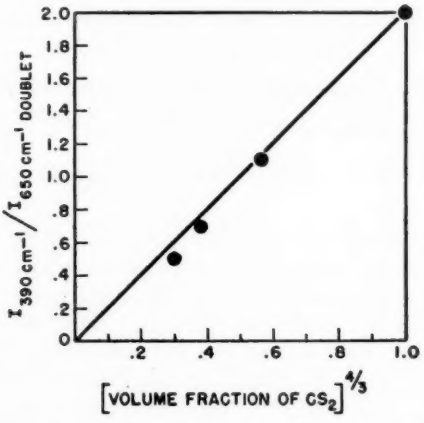

FIG. 5. Relative intensity of the 390 cm.$^{-1}$ band of CS_2 as a function of (concentration)$^{4/3}$.

proportional to the (molecular-volume)$^{1/3}$ then according to Buchheim the relative intensity of the 390 cm.$^{-1}$ band should be proportional to (volume-fraction)$^{4/3}$. This plot is shown in Fig. 5.

The reason the forbidden bands ν_2 and ν_3 appear in the Raman spectrum is to be found in the effects of the interaction field. In CO_2 the field distorted the molecule in the direction of the OCO axis giving essentially $C_{\infty v}$ symmetry (9) with its allowed Raman spectrum of two polarized (ν_1, ν_3) and one depolarized line (ν_2). In the case of CS_2 however both ν_3 and ν_2 are found to be polarized. This suggests that the distortion of the CS_2 molecule is such as to leave the molecule with a plane of symmetry only (C_s), in which case all three fundamentals are allowed in the Raman effect and should be polarized. This would imply not only distortion along the SCS axis but also at right angles to it. This would correspond to the interaction between CS_2 molecules taking place between a C atom of one molecule and only one of the S atoms of the other so that a real difference in field is experienced by the S atoms. Further, this difference is not only along the CS bond but also at right angles to it. On the basis of these spectroscopic data for liquid CS_2 and CO_2 one might expect the crystal structure of CS_2 to be different from that of CO_2.

REFERENCES

1. BERNSTEIN, H. J. and ALLEN, G. J. Opt. Soc. Amer. 45: 237. 1955.
2. BHAGAVANTAM, S. Phys. Rev. 39: 1020. 1932.
3. BUCHHEIM, W. Physik. Z. 36: 694. 1935.
4. HERZBERG, G. Infrared and Raman spectra. D. Van Nostrand Company, Inc., N.Y. 1945. p. 277.
5. MESNAGE, P. L. J. phys. radium, 2: 403. 1931.
6. PIENKOWSKI, S. Acta Phys. Polon. 1: 87. 1932.
7. PLACZEK, G. Handb. Radiol. 6: 328. 1934.
8. RANK, D. H. and KAGARISE, R. E. J. Opt. Soc. Amer. 40: 89. 1950.
9. WELSH, H. L., PASHLER, P. E., and STOICHEFF, B. P. Can. J. Phys. 30: 99. 1952.
10. WHITE, J. U., ALPERT, N., and DEBELL, A. G. J. Opt. Soc. Amer. 45: 154. 1955.

THE DIFFERENTIAL EQUATIONS OF CONSECUTIVE REACTIONS[1]

By A. E. R. Westman and D. B. DeLury

ABSTRACT

The differential equations of consecutive first-order reactions are formulated in a general manner. The solutions of these equations are shown to fall into a pattern, according to which the solutions to all such systems can be written down without resort to formal integration. The pattern is also convenient for making numerical calculations.

A SPECIAL CASE

Suppose that a molecule of tetraphosphate breaks down under hydrolysis to form one molecule of triphosphate and one of orthophosphate, that triphosphate breaks down into one molecule of pyrophosphate and one of orthophosphate, and that one molecule of pyrophosphate breaks down into two of orthophosphate. Let the symbols $\mathscr{A}$. $\mathscr{B}$. $\mathscr{C}$. $\mathscr{D}$ refer to these phosphates and let α, β, γ, δ stand for the numbers of phosphorous atoms in them ($\alpha = 4$, $\beta = 3$, $\gamma = 2$, $\delta = 1$). Let a, b, c, d ($a+b+c+d = 1$) represent the proportions of the phosphorus atoms, at time t, which are present as $\mathscr{A}$. $\mathscr{B}$. $\mathscr{C}$. $\mathscr{D}$ and let a_0, b_0, c_0, d_0 represent their values when $t = 0$. Then, if the reactions are first order and independent of each other and if their rate constants A, B, C* are known, the proportions a, b, c, d at any time t are defined by the following system of differential equations:

$$\text{[I]} \qquad \begin{aligned} (1) \quad -da/dt &= Aa, \\ (2) \quad -db/dt &= Bb-(\beta/\alpha)Aa, \\ (3) \quad -dc/dt &= Cc-(\gamma/\beta)Bb, \end{aligned}$$

with initial conditions $a = a_0$, $b = b_0$, $c = c_0$, $d = d_0$ when $t = 0$. The value of d can be specified either by a differential equation or more simply by the relation

$$d = 1-a-b-c.$$

With a view to generalization later on, the symbol $(\mathscr{P}.\mathscr{Q})$ will be introduced here to stand for the fraction of the phosphorus lost to $\mathscr{P}$ that goes directly into $\mathscr{Q}$. In terms of these symbols, the reaction described above is specified by

$$\begin{aligned} (\mathscr{A}.\mathscr{B}) &= \beta/\alpha, \quad & (\mathscr{A}.\mathscr{C}) &= 0, \quad & (\mathscr{A}.\mathscr{D}) &= 1-(\beta/\alpha); \\ & & (\mathscr{B}.\mathscr{C}) &= \gamma/\beta, \quad & (\mathscr{B}.\mathscr{D}) &= 1-(\gamma/\beta); \\ & & & & (\mathscr{C}.\mathscr{D}) &= 1. \end{aligned}$$

The ratios β/α and γ/β in Equations [I] will be replaced by $(\mathscr{A}.\mathscr{B})$ and $(\mathscr{B}.\mathscr{C})$.

The explicit solution of a set of equations like [I] offers no mathematical difficulty, but the resulting formulae are elaborate and cumbersome and offer too many opportunities for mistakes in calculation. The purposes of this note

[1]*Manuscript received April 27, 1956.*
Contribution from the Department of Chemistry and the Department of Mathematical Statistics, Ontario Research Foundation, Toronto 5, Ontario.

**Symbols A, B, etc., have been used to represent rate constants, instead of the conventional symbols k_A etc., to make the symmetry of the equations more apparent.*

are to put forward an orderly notation for writing the solutions and to point out that, once the underlying pattern of the solutions is perceived, the solutions may be written down directly without resort to formal integration of the differential equations.

Direct integration of Equation (1) yields the solution

$$a = a_0 e^{-At},$$

which will be rewritten in the form

$$a = -a_0(1-e^{-At})+a_0.$$

Again, integration of Equation (2) produces the formula

$$b = a_0\left[-(\mathscr{A}\mathscr{B})\frac{A}{A-B}e^{-At}+(\mathscr{A}\mathscr{B})\frac{A}{A-B}e^{-Bt}\right]+b_0e^{-Bt},$$

which will be rearranged in the form

$$b = a_0\left[(\mathscr{A}\mathscr{B})\frac{A}{A-B}(1-e^{-At})-(\mathscr{A}\mathscr{B})\frac{A}{A-B}(1-e^{-Bt})\right]-b_0(1-e^{-Bt})+b_0.$$

Solutions for c, d, . . . can be expressed in the same manner, but the formulae soon become extremely elaborate. It is suggested here that a form of matrix notation simplifies the statements of these formulae and provides a pattern for writing directly the solutions to any such system of equations. One convenient scheme is the following. Write in a column the arguments $1-e^{-At}$, $1-e^{-Bt}$, etc., and finally, 1. Write in a row the initial amounts a_0, b_0, . . . , as shown in Table I. Then the cell of the table corresponding to an argument and an initial amount receives the appropriate multiplier.

The full pattern of the solution can be seen in the formula for c. The column of multipliers corresponding to a_0 all have the coefficient $(\mathscr{A}\mathscr{B})(\mathscr{B}\mathscr{C})$ which reflects the route by which a_0 has contributed to c. Likewise, they all contain the product of the rate constants AB, the two rates which are associated with this path. The denominators are selections from the differences $A-B$, $A-C$,

TABLE I

		a_0	b_0	c_0
a	$1-e^{-At}$	-1		
	1	1		
	$1-e^{-At}$	$+(\mathscr{A}\mathscr{B})\frac{A}{A-B}$		
b	$1-e^{-Bt}$	$-(\mathscr{A}\mathscr{B})\frac{A}{A-B}$	-1	
	1		1	
	$1-e^{-At}$	$-(\mathscr{A}\mathscr{B})(\mathscr{B}\mathscr{C})\frac{AB}{(A-B)(A-C)}$		
c	$1-e^{-Bt}$	$+(\mathscr{A}\mathscr{B})(\mathscr{B}\mathscr{C})\frac{AB}{(A-B)(B-C)}$	$+(\mathscr{B}\mathscr{C})\frac{B}{B-C}$	
	$1-e^{-Ct}$	$-(\mathscr{A}\mathscr{B})(\mathscr{B}\mathscr{C})\frac{AB}{(A-C)(B-C)}$	$-(\mathscr{B}\mathscr{C})\frac{B}{B-C}$	-1
	1			1

$B-C$, all taken according to the order of the sequence. The denominator in the multiplier of $1-e^{-At}$ is the product of those differences in which A appears, that of $1-e^{-Bt}$ is the product of those in which B appears, and so on. Lastly, the signs are alternately plus and minus, *starting with a minus sign at the foot of the column*. Similar observations apply to the b_0 column. The final column always consists simply of the -1 and 1.

Application of these rules provides the solutions to any such system of equations provided the conditions $(\mathscr{A}\mathscr{C}) = 0$, etc. are met. A useful check when the multipliers are being calculated numerically is provided by the fact that the multipliers must sum to zero in each cell. This is easily demonstrated algebraically and corresponds to the fact that, as t goes to infinity, the proportions of $\mathscr{A}, \mathscr{B}, \mathscr{C}$, etc. go to zero. (This must be modified if a rate constant is zero. See Appendix II.)

If, as an alternative to the assumption which led to System I, it is assumed that tetraphosphate hydrolyzes directly into pyrophosphate, which in turn breaks down into orthophosphate, System I must be replaced by another set of differential equations whose solutions are not included among those of System I. The solutions to the new system can, of course, be written out, but it seems worth while to lay out a general system of differential equations which includes as special cases those already mentioned and many others and to develop a rule for writing the solutions to the general system.

THE GENERAL SYSTEM

A reaction in which each of a sequence of substances $\mathscr{A}, \mathscr{B}, \mathscr{C}, \mathscr{D}, \ldots$ breaks down to form some or all of the substances which follow it in the sequence, but not those which precede it, will be termed a consecutive reaction. In terms of the symbols and assumptions introduced earlier, the differential equations for this reaction are

$$\text{[II]} \qquad \begin{aligned} (1) \quad -da/dt &= Aa, \\ (2) \quad -db/dt &= Bb-(\mathscr{A}\mathscr{B})Aa, \\ (3) \quad -dc/dt &= Cc-(\mathscr{A}\mathscr{C})Aa-(\mathscr{B}\mathscr{C})Bb, \end{aligned}$$

and so on.

The pattern for writing the solutions to System II is easily built up from the rules developed for System I. Equations (1) and (2) are the same in both systems, but Equation (3) in System II includes a term which provides for the path $\mathscr{A} \rightarrow \mathscr{C}$. The contribution from this path is provided for in the solution by the rule given earlier for a path like $\mathscr{A} \rightarrow \mathscr{B}$, with $\mathscr{B}$ replaced by $\mathscr{C}$ and B by C. The a_0 column in the formula for c is shown in Table II.

Once the solutions to the general system are written out, they may be reduced to any special case by giving the appropriate values to the symbols $(\mathscr{A}\mathscr{B})$, etc. and, when necessary, to the rate constants. For example, the situation tetra- $\rightarrow$ pyro- $\rightarrow$ ortho-, tri- $\rightarrow$ pyro-+ortho-, mentioned above, is specified by the values

$$\begin{aligned} (\mathscr{A}\mathscr{B}) &= 0, \quad & (\mathscr{A}\mathscr{C}) &= 1, \quad & (\mathscr{A}\mathscr{D}) &= 0; \\ & & (\mathscr{B}\mathscr{C}) &= \gamma/\beta, \quad & (\mathscr{B}\mathscr{D}) &= 1-(\gamma/\beta); \\ & & & & (\mathscr{C}\mathscr{D}) &= 1. \end{aligned}$$

COMPLETE FORMULA FOR d, GENERAL SYSTEM

	a_0	b_0	c_0	d_0
$1-e^{-At}$	$+(\mathscr{A},\mathscr{B})(\mathscr{B},\mathscr{C})(\mathscr{C},\mathscr{D})\frac{ABC}{(A-B)(A-C)(A-D)}-(\mathscr{A},\mathscr{B})(\mathscr{B},\mathscr{D})\frac{AB}{(A-B)(A-D)}-(\mathscr{A},\mathscr{C})(\mathscr{C},\mathscr{D})\frac{AC}{(A-C)(A-D)}+(\mathscr{A},\mathscr{D})\frac{A}{A-D}$			
$1-e^{-Bt}$	$-(\mathscr{A},\mathscr{B})(\mathscr{B},\mathscr{C})(\mathscr{C},\mathscr{D})\frac{ABC}{(A-B)(B-C)(B-D)}+(\mathscr{A},\mathscr{B})(\mathscr{B},\mathscr{D})\frac{AB}{(A-B)(B-D)}$	$-(\mathscr{B},\mathscr{C})(\mathscr{C},\mathscr{D})\frac{BC}{(B-C)(B-D)}+(\mathscr{B},\mathscr{D})\frac{B}{B-D}$		
$1-e^{-Ct}$	$+(\mathscr{A},\mathscr{B})(\mathscr{B},\mathscr{C})(\mathscr{C},\mathscr{D})\frac{ABC}{(A-C)(B-C)(C-D)}$ $+(\mathscr{A},\mathscr{C})(\mathscr{C},\mathscr{D})\frac{AC}{(A-C)(C-D)}$	$+(\mathscr{B},\mathscr{C})(\mathscr{C},\mathscr{D})\frac{BC}{(B-C)(C-D)}$	$+(\mathscr{C},\mathscr{D})\frac{C}{C-D}$	
$1-e^{-Dt}$	$-(\mathscr{A},\mathscr{B})(\mathscr{B},\mathscr{C})(\mathscr{C},\mathscr{D})\frac{ABC}{(A-D)(B-D)(C-D)}-(\mathscr{A},\mathscr{B})(\mathscr{B},\mathscr{D})\frac{AB}{(A-D)(B-D)}-(\mathscr{A},\mathscr{C})(\mathscr{C},\mathscr{D})\frac{AC}{(A-D)(C-D)}-(\mathscr{A},\mathscr{D})\frac{A}{A-D}$	$-(\mathscr{B},\mathscr{C})(\mathscr{C},\mathscr{D})\frac{BC}{(B-D)(C-D)}-(\mathscr{B},\mathscr{D})\frac{B}{B-D}-(\mathscr{C},\mathscr{D})\frac{C}{C-D}$	-1	
1				1

FORMULA FOR d SPECIALIZED AS DESCRIBED IN APPENDIX II

	a_0	b_0	c_0	d_0
$1-e^{-At}$	$+(\mathscr{A},\mathscr{B})(\mathscr{B},\mathscr{C})(\mathscr{C},\mathscr{D})\frac{BC}{(A-B)(A-C)}-(\mathscr{A},\mathscr{B})(\mathscr{B},\mathscr{D})\frac{B}{A-B}-(\mathscr{A},\mathscr{C})(\mathscr{C},\mathscr{D})\frac{C}{A-C}+(\mathscr{A},\mathscr{D})$			
$1-e^{-Bt}$	$-(\mathscr{A},\mathscr{B})(\mathscr{B},\mathscr{C})(\mathscr{C},\mathscr{D})\frac{AC}{(A-B)(B-C)}+(\mathscr{A},\mathscr{B})(\mathscr{B},\mathscr{D})\frac{A}{A-B}$	$-(\mathscr{B},\mathscr{C})(\mathscr{C},\mathscr{D})\frac{C}{B-C}+(\mathscr{B},\mathscr{D})$		
$1-e^{-Ct}$	$+(\mathscr{A},\mathscr{B})(\mathscr{B},\mathscr{C})(\mathscr{C},\mathscr{D})\frac{AB}{(A-C)(B-C)}$ $+(\mathscr{A},\mathscr{C})(\mathscr{C},\mathscr{D})\frac{A}{A-C}$	$+(\mathscr{B},\mathscr{C})(\mathscr{C},\mathscr{D})\frac{B}{B-C}$	$+(\mathscr{C},\mathscr{D})$	
1				1

TABLE II

		a_0
	$1-e^{-At}$	$-(\mathscr{A}\mathscr{B})(\mathscr{B}\mathscr{C})\frac{AB}{(A-B)\ (A-C)}+(\mathscr{A}\mathscr{C})\frac{A}{A-C}$
c	$1-e^{-Bt}$	$+(\mathscr{A}\mathscr{B})(\mathscr{B}\mathscr{C})\frac{AB}{(A-B)\ (B-C)}$
	$1-e^{-Ct}$	$-(\mathscr{A}\mathscr{B})(\mathscr{B}\mathscr{C})\frac{AB}{(A-C)\ (B-C)}-(\mathscr{A}\mathscr{C})\frac{A}{A-C}$
	1	

Again, if it were assumed that, of the portion of $\mathscr{A}$ which reacts, a fraction p follows the path $\mathscr{A}\rightarrow\mathscr{B}$ and the fraction $1-p$ follows the path $\mathscr{A}\rightarrow\mathscr{C}$ the system is specified by

$$(\mathscr{A}\mathscr{B}) = (\beta/\alpha)p, \qquad (\mathscr{A}\mathscr{C}) = (1-p), \qquad (\mathscr{A}\mathscr{D}) = p[1-(\beta/\alpha)];$$
$$(\mathscr{B}\mathscr{C}) = \gamma/\beta, \qquad (\mathscr{B}\mathscr{D}) = 1-\gamma/\beta;$$
$$(\mathscr{C}\mathscr{D}) = 1.$$

APPENDIX I

The complete formula for d is given here to display the full pattern of the solutions to the general system. d is determined by the differential equation

$$-dd/dt = Dd-(\mathscr{A}\mathscr{D})Aa-(\mathscr{B}\mathscr{D})Bb-(\mathscr{C}\mathscr{D})Cc,$$

where a, b, c are given by Equations (1), (2), (3) of System II.

APPENDIX II

The general formula for d is here specialized to describe the case in which $\mathscr{D}$ is the final substance in the sequence. That is, $\mathscr{D}$ does not break down ($D = 0$) and all the other substances break down, by all possible routes, into $\mathscr{D}$ and nothing else. It follows that

$$(\mathscr{C}\mathscr{D}) = 1, \qquad (\mathscr{B}\mathscr{C})+(\mathscr{B}\mathscr{D}) = 1, \qquad (\mathscr{A}\mathscr{B})+(\mathscr{A}\mathscr{C})+(\mathscr{A}\mathscr{D}) = 1.$$

The solution corresponding to these conditions is obtained from the general formula given in Appendix I simply by substituting $D = 0$. The form of the solution is altered somewhat by this substitution, because the argument $1-e^{-Dt}$ vanishes and therefore the corresponding row of multipliers is dropped. The resulting formula for d has the property that the sum of the coefficients in each cell is unity. This corresponds to the fact that, when t becomes infinite,

$$d = a_0+b_0+c_0+d_0 = 1.$$

THE INFRARED AND RAMAN SPECTRA OF ALLENE-1,1-d_2 [1]

By J. C. Evans,[2] J. K. Wilmshurst,[3]
and H. J. Bernstein

The infrared spectrum of allene-1,1-d_2 vapor has been observed from 2 to 35 μ (Fig. 1) using a Perkin Elmer Model 12C double pass spectrometer equipped with LiF, NaCl, and CsBr optics and the Raman spectrum obtained for the liquid at $-50°$ C. (Fig. 2) with a White grating Raman spectrometer (8) with photoelectric recording. The depolarization ratios of the Raman lines were obtained by the method of Edsall and Wilson (3).

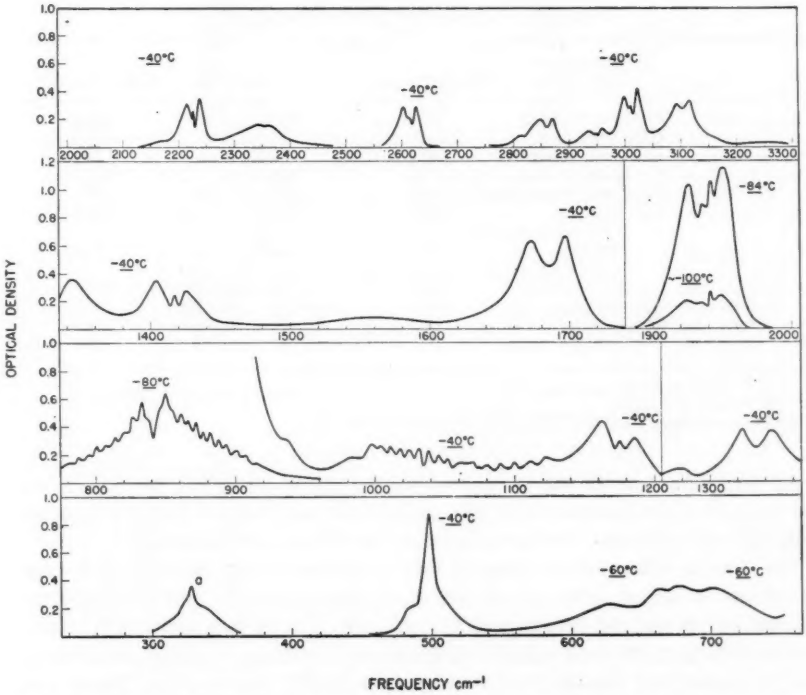

FIG. 1. The infrared spectrum of $H_2C{=}C{=}CD_2$ vapor in a 10 cm. cell at the vapor pressure of the liquid for the temperature shown; (*a*) 6 cm. cell, liquid at $-50°$C.

[1]*Issued as N.R.C. No. 4011.*
[2]*National Research Laboratories Postdoctorate Fellow 1953–1955.*
[3]*National Research Laboratories Postdoctorate Fellow 1955– .*

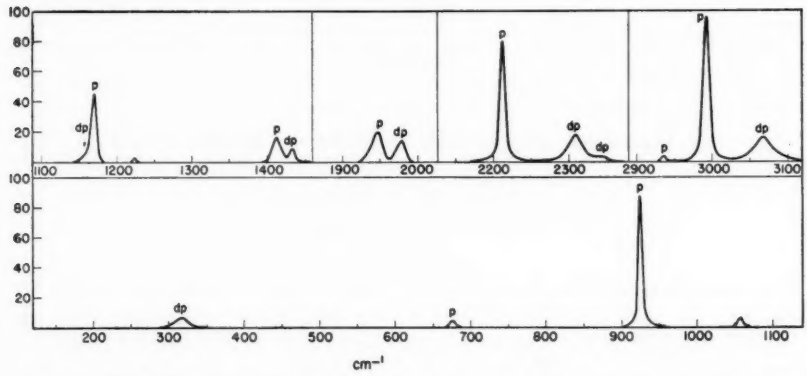

FIG. 2. The Raman spectrum of liquid $H_2C{=}C{=}CD_2$ (slits ~7 cm.$^{-1}$). The intensity of the band at ~3000 cm.$^{-1}$ is taken as 100. dp = depolarized, p = polarized.

TABLE I

FREQUENCY ASSIGNMENT FOR ALLENE-1,1-d_2

V_d	C_{2v}		Approximate description	$CH_2{=}C{=}CH_2$	$CH_2{=}C{=}CD_2$	$CD_2{=}C{=}CD_2$
a_1	a_1	ν_1	C—H stretching	2996	2995 R	2195
a_1	a_1	ν_2	CH_2 bending	1440	1169 R	1228
a_1	a_1	ν_3	C=C=C stretching	1076	924 R	874
b_2	a_1	ν_5	C—H stretching	3005	2226 IR	2230
b_2	a_1	ν_6	C=C=C stretching	1957	1941 IR	1921
b_2	a_1	ν_7	CH_2 bending	1398	1416 IR	1034
b_1	a_2	ν_4	Torsion	865	(750)	615
e	b_1,b_2	ν_8	C—H stretching	3085	3105 IR, 2309 R	2330
e	b_1,b_2	ν_9	CH_2 rocking	1015	1058 R, 842 IR	830
e	b_1,b_2	ν_{10}	CH_2 rocking	842	676 R, 842 IR	667
e	b_1,b_2	ν_{11}	C=C=C bending	354	317 R, 317 R	306

R = Raman band.
IR = infrared band.
(750) = calculated from the Teller Redlich product rule (5).

An assignment of all the fundamentals for allene-1,1-d_2 has been made on the basis of C_{2v} symmetry and this assignment is given in Table I together with that of Lord and Venkateswarlu (6) for allene and allene-d_4.

The type a_1 vibrations in allene-1,1-d_2, corresponding to the a_1 and b_2 type vibrations in allene, give rise to polarized Raman bands and parallel type infrared bands and can be assigned immediately. The type b_1 and b_2 vibrations, corresponding to the type e doubly degenerate vibrations of allene, should give rise to depolarized Raman bands and perpendicular type infrared bands and are assigned by comparison with allene and allene-d_4. A partial resolution of the two perpendicular bands at 842 and 1058 cm.$^{-1}$ was obtained. The a_2 torsional frequency was not observed but was computed from the Teller Redlich product rule (5). All the remaining observed frequencies can be easily

assigned, in terms of these fundamentals, to overtone or combination bands (Table II). The Raman band at 1223 cm.$^{-1}$ is probably ν_1 (2995 cm.$^{-1}$) excited by the 4047 Å mercury line.

The Teller Redlich product rule (5), Decius–Wilson sum rule (2), and Bernstein–Pullin sum rule (1) are consistent with the present assignment (Table III).

On attempting a direct comparison of the a_1 and b_2 frequencies in allene with the a_1 frequencies in allene-1,1-d_2, it is found that an interesting change has

TABLE II

OVERTONE AND COMBINATION BANDS FOR ALLENE-1,1-d_2

Obs. frequency	Assignment	Calc.
498* IR	$\nu_9(b_2)-\nu_{11}(b_2)$	525
626 IR	$2\nu_{11}$	634
1158 R	$\nu_9(b_2)+\nu_{11}(b_1)$	1159
~1285 IR	$\nu_8(b_2)-$[1008]	1301
1334 IR	$2\times\nu_{10}$	1352
1433 R	$\nu_{10}(b_1)+\nu_4(a_2)$	1426
~1566 IR	$\nu_4(a_2)+\nu_9(b_2)$	1592
1686 IR	$2\times\nu_9(b_2)$	1684
1935 IR	$\nu_6(a_1)+\nu_{11}-\nu_{11}$†	1941
1977 R	?	
2173 IR	2×[1086]	2172
2615 IR	$\nu_8(b_2)+\nu_{11}(b_2)$	2626
2812 IR	$2\times\nu_7(a_1)$	2832
2860 IR	2×[1086]$+\nu_{10}(b_1)$	2848
2949 IR	$\nu_6(a_1)+$[1008]	2949

[1086] and [1008] are the estimated positions of the unperturbed fundamentals $\nu_2(a_1)$ and $\nu_3(a_1)$.

*May be due to $CH_3C{\equiv}CD$ impurity which has its strongest infrared band at 498 cm.$^{-1}$ (4).

†Consistent with corresponding assignments in allene and allene-d_4 (6).

TABLE III

PRODUCT RULE RATIOS

		Symmetry species used for ratio calculation		
Theor.	Obs.	CH_2CCH_2	CH_2CCD_2	CD_2CCD_2
0.513	0.519	a_1, b_2	a_1	
0.512	0.527		a_1	a_1, b_2
0.866	—	b_1	a_2	
0.816	—		a_2	b_1
0.382	0.426	e	b_1, b_2	
0.461	0.457		b_1, b_2	e

APPLICATION OF SUM RULES TO ALLENE-1,1-d_2

	$\Sigma\nu^2$, cm.$^{-2}$		$\Sigma\nu$, cm.$^{-1}$	
Species	Theor.	Obs.	Calc.	Obs.
a_1	2.192×10^7	2.192×10^7	10,677	10,671
b_1, b_2	1.792×10^7	1.817×10^7	9,415	9,466

occurred and two bands in the 1000–1400 cm.$^{-1}$ region, one due to the symmetrical CH_2 bending and the other due to the symmetrical C=C=C stretching frequency, have undergone major changes upon deuterium substitution. This change is explained by the coupling of the symmetrical CD_2 bending mode with the symmetrical C=C=C stretching mode, which give rise to frequencies in the 1000–1100 cm.$^{-1}$ region, causing one frequency to increase to 1169 cm.$^{-1}$, and the other to drop to 924 cm.$^{-1}$. This coupling is also present in allene-d_4, but to a slightly greater extent, the two resultant frequencies being at 1228 cm.$^{-1}$ and 874 cm.$^{-1}$.

The sample of allene-1,1-d_2 was prepared for us through the courtesy of Morse and Leitch (7).

1. Bernstein, H. J. and Pullin, A. D. E. J. Chem. Phys. 21: 2188. 1953.
2. Decius, J. C. and Wilson, E. B., Jr. J. Chem. Phys. 19: 1409. 1951.
3. Edsall, J. T. and Wilson, E. B., Jr. J. Chem. Phys. 6: 124. 1938.
4. Grisenthwaite, R. J. and Thompson, H. W. Trans. Faraday Soc. 50: 212. 1954.
5. Herzberg, G. Infrared and Raman spectra of polyatomic molecules. D. Van Nostrand Company, Inc., New York. 1945. p. 232.
6. Lord, R. C. and Venkateswarlu, P. J. Chem. Phys. 20: 1237. 1952.
7. Morse, A. T. and Leitch, L. C. To be published.
8. White, J. U., Alpert, N., and De Bell, A. G. J. Opt. Soc. Amer. 45: 154. 1955.

Received April 25, 1956.
Division of Pure Chemistry,
National Research Council,
Ottawa, Canada.

A NOTE ON THE SYSTEM WOLFRAM–TELLURIUM

By Osvald Knop and Haakon Haraldsen

Goldschmidt (2) considered wolfram ditelluride to be isostructural with wolfram disulphide and wolfram diselenide, but this has never been confirmed by a structural investigation. In fact, in a preliminary study of the binary systems of wolfram with sulphur, selenium, and tellurium, Stangebye (7) showed that the compound WTe_2, prepared by heating stoichiometric amounts of the elements *in vacuo*, did not give X-ray powder diffraction photographs similar to those of the disulphide and diselenide.

This observation was fully confirmed in the present investigation. The rotation and Weissenberg photographs of a single crystal found in the mass of fine ditelluride powder showed that the compound had an orthorhombic structure with the unit-cell dimensions $a = 3.490 \pm 0.006$ Å, $b = 6.277 \pm 0.015$ Å, and $c = 14.07 \pm 0.02$ Å. The volume of the unit cell based on these dimensions, 308 ± 2 Å^3, and the experimental density, $d_4^{20} = 9.40$, led to four WTe_2 units per unit cell. Reflections of the type $(h0l)$ were absent when $h+l = 2n+1$. The space groups consistent with these systematic absences are $D_{2h}^{13} - Pmnm$, $C_{2v}^{7} - Pmn$, and $D_2^3 - P2_122_1$.

Unless WTe_2 is polymorphic—and we obtained no evidence to that effect—it cannot be considered isostructural with the *C*7-type compounds, i.e., with MoS_2, $MoSe_2$, WS_2, and WSe_2. There are indications, however, that it has a

layer-like structure closely related to the *C*7 type. The axial ratio of WTe_2, $c/a = 4.03$, does not differ greatly from the values 3.92–3.93 and 3.94 for the corresponding sulphur and selenium compounds (9, 10), and a value for b about 3.7% lower than the above value would give an axial ratio $b/a = \sqrt{3}$ required for an orthohexagonal cell. This suggests a modified double unit cell of the *C*7 type. A Patterson projection on the (010) plane seemed to confirm this similarity but the intensity data on which it was based were rather inaccurate. The single crystal used was a very thin plate of irregular shape, with the approximate dimensions 0.15, 0.08, and 0.02 mm. along the *a*-, *b*-, and *c*-axes, respectively, and there must have been heavy irregular absorption of X-rays in the crystal. Powder photographs taken both with an ordinary and with a microfocus camera contained too many diffuse and overlapping lines to permit an intensity evaluation. Attempts are being made to secure more suitable single crystals of WTe_2 that will provide reliable data for a structure determination.

No line shift outside the usual measurement spread was detected in the powder photographs of samples having the gross compositions $WTe_{1.90}$ and WTe_3. These samples were prepared in the same manner as WTe_2 and were annealed *in vacuo* at 500°C. for several days. It seems likely that the homogeneity range of wolfram ditelluride is very narrow (compare the slight variation in the lattice constants reported for WS_2 (9)). This indicates that if the composition of the single crystal used deviated at all from the stoichiometric composition, it could have been only by a very small amount.

In agreement with the results of Stangebye (7) and Morette (4, 5) no compound other than WTe_2 was detected in alloys obtained by direct synthesis *in*

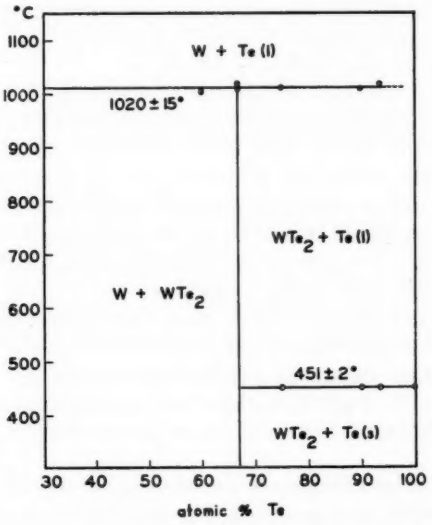

FIG. 1. Phase relationships in the system wolfram–tellurium under orthobaric conditions.

vacuo. Combined evidence from X-ray powder photography, and from thermal analysis of samples sealed in small evacuated quartz containers, suggests phase relationships as represented in Fig. 1, with the system under its own pressure. However, one cannot exclude the possibility that other compounds might be obtained by low-temperature annealing of intimate mixtures of WTe_2 and tellurium or wolfram for long periods of time. As is evident from Morette's examination of polished sections of alloys rich in tellurium (5), the solubility of wolfram in tellurium at temperatures below 500°C. must be quite low, as a solidified alloy with 0.33 at. % W still contained crystals of the ditelluride embedded in a matrix of tellurium.

A fuller account of the continued investigation, and of a similar investigation in the system molybdenum–tellurium now in progress, will be published later.

EXPERIMENTAL

The wolfram used in this investigation was prepared by reducing calcined WO_3 (c.p. grade) with hydrogen at temperatures between 650° and 800°C. The lattice constant of the resulting lightly-sintered powder was found to be 3.1647 ± 0.0003 Å at room temperature, in very good agreement with the value 3.16477 ± 0.00008 Å reported by Cohen (1). Both reduced metal and a commercial wolfram powder reported to contain 99.8% W and 0.2% Mo were used in the preparation of samples with the composition $WTe_{2.00}$. No differences in the properties of the resulting powders were observed.

A grant of tellurium of about 99.9% purity was kindly made by the Research and Development Department of the Canadian Copper Refiners, Limited, Montreal. According to the analysis supplied the main impurity was selenium. The lattice constants of the material were determined as 4.456 ± 0.002 Å and 5.925 ± 0.002 Å, in satisfactory agreement with the values of Straumanis (8), 4.45591 ± 0.00012 Å and 5.92687 ± 0.00002 Å.

Accurately weighed amounts of the elements totalling 15–20 gm. were introduced into degassed clear-quartz tubes which were then evacuated to 10^{-6} mm. Hg, sealed off, and put into a deep vertical tubular furnace at 700–800°C. After several hours the power was turned off and the samples allowed to cool in the furnace. The alloys were then crushed and ground to 100 mesh, thoroughly mixed, and annealed at 500°C. for several days in sealed evacuated quartz tubes. Samples of the gross compositions $WTe_{1.50}$, $WTe_{1.90}$, $WTe_{2.00}$, WTe_3, WTe_4, WTe_9, and WTe_{15} were prepared.

The density of the ditelluride was determined pycnometrically with water as displacement liquid, about 1 cm.^{3} of powder being used in separate determinations. The average of several determinations gave $d_4^{20} = 9.40$. Morette (4, 5) reported $d_4^{15} = 9.44 \pm 0.02$, without mentioning details of his method, while the value calculated from the above lattice constants is 9.46 ± 0.06 gm./cm.^{3}

Although there was practically no loss of material during the handling of the powders, all samples were analyzed. The determination of tellurium using sulphur dioxide and hydrazine hydrate (3) gave satisfactory results. Wolfram was determined as WO_3. The analytical results were in close agreement with

the intended gross compositions. Indeed, any discrepancies between the analytical results and the compositions of the samples as obtained by weighing are likely to have originated in the inaccuracies inherent in the analytical method.

The samples for thermal analysis were sealed in evacuated containers of clear quartz having internal free volumes of about 3 cm.^{3} An average of about 5 gm. of sample was used in individual runs. There was a pronounced tendency to supercooling, and the geometry of the heating curves depended considerably on the heating rates.

Filtered or unfiltered CuK-radiation ($\lambda\alpha_1 = 1.53740$ kX, $\lambda\alpha_2 = 1.54123$ kX) from a hot-cathode tube was used throughout. The powder photographs were taken in a Straumanis-type camera with a nominal diameter of 114.6 mm., and the rotation and equi-inclination Weissenberg photographs of the single crystal about the a- and b-axes (three and four zones, respectively) were taken in a Unicam instrument, using the multiple-film technique. The intensities were estimated visually. Nelson and Riley's method (6) was used in the treatment of the lattice constants. Difficulties were encountered in the measurement of the films, as WTe_2 did not give good powder photographs.

ACKNOWLEDGMENTS

This work was begun by the first author in 1948 during his stay at the Institute of Inorganic Chemistry of the University of Oslo, as a part of the studies of the chalkogenides of the transition elements pursued at the Institute for a number of years. A grant from the Norwegian Unesco Committee which enabled him to stay at the Institute is hereby gratefully acknowledged. The investigation was continued at the Nova Scotia Technical College, with financial assistance from the Nova Scotia Research Foundation. The authors wish to express their gratitude to Professor G. V. Douglas for the use of his X-ray diffraction unit; to Dr. D. R. Ryan for the analytical work; to Miss Patricia M. Beatty for assistance with the computations; and to Dr. C. M. Mitchell for a powder photograph of the ditelluride taken with a microfocus unit.

1. Cohen, M. U. Z. Krist. 94: 288. 1936.
2. Goldschmidt, V. M. Trans. Faraday Soc. 25: 279. 1919.
3. Lenher, V. and Homberger, A. W. J. Am. Chem. Soc. 30: 387. 1908.
4. Morette, A. Compt. rend. 216: 566. 1943.
5. Morette, A. Ann. chim. (11), 19: 130. 1944.
6. Nelson, J. B. and Riley, D. P. Proc. Phys. Soc. (London), 57: 160. 1945.
7. Stangebye, E. Thesis. University of Oslo, Oslo, Norway. 1946.
8. Straumanis, M. Z. Krist. 102: 432. 1940.
9. Structure Reports. Vol. 11. 1947–1948. Utrecht, 1951. Intern. Union of Crystallography. p. 260.
10. Strukturbericht. Bd. I. 1915–1928. Ergänzungsband zur Z. Krist. Leipzig, 1931. pp. 164, 215.

Received February 24, 1956.
Department of Chemical Engineering,
Nova Scotia Technical College,
Halifax, Nova Scotia,
and
Institute of Inorganic Chemistry,
University of Oslo,
Blindern, Norway.

HELVETICA CHIMICA ACTA

EDENDA CURAT SOCIETAS CHIMICA HELVETICA

Since 1918 the Swiss Chemical Society has been editing its own periodical for Pure Chemistry which is published under the title *Helvetica Chimica Acta*.

HELVETICA CHIMICA ACTA are published yearly in 8 numbers with a total of approximately 2300 pages, the year beginning on the 1st February. The subscription for the current volume is Swiss frs. 80.—, plus postage (abroad fr. 7.50). Back volumes can be supplied as follows: reprint volumes, I–XIV cloth bound, set $400; single volumes, paper bound, $25 each, plus postage; from Vol. XV, Swiss frs. 100.— each; from Vol. XXV, Swiss frs. 80.— each, plus postage. The price for single numbers is Swiss frs. 12.—, plus postage.

Please send your order to Messrs.

SCHWEIZERISCHE CHEMISCHE GESELLSCHAFT
VERLAG HELVETICA CHIMICA ACTA
POSTFACH BASEL 7 SWITZERLAND

CANADIAN JOURNAL OF CHEMISTRY

Notes to Contributors

Manuscripts

(i) ***General.*** Manuscripts, in English or French, should be typewritten, double spaced, on paper 8½ × 11 in. **The original and one copy are to be submitted.** Tables and captions for the figures should be placed at the end of the manuscript. Every sheet of the manuscript should be numbered.

Style, arrangement, spelling, and abbreviations should conform to the usage of this journal. Names of all simple compounds, rather than their formulas, should be used in the text. Greek letters or unusual signs should be written plainly or explained by marginal notes. Superscripts and subscripts must be legible and carefully placed.

Manuscripts and illustrations should be carefully checked before they are submitted. Authors will be charged for unnecessary deviations from the usual format and for changes made in the proof that are considered excessive or unnecessary.

(ii) ***Abstract.*** An abstract of not more than about 200 words, indicating the scope of the work and the principal findings, is required, except in Notes.

(iii) ***References.*** References should be listed **alphabetically by authors' names,** numbered, and typed after the text. The form of the citations should be that used in this journal; in references to papers in periodicals, titles should not be given and only initial page numbers are required. The names of periodicals should be abbreviated in the form given in the most recent *List of Periodicals Abstracted by Chemical Abstracts*. All citations should be checked with the original articles and each one referred to in the text by the key number.

(iv) ***Tables.*** Tables should be numbered in roman numerals and each table referred to in the text. Titles should always be given but should be brief; column headings should be brief and descriptive matter in the tables confined to a minimum. Vertical rules should be used only when they are essential. Numerous small tables should be avoided.

Illustrations

(i) ***General.*** All figures (including each figure of the plates) should be numbered consecutively from 1 up, in arabic numerals, and each figure referred to in the text. The author's name, title of the paper, and figure number should be written in the lower left corner of the sheets on which the illustrations appear. Captions should not be written on the illustrations (see Manuscripts (i)).

(ii) ***Line Drawings.*** Drawings should be carefully made with India ink on white drawing paper, blue tracing linen, or co-ordinate paper ruled in blue only; any co-ordinate lines that are to appear in the reproduction should be ruled in black ink. Paper ruled in green, yellow, or red should not be used unless it is desired to have all the co-ordinate lines show. All lines should be of sufficient thickness to reproduce well. Decimal points, periods, and stippled dots should be solid black circles large enough to be reduced if necessary. Letters and numerals should be neatly made, preferably with a stencil (**do NOT use typewriting**) and be of such size that the smallest lettering will be not less than 1 mm. high when reproduced in a cut 3 in. wide.

Many drawings are made too large; originals should not be more than 2 or 3 times the size of the desired reproduction. In large drawings or groups of drawings the ratio of height to width should conform to that of a journal page but the height should be adjusted to make allowance for the caption.

The original drawings and one set of clear copies (e.g. small photographs) are to be submitted.

(iii) ***Photographs.*** Prints should be made on glossy paper, with strong contrasts. They should be trimmed so that essential features only are shown and mounted carefully, with rubber cement, on white cardboard with no space or only a **very** small space (less than 1 mm.) between them. In mounting, full use of the space available should be made (to reduce the number of cuts required) and the ratio of height to width should correspond to that of a journal page (4¾ × 7¼ in.); however, allowance must be made for the captions. Photographs or groups of photographs should not be more than 2 or 3 times the size of the desired reproduction.

Photographs are to be submitted in duplicate; if they are to be reproduced in groups one set should be mounted, the duplicate set unmounted.

Reprints

A total of 50 reprints of each paper, without covers, are supplied free. Additional reprints, with or without covers, may be purchased.

Charges for reprints are based on the number of printed pages, which may be calculated approximately by multiplying by 0.6 the number of manuscript pages (double-spaced typewritten sheets, 8½ × 11 in.) and including the space occupied by illustrations. An additional charge is made for illustrations that appear as coated inserts. The cost per page is given on the reprint requisition which accompanies the galley.

Any reprints required in addition to those requested on the author's reprint requisition form must be ordered officially as soon as the paper has been accepted for publication.

Contents

Page

Thermal Neutron Capture Cross Section of Ce^{142}—*L. P. Roy and L. Yaffe* - 1023

Graft Copolymers of Styrene and Methyl Methacrylate. Part II: Viscosity Behavior—*M. H. Jones* - - - - - - - - - - - 1027

The Vibrational Spectra of Isobutane and Isobutane-d_1—*J. C. Evans and H. J. Bernstein* - - - - - - - - - - - - - - - 1037

Adsorption of Oxygen by a Silver Catalyst—*W. W. Smeltzer, E. L. Tollefson, and A. Cambron* - - - - - - - - - - - - - 1046

The Reaction of Deuterium Atoms with Ethylene—*S. Toby and H. I. Schiff* - 1061

The Reactions of Active Nitrogen with Alkyl Chlorides—*B. Dunford, H. G. V. Evans, and C. A. Winkler* - - - - - - - - - - 1074

The Vibrational Spectra of Acetaldehyde and Acetaldehyde-d_1—*J. C. Evans and H. J. Bernstein* - - - - - - - - - - - 1083

Hydrolysis and Hydrazinolysis of Esters of N,N-dimethyldithiocarbamic Acid. A Method for the Preparation of Mercaptans—*Marshall Kulka* - - - - - - - - - - - - - - - - - - - 1093

The Application of Interpolation Theory to Data on the Adsorption of Nitrogen, Oxygen, and Argon on Rutile—*J. M. Honig and L. H. Reyerson* - - - - - - - - - - - - - - - - - - 1101

The Entropies of Ions in Aqueous Solution. I. Dependence on Charge and Radius—*K. J. Laidler* - - - - - - - - - - - - 1107

The Adsorption of Nitrogen by Brominated Graphite and Carbon Black—*H. L. McDermot and J. C. Arnell* - - - - - - - - 1114

Intensity in the Raman Effect. V. The Effect of Intermolecular Interaction on the Raman Spectrum of Carbon Disulphide—*J. C. Evans and H. J. Bernstein* - - - - - - - - - - - - 1127

The Differential Equations of Consecutive Reactions—*A. E. R. Westman and D. B. DeLury* - - - - - - - - - - - - - - 1134

Notes:

The Infrared and Raman Spectra of Allene-1,1-d_2—*J. C. Evans, J. K. Wilmshurst, and H. J. Bernstein* - - - - - - - - 1139

A Note on the System Wolfram–Tellurium—*Osvald Knop and Haakon Haraldsen* - - - - - - - - - - - - - - - - 1142

Printed in Canada by University of Toronto Press